SHORTED ANNULAR PATCH ANTENNAS FOR MULTIPATH REJECTION IN GPS-BASED ATTITUDE DETERMINATION SYSTEMS

Luigi Boccia,[1] Giandomenico Amendola,[2] Giuseppe Di Massa,[1] and Luisella Giulicchi[2]
[1] Dipartimento di Elettronica, Informatica e Sistemistica
University of Calabria
87036 Rende, Italy
[2] European Space Agency (ESA – Estec)
Noordwijk, The Netherlands

Received 11 July 2000

ABSTRACT: *In the past years, ESA has been considering the use of the Global Positioning System (GPS) as a medium-accuracy attitude sensor for low-earth-orbit missions. This paper describes the design of a compact GPS antenna with improved multipath rejection to counteract the effects of the spurious reflections. In particular, a shorted annular patch that is a variant of the classical annular patch and has its inner edge shorted by a cylindrical conducting wall is proposed. It is shown that the radiation characteristics of the antenna offer the possibility to fulfill the multipath rejection radiation requirements without using an array solution.* © 2001 John Wiley & Sons, Inc. Microwave Opt Technol Lett 28: 47–51, 2001.

Key words: *GPS; attitude; antenna; multipath*

1. INTRODUCTION

Recently, the Global Positioning System has been demonstrated to be a very promising medium-accuracy attitude sensor for low-earth-orbit missions [1, 2]. A GPS-based attitude determination system represents a hybrid sensor that gives a continuous pointing knowledge, completely immune to drift phenomena, and therefore without the necessity to be calibrated by a reference sensor. Furthermore, it gives a reduction in size, power, and cost of the sensor hardware.

The basic measurable in GPS-based attitude determination is a differential measurement across two antennas of the phase of the GPS signal. The largest error source on this measurement is due to reflections or diffractions from surfaces around the antennas (the spacecraft body, solar panels, etc.) that introduce differential phase distortions. This error is normally referred to as multipath error (Fig. 1), and currently represents the limiting factor in the achievable accuracy of GPS-based attitude determination.

The multipath effect on differential phase measurements and attitude estimation can be mitigated with software processing using measurement redundancy or error predictability [3, 4]. With such methods, a reduction of the multipath error of about 50% can be achieved.

Nevertheless, signal processing in a GPS receiver cannot completely satisfy the accuracy requirements of the GPS-based attitude sensor, and a receiving antenna that can reject multipath signals is required.

Antennas can be optimized for GPS-based attitude determination in two ways. First, they can be designed with high rejection to left-hand circularly polarized (LHCP) signals. This reduces the impact of multipath because the GPS signal is right-hand circularly polarized (RHCP), while odd reflections are LHCP. Hence, using antennas with a good rejection of LHCP signals, multipath effects arising from direct reflections can be potentially eliminated. Effects due to double reflections remain, but they are normally much weaker.

Second, attitude measurement performance can be improved by shaping the antenna gain pattern to reject low-elevation signals. This is beneficial because reflected signals often impinge on the antenna at low elevations. Hence, a narrow beam minimizes their impact. Notice, however, that, in order to perform attitude determination, at least two GPS satellites must be tracked at all times. For this reason, the antenna field of view must be large enough to ensure that two or more satellites are visible throughout the satellite orbit. In practice, this means that the antenna pattern aperture must be greater than 120° (supposing that only GPS is used, a less constraining bound can be found if simultaneous use of Glonass is assumed).

Besides, a new antenna will be suitable for aerospace applications only if its size is small enough to permit an easy implementation on the spacecraft. Indeed, one essential advantage of using GPS for attitude determination is that different sensors and their interfaces can be eliminated and, in turn, costs, power requirements, weight, and complexity can be reduced.

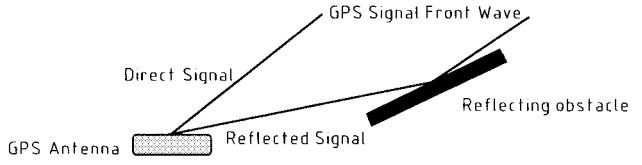

Figure 1 Origin of the multipath error

In this paper, it will be shown that the low-multipath requirements on a GPS antenna for spacecraft attitude determination can be fulfilled with a single radiator by considering a shorted annular patch antenna.

In the following, the radiation characteristics of the shorted annular patch will be resumed. In particular it will be shown that, with a proper choice of the inner and outer radii of the ring, a narrow radiation pattern can be obtained, suppressing, at the same time, surface-wave emissions, thus limiting their effects on the cross-polar and back-radiation levels.

A design of a circularly polarized shorted ring then will be presented, and both its theoretical and measured characteristics will be shown. Furthermore, in order to prove the low-multipath performances of the proposed antenna, the results of comparative measurements performed on the *on-ground* GPS Test Facility at the European Space Agency (ESA) will be presented and discussed.

2. ANTENNA DESIGN

The shorted annular patch antenna [5] is a derivation of the standard circular patch. It presents the same radiating characteristics, but a wider bandwidth and easier matching.

The geometrical configuration of the antenna is shown in Figure 2, with the exclusion of the feeding network.

This antenna has several advantages with respect to the standard circular patch. In fact, a circular disk antenna has an input impedance that ranges from 0 Ω at the center up to 200–300 Ω at the edge. To get a good match, the feed should be then inserted near the center with a small tolerance. A shorted annular patch has an input impedance of about 100 Ω at the edge; therefore, the position of the feed is less critical, and the antenna can be fed with a coplanar microstrip.

Furthermore, the presence of the cylindrical conductor in the central zone of the antenna reduces the energy stored under the patch, resulting in a lower antenna quality factor and in a bandwidth wider than the one of a standard circular disk.

The essential feature of the antenna is that the low-multipath radiation pattern requirements can be fulfilled using a single radiator (i.e., without adopting an array solution), as the pattern of the shorted annular patch can be easily controlled by varying the antenna geometry without degrading the radiation characteristics.

In fact, it is easy to show that [5], when working on its dominant mode TM_{11}, the shorted ring has equivalent magnetic current distribution of a conventional disk that results in a similar radiation pattern. As a consequence, with a proper choice of the external and internal radii, narrower radiation patterns that maintain the radiation characteristics of a circular disk can be obtained. This is clearly shown in Figure 3, where the simulated radiation patterns of three shorted ring antennas resonating at 1.57542 GHz, with an external radius of 45, 55.7, and 66 mm, are reported, together with that of a circular disk antenna. The effects of a larger ring radius are quite evident. For the ring with a larger radius, sidelobes on the *H*-plane cut are observed, which limit the range of the values admitted for the choice of the patch size.

A further requirement for the ideal antenna is that it should control surface-wave emissions in order to reduce their effects on the radiation pattern, and in particular on the cross-polar level.

As is well known [6], the surface waves can be inhibited if a shorted annular patch with an external radius

$$a = \frac{x'_{1n}}{k} \tag{1}$$

is taken. In Eq. (1), which is valid for thin substrates [7], x'_{1n} are the zeros of the derivative of the first-order Bessel function, and k is the free-space propagation constant.

An antenna design fulfilling the constraints previously described has been realized at the GPS L2 frequency $f =$ 1.57542 GHz. In order to obtain a narrow radiation pattern, the first zero in Eq. (1) is taken. This choice has given an

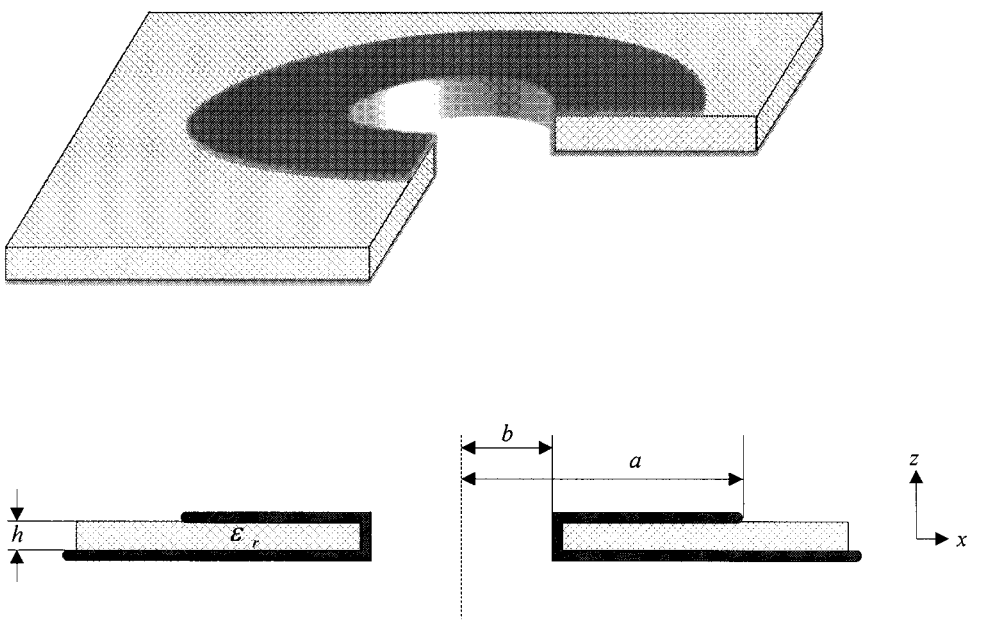

Figure 2 Shorted annular patch geometry

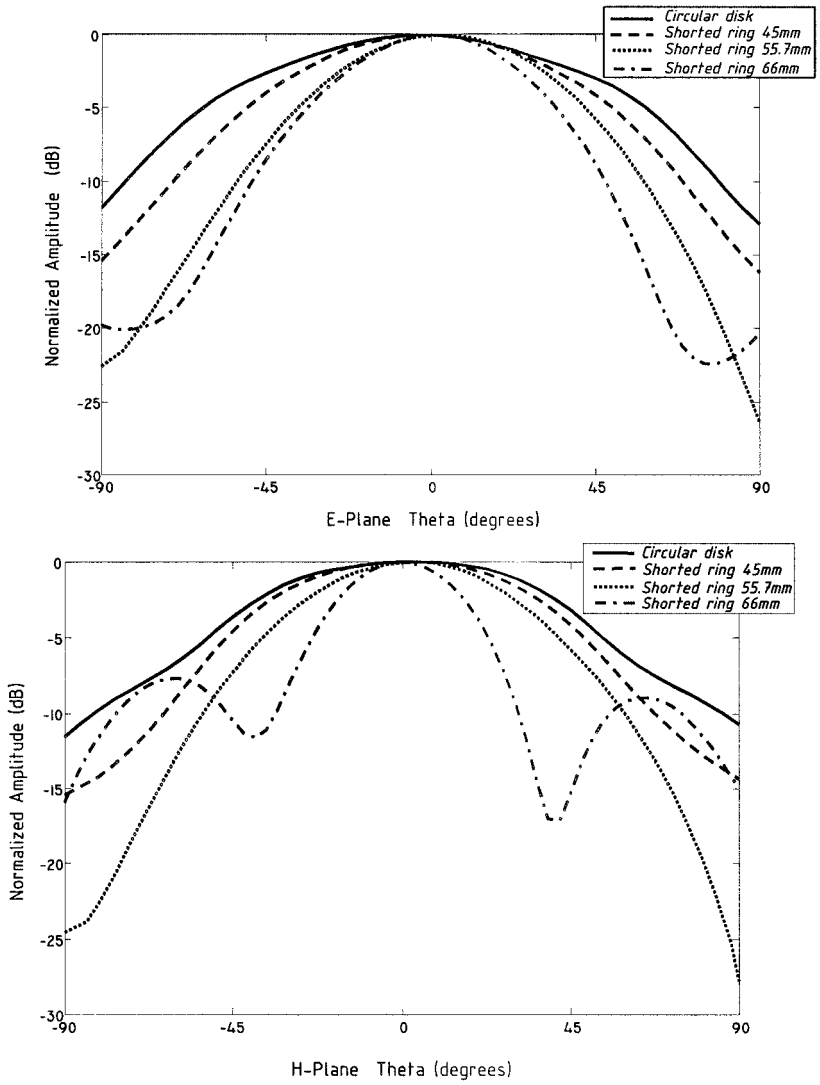

Figure 3 Radiation patterns of a circular disk with radius 34.3 mm, and of three shorted annular patch antennas having external radius of 45, 55.7, and 66 mm, respectively. The four antennas resonate at 1.57542 GHz

external radius a of 5.57 cm for a substrate with $\varepsilon_R = 2.33$ and 0.159 cm thick. In order to make the patch resonate on the desired frequency, an inner radius b of 2.79 cm has been taken. The antenna frequency has been determined with a simple, but effective cavity model, and the whole structure has been simulated with a finite-element package [8] to take into account the effects of the finite substrate in order to estimate the back-radiation level. The prototype antenna is shown in Figure 4.

As can be seen, circular polarization is obtained with a dual-fed solution. Two 50 Ω feeding lines with a 90° phase difference have been adopted. The offset feeding lines are set inside the edges of the patch, and a quarter-wave transformer allows the match between the parallel connection of the two lines and the power-divider output.

To obtain a good match, the antenna has been fed with a recessed microstrip [9]. The reactance generated in the microstrip portion internal to the patch is avoided, introducing a gap of 1.5 mm on each side of the line. The measured S_{11} of the antenna is reported in Figure 5, showing a good match.

In Figure 6, the simulated copolar and cross-polar patterns in the two principal planes are presented. As can be seen, the antenna shows a good behavior in terms of both the copolar and back-radiation level and, even if the antenna is fed with coplanar lines, the effects of the spurious radiation do not deteriorate the radiation patterns. Furthermore, considering the absence of sidelobes, the back-radiation level can be further reduced by slightly enlarging the antenna ground plane [10].

For comparison, the copolar components of the radiation pattern measured in the compact antenna test range of the ESA are also presented in Figure 7, together with the simulated ones, showing a good agreement.

3. EXPERIMENTAL RESULTS

The effectiveness of the proposed design has been verified through comparative measurements performed on an *on-ground* GPS test facility [11] of the ESA.

The basic measurable in the GPS-based attitude determination is the differential measurement across the two anten-

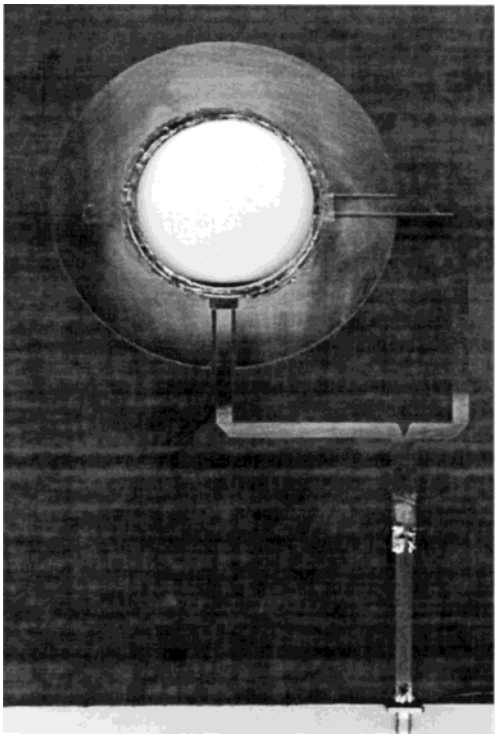

Figure 4 Top view of a shorted annular patch antenna having external radius $a = 5.57$ cm, internal radius $b = 2.79$ cm, and realized on a substrate with $\varepsilon_R = 2.33$ and 1.59 mm thick

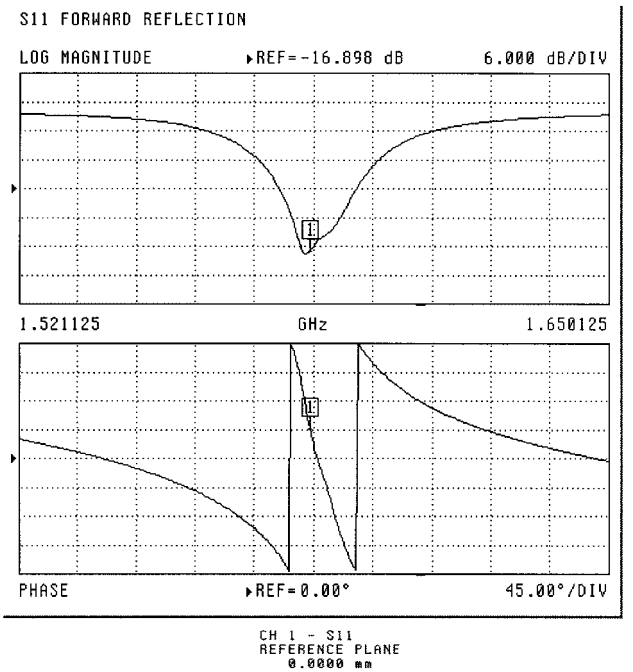

Figure 5 Measured reflection coefficient for the antenna shown in Figure 4

nas of the phase of the GPS signal. In order to evaluate the behavior of the shorted ring, 24-h tests to collect sets of differential phase measurements have been performed, and the results have been compared with the ones obtained using standard GPS patch antennas.

In order to have a complete statistical evaluation of the multipath error rejection performances, the mean, the standard deviation, and the root-mean square (rms) of the differential phase error over all of the collecting time have been considered.

The results obtained are reported in Table 1. They are very promising, and demonstrate that a performance improvement of 50% can be achieved through specific antenna design that is compliant with size, mass, and cost requirements. Furthermore, considering that the multipath error can be mitigated with software processing, we can expect another 50% reduction of the multipath level. Therefore, by implementing both the software and hardware solutions, the GPS sensor would become very interesting and, by reaching accu-

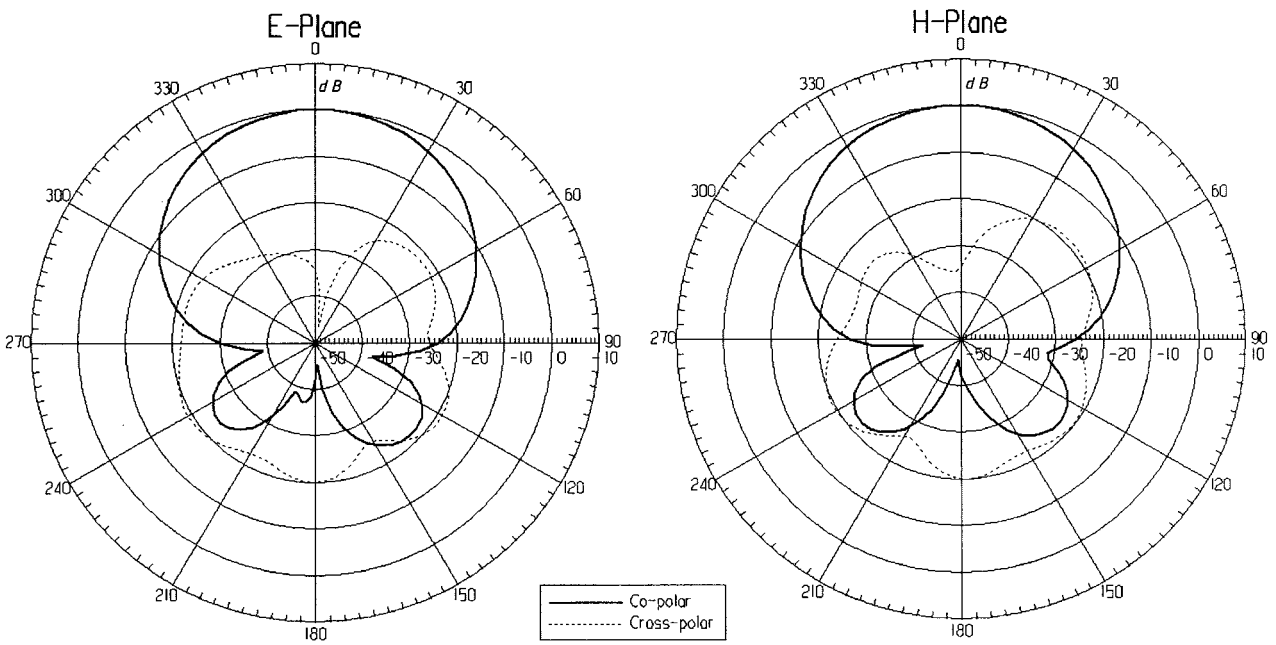

Figure 6 Simulated copolar and cross-polar radiation patterns (dB versus theta) of the shorted annular patch of Figure 4

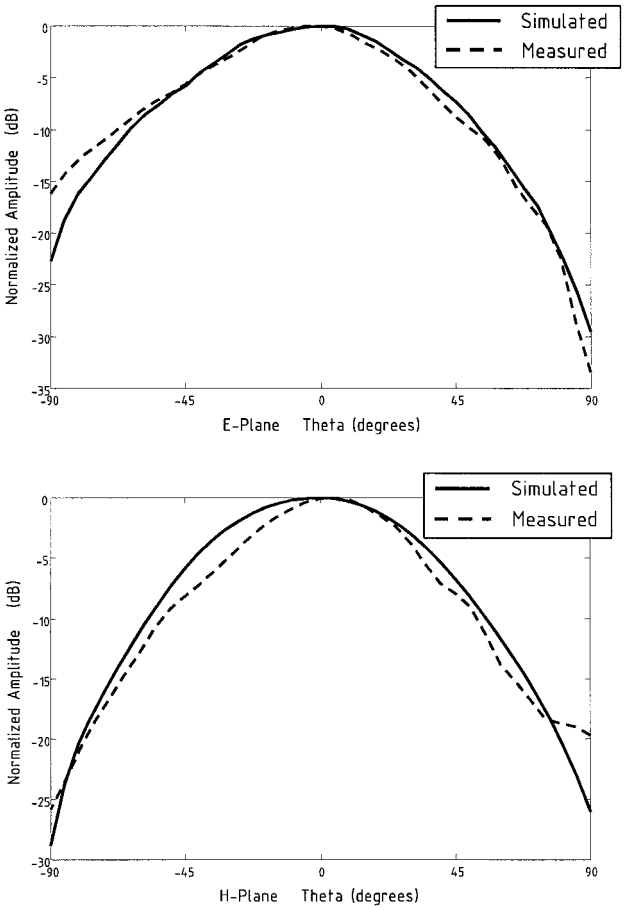

Figure 7 Measured and simulated copolar radiation pattern

TABLE 1 Experimental Results: Statistical Summary

Multipath Error	Shorted Annular Patch	Reference GPS Patch	Multipath Error Reduction
Mean (deg)	−1.2	5.4	74.5
Standard deviation (deg)	10.0	19.1	47.4
rms (deg)	13.1	26.2	50.1

racies below the 1° (1-sigma) currently achievable, it would comply to a wider range of mission requirements.

4. CONCLUSIONS

In this paper, the design of a shorted annular patch for attitude determination with a high-multipath rejection has been proposed. The antenna characteristics made possible an effective design, fulfilling the requirements on the radiation pattern needed to reduce multipath effects on differential phase measurements.

The antenna has been tested by means of measurements collected on an *on-ground* GPS test facility. Experimental results indicate that the shorted annular patch antenna reduces the multipath error, with respect to the standard GPS antenna, up to 50% rms. Additionally, the shorted ring, inheriting all of the advantages of the microstrip antennas in term of cost, weight, and easy manufacturing, is well suited for aerospace applications.

REFERENCES

1. C.E. Choen, Attitude determination using GPS, Ph.D. dissertation, Stanford University, 1992.
2. L. Vaillon (MMS-Toulouse), Attitude determination using GPS, Summary rep from Estec Study Contract 9558/91/NL/JG, Apr. 1998.
3. L. Giulicchi and A. Pasetti, GPS test system series: Multipath bias compensation, Estec rep GTS-ES-AP-02, issue 2, Nov. 1998.
4. A. Pasetti and L. Giulicchi, GPS test system series: Multipath frequency compensation, Estec rep GTS-ES-AP-03, issue 2, Sept. 1998.
5. G. Di Massa and G. Mazzarella, Shorted annular patch antenna, Microwave Opt Technol Lett 8 (1995).
6. D.R. Jackson, J.T. Williams, A.K. Bhattacharyya, R.L. Smith, S.J. Buchheit, and S.A. Long, Microstrip patch designs that do not excite surface waves, IEEE Trans Antennas Propagat 41 (1993).
7. D.M. Pozar, Input impedance and mutual coupling of rectangular microstrip antennas, IEEE Trans Antennas Propagat 40 (1992).
8. Ansoft High Frequency Structure Simulator v.6, Ansoft Corp.
9. G. Amendola, G. DiMassa, and G. Mazzarella, Planar shorted annular patch antenna, Int Conf Electromag Adv Appl, Torino, Italy, 1995.
10. R. Marg, I. Schon, and A.F. Jacob, Finite ground plane effects on the radiation pattern of small microstrip arrays, Proc Inst Elect Eng 147 (2000).
11. A. Pasetti, A. Medina, and P. Colmenarejo, GPS test system series: System architecture, Estec-WSC TN GTS-WS-AP-01, issue 2, Jan. 20, 1998.

Progress In Electromagnetics Research C, Vol. 35, 123–134, 2013

WIDEBAND SHORTED ANNULAR STACKED PATCH ANTENNA FOR GLOBAL NAVIGATION SATELLITE SYSTEM APPLICATION WITH COMPACT SIZE AND BROAD BEAMWIDTH CHARACTERISTICS

Xi Li*, Lin Yang, Min Wang, Yi Wang, Xi Chen, and Juan Lei

National Laboratory of Science and Technology on Antennas and Microwaves, Xidian University, Xi'an, Shaanxi, China

Abstract—A compact circularly polarized shorted annular stacked patch antenna has been proposed for global navigation satellite system (GNSS) in this paper. The antenna has been designed to operate for the satellite navigation frequencies including GPS, GLONASS, Galileo and Compass (1100 MHz–1600 MHz). In order to obtain wideband characteristics, broadband 90° hybrids have been used as a secondary network. The designed antenna has a 73.7% (10-dB) return loss bandwidth from 0.9 GHz to 1.95 GHz, and 60.1% 3-dB axial ratio bandwidth from 0.96 GHz to 1.8 GHz, respectively. Shorted annular stacked patch structure is incorporated into the antenna design helping to obtain stable gain bandwidth, broad beamwidth characteristics and good axial ratio at low elevation. The designed antenna occupies a compact size of 100 mm × 100 mm × 15.5 mm.

1. INTRODUCTION

With the development of global navigation satellite system (GNSS), the requests for multi-system navigation ability increase. To fulfill the needs of this application, antennas should be wideband, with stable gain bandwidth, broad beamwidth and compact size. Quadrifilar helical antenna has exciting radiation characteristics of broad beamwidth [1, 2]. However, the disadvantages of big size and narrow bandwidth limit its applications. Microstrip patch antennas [3–6, 8–11, 13–21] are often used in the applications needing circular polarization due to their low-profile, low cost, easy fabrication and

Received 19 October 2012, Accepted 12 December 2012, Scheduled 13 December 2012

* Corresponding author: Xi Li (xli@xidian.edu.cn).

compatibility with integrated circuit technology. However, the general limitations of the traditional microstrip antennas are achievable impedance and axial-ratio (AR) bandwidths. There are many methods to achieve broadband performance of microstrip antennas, such as using two or more radiating structures which work at different but contiguous resonant frequencies, using coupling feeding scheme, adding external matching circuits and so on. Several multi-band or wideband low-profile antennas have been proposed in the literature [7–11] for GPS or GNSS application. However, few of them can obtain broad beamwidth characteristics and good axial ratio at low elevation, which are useful to suppressing multipath interferences.

In this paper, a novel proximity-coupled probe-fed shorted annular stacked patch antenna design for GNSS application has been presented, which can be used in all four satellite navigation services. The presented antenna is characterized by the following features: 1) in order to obtain wideband impedance and AR bandwidths, broadband 90° hybrids and printed L-probes coupling feeding schemes are used. 2) The ground plane and feeding network are printed on the lower and higher side of the substrate respectively. In this case, the network can be fed by an SMA connector from the bottom of substrate, which is propitious to feeding the array. This structure can also make the antenna symmetrical and have a symmetrical radiation performance. 3) The feeding network is arranged along the diagonal of the substrate, helping to optimize the space utilization. 4) The usage of shorted annular stacked patch as radiator instead of conventional patch, which can provide stable gain bandwidth, broad beamwidth characteristics and good axial ratio at low elevation.

In Section 2, the antenna configuration and design principle are described. The simulated and measured antenna parameters are given in Section 3, followed by a brief conclusion in Section 4.

2. ANTENNA CONFIGURATION AND DESIGN

Figure 1 presents the structure of the proposed shorted annular stacked patch antenna. The antenna design includes five layers. The upper annular patch is printed on the top of the first substrate layer and the lower annular patch printed on the back. The upper and lower patches are shorted by the metal wall. The second substrate layer acts as the support and isolates the lower patch and L-probe. The L-probes are proposed to achieve broadband matching. In this design, four L-probes are placed under the radiating patch to excite the annular ring and transform the input impedance. The L-probes are composed of four square metal strips, printed on the top of the third substrate and

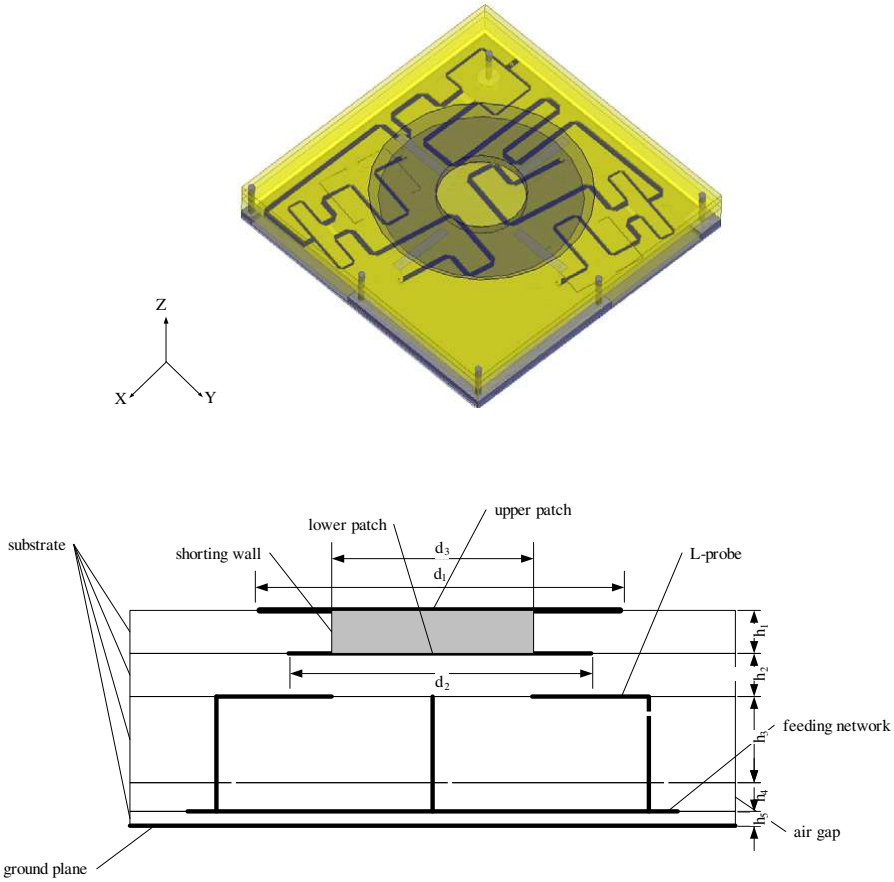

Figure 1. The structure of the proposed antenna.

the posts, which go through the substrate and are connected to the broadband 90° hybrid port. The dimensions of the probes and the distances between strips and annular patch affect the coupling. The fourth layer is the air layer, which can decrease the effect between the feeding network and the substrate. The feeding network is printed on the top of the top of the fifth substrate layer and the ground plane is printed on its back. The feeding network is composed of one common two-way power divider with 180° phase offset acting as the primary network and two wideband 90° hybrids acting as the secondary network. In this case, the feeding network can provide good 90° phase differences between two adjacent ports which are connected to the same wideband 90° hybrids. The structure of the feeding network is shown

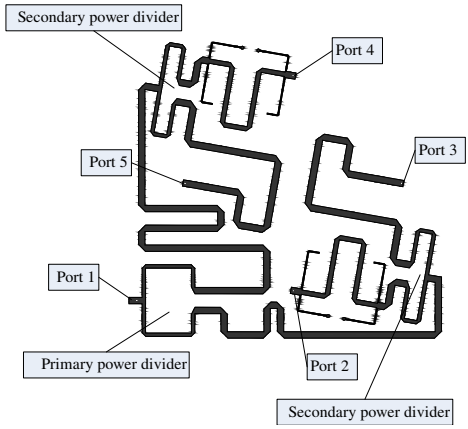

Figure 2. Layout graph of the feeding circuit.

Table 1. Key dimensions of the structure.

L	ε_r (all substrate layer)	d_1	d_2	d_3
100 mm	4.4	67 mm	60.8 mm	27 mm
h_1	h_2	h_3	h_4	h_5
3 mm	3 mm	6 mm	2.5 mm	1 mm

in Figure 2. Figure 3 displays the simulated (using HFSS ver.13 [22]) and measured return loss, magnitude response and phase differences of the feeding network. We observe that the magnitude variation is less than 0.5 dB and the phase shift unbalance less than 5° in the band of 1.1–1.6 GHz using the proposed feeding network. It is important for the antenna design to obtain excellent circular polarization performances.

The key dimensions of the structure are shown in Table 1.

3. RESULTS AND DISCUSSION

Figure 4 provides the graphs of the fabricated antenna. The overall size of the antenna is 100 mm × 100 mm × 15.5 mm. Figure 5 presents the variety of VSWR affected by the height of the third substrate (h_3) and the thickness of air gap (h_4). As can be seen in the figure, when $h_3 > 6$ mm and $h_4 > 2.5$ mm, VSWR < 2 in the whole band for GNSS. The VSWR measured using Agilent E8363B network analyzer along with the simulation data using HFSS are presented in Figure 6. It can be observed that the impedance bandwidth for VSWR < 2 is 73.7%, providing the working range of 0.9 to 1.95 GHz.

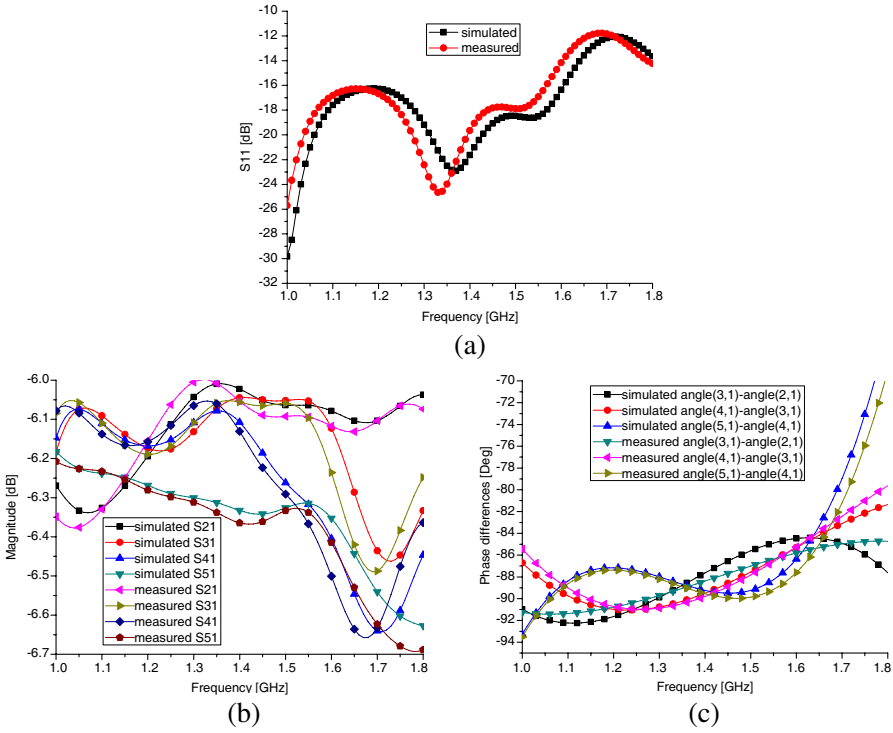

Figure 3. Simulated and measured performances of the feeding network. (a) Simulated and measured return loss of the feeding network. (b) Simulated and measured magnitude response of the feeding network. (c) Simulated and measured phase differences of the feeding network.

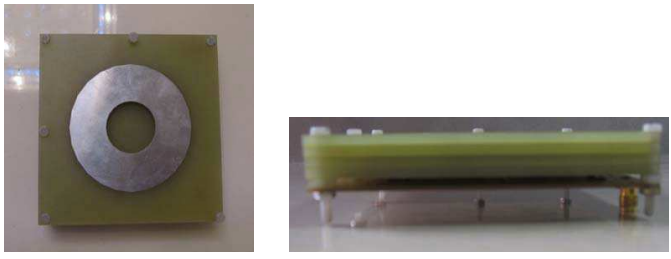

(a) Front view (b) Side view

Figure 4. The photo of the proposed antenna.

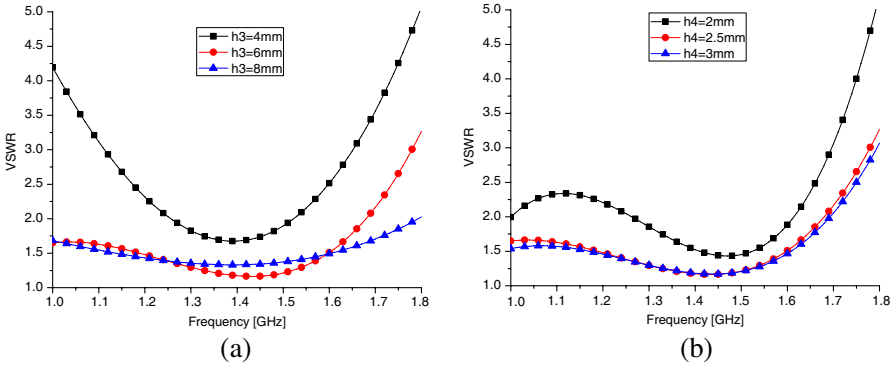

Figure 5. Simulated return loss of the proposed antenna for various h_3 and h_4.

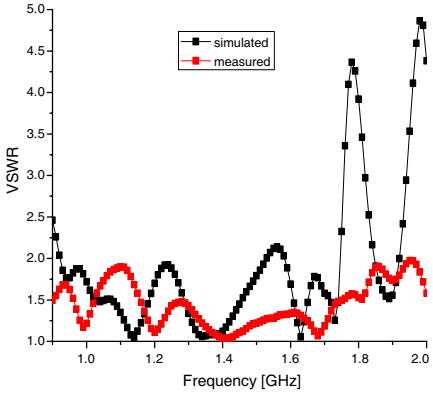

Figure 6. Simulated and measured VSWR.

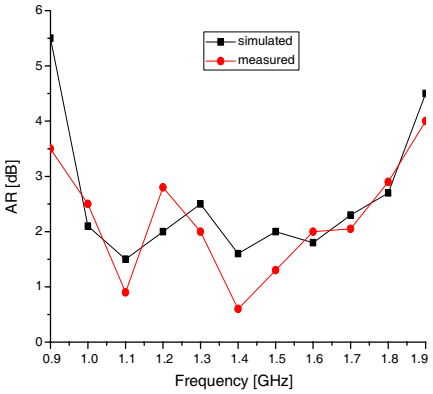

Figure 7. Simulated and measured AR.

The radiation performances were measured in an anechoic chamber. Two Archimedean spiral antennas were used to measure right-hand circular polarization and left-hand circular polarization radiation, respectively. From Figure 7, the 3-dB AR bandwidth of the proposed antenna is 60.1% providing the working range of 0.96 to 1.8 GHz. It owes to applying four ports L-probes coupling feeding schemes, which enhance the AR bandwidth extremely. As can be seen in the figure, the impedance and AR bandwidths are sufficient to cover GNSS frequencies. The simulated and measured AR patterns in the X-Z and Y-Z planes at 1.2, 1.4 and 1.6 GHz are presented in Figure 8. As seen, the elevation angles for AR < 5 dB are $-50°$–$50°$ at X-Z

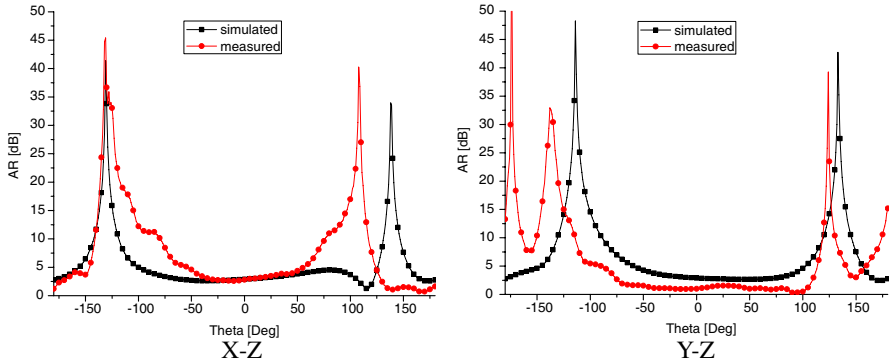

(a) Simulated and measured AR patterns at 1.2 GHz

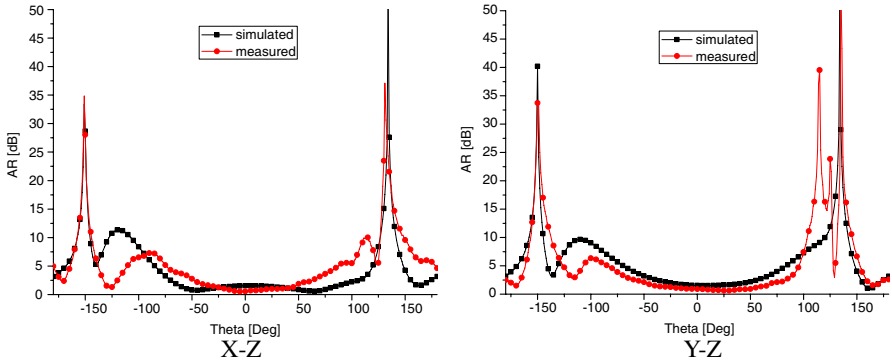

(b) Simulated and measured AR patterns at 1.4 GHz

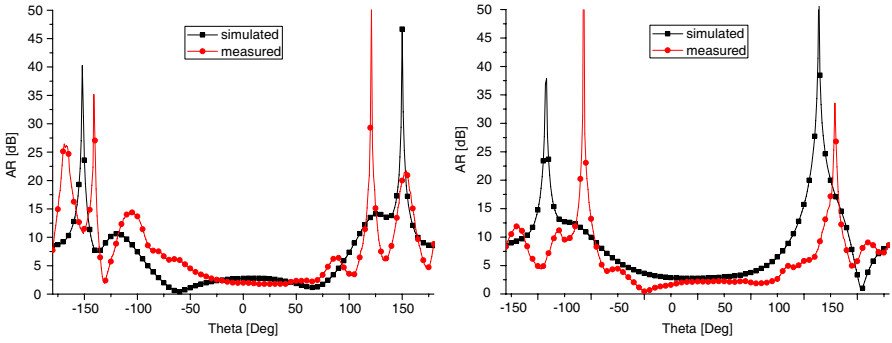

(c) Simulated and measured AR patterns at 1.6 GHz

Figure 8. Simulated and measured AR patterns.

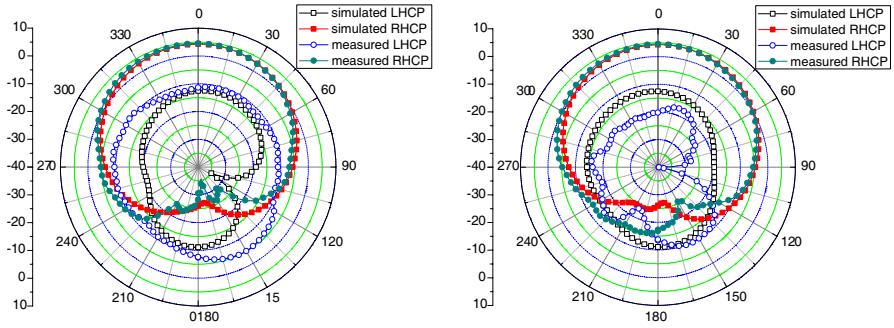

(a) Simulated and measured radiation patterns at 1.2 GHz

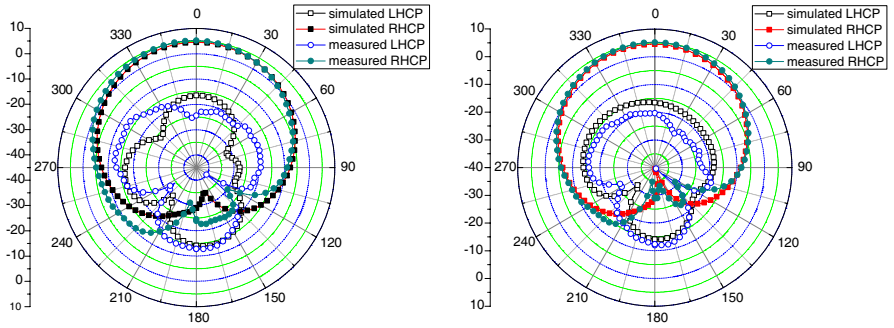

(b) Simulated and measured radiation patterns at 1.4 GHz

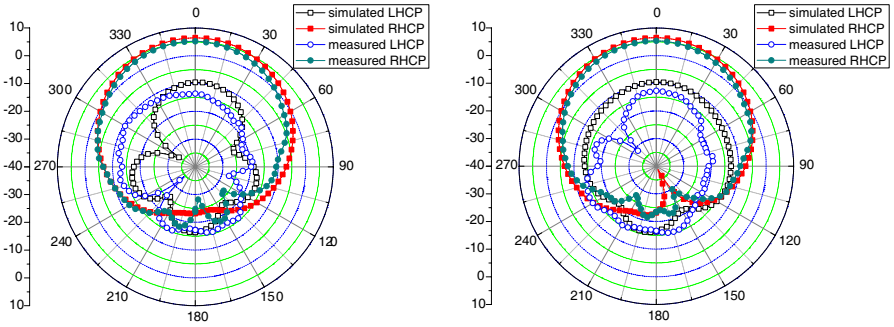

(c) Simulated and measured radiation patterns at 1.6 GHz

Figure 9. Simulated and measured radiation patterns.

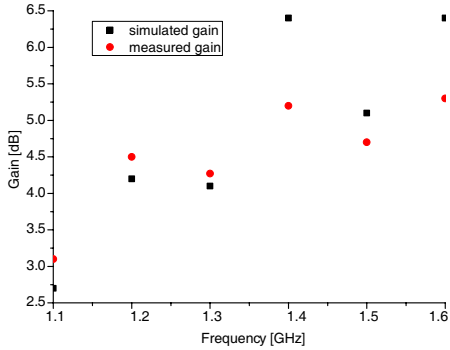

Figure 10. Simulated and measured gain of the proposed antenna.

Table 2. Axial ratio and gain characteristics at low elevation.

Literature	Elevation angles for gain > -5 dBi	Elevation angles for AR < 5 dB
7	About 20°	Not mentioned
8	About 20°	Not mentioned
9	About 20°	Not mentioned
11	About 30°	Not mentioned
12	About 30°	Not mentioned
13	About 30°	About 28°
Proposed	About 15°	About 15° expect x-z plane at 1.2 GHz and x-z plane at 1.6 GHz

plane and −80°–110° at Y-Z plane respectively at 1.2 GHz, −75°–85° at X-Z plane and −75°–90° at Y-Z plane respectively at 1.4 GHz, −50°–75° at X-Z plane and −85°–85° at Y-Z plane respectively at 1.6 GHz. The asymmetry of the AR patterns is mainly due to the machine and measurement errors. Figure 9 shows the simulated and measured radiation patterns in the X-Z and Y-Z planes at three different frequencies 1.2, 1.4 and 1.6 GHz. Broad pattern coverage and high gain at low elevation angles (more than −5 dBi at elevation angles $> 15°$) are achieved. The excellent performances of the antenna are mainly due to the shorted annular stacked patch structure and four ports proximity-coupled probe-fed feeding mechanism. Axial ratio and gain characteristics at low elevation are better than other structures reported in the literatures [7–9, 11–13], which can be seen in Table 2. It is noted that literature [13] can achieve excellent AR

performance at low elevation angles by mounting the antenna on a cylinder housing. However, it will increase the overall size obviously. The simulated and measured RHCP gain of the antenna at different frequencies is presented in Figure 10, and it is observed that the stable gain bandwidth can be obtained for gain > 3 dBi.

4. CONCLUSION

In this paper, the results of the design for a novel compact circularly polarized shorted annular stacked patch antenna are reported. The antenna is fed by four ports feeding network composed of one common Wilkinson power divider and two broadband 90° hybrids. Using the proposed proximity-coupled probe-fed feeding scheme, the antenna exhibits an effective bandwidth of 60.1% from 0.96 to 1.8 GHz for VSWR < 2 and AR < 3 dB. Shorted annular stacked patch structure is incorporated into the antenna design. The proposed antenna not only has a compact size of 100 mm $\times$ 100 mm $\times$ 15.5 mm, but also can provide stable gain bandwidth, broad beamwidth characteristics and good axial ratio at low elevation. Measured parameters show good agreement with the modeling and conform that such antennas can be successful used for GNSS applications.

REFERENCES

1. Kilgus, C., "Resonant quadrifilar helix," *IEEE Transactions on Antennas and Propagation*, Vol. 17, No. 3, 349–351, 1969.
2. Amin, M. and R. Cahill, "Compact quadrifilar helix antenna," *Electronics Letters*, Vol. 41, 672–674, 2005.
3. Huang, J. and V. Jamnejad, "A microstrip array feed for land mobile satellite reflector antennas," *IEEE Transactions on Antennas and Propagation*, Vol. 37, No. 2, 153–158, 1989.
4. Chebolu, S., S. Dey, R. Mittra, and M. Itoh, "A dual-band stacked microstrip antenna array for mobile satellite applications," *Antennas and Propagation Society International Symposium, 1995, AP-S Digest*, Vol. 1, 598–601, 1995.
5. Wu, J. Y., J. S. Row, and K. L. Wong, "A compact dual-band microstrip patch antenna suitable for DCS/GPS operations," *Microwave and Optical Technology Letters,* Vol. 29, No. 6, 410–412, 2001.
6. Guo, Y. X., L. Bian, and X. Q. Shi, "Broadband circularly polarized annular-ring microstrip antenna," *IEEE Transactions on Antennas and Propagation*, Vol. 57, No. 8, 2474–2477, 2009.

7. Zhou, Y., S. Koulouridis, G. Kizitas, and J. L. Volakis, "A novel 1.5″ quadruple antenna for tri-band GPS applications," *IEEE Antennas and Wireless Propagation Letters*, Vol. 5, 224–227, 2006.
8. Zhou, Y., C. C. Chen, and J. L. Volakis, "Dual band proximity-fed stacked patch antenna for tri-band GPS applications," *IEEE Transactions on Antennas and Propagation*, Vol. 55, No. 1, 220–223, 2007.
9. Wang, Z. B., S. J. Fang, S. Q. Fu, and S. W. Lu, "Dual-band probe-fed stacked patch antenna for GNSS applications," *IEEE Antennas and Wireless Propagation Letters*, Vol. 8, 100–103, 2009.
10. Pimenta, M. S., F. Ferrero, R. Staraj, and J. M. Ribero, "Low-pofile circularly polarized GNSS antenna," *Microwave and Optical Technology Letters*, Vol. 54, No. 12, 2811–2814, 2012.
11. Ma, J. P., A. B. Kouki, and R. Landry, Jr., "Wideband circularly polarized single probe-fed patch antenna," *Microwave and Optical Technology Letters*, Vol. 54, No. 8, 1803–1808, 2012.
12. Zheng, L. and S. Gao, "Compact dual-band printed square quadrifilar helix antenna for global navigation satellite system receivers," *Microwave and Optical Technology Letters*, Vol. 53, No. 5, 993–997, 2011.
13. Moernaut, G. J. K. and G. A. E. Vandenbosch, "Concept study of a shorted annular patch antenna: Design and fabrication on a conducting cylinder," *IEEE Transactions on Antennas and Propagation*, Vol. 59, No. 1, 2097–2102, 2011.
14. Kasabegoudar, V. G. and K. J. Vinoy, "A broadband suspended microstrip antenna for circular polarization," *Progress In Electromagnetics Research*, Vol. 90, 353–368, 2009.
15. Bao, X. L. and M. J. Ammann, "Comparison of several novel annular-ring microstrip patch antennas for circular polarization," *Journal of Electromagnetic Waves and Applications*, Vol. 20, No. 11, 1427–1438, 2006.
16. Liu, W. C. and P. C. Kao, "Design of a probe-fed H-shaped microstrip antenna for circular polarization," *Journal of Electromagnetic Waves and Applications*, Vol. 21, No. 7, 857–864, 2007.
17. Chang, T. N. and J. H. Jiang, "Enhance gain and bandwidth of circularly polarized microstrip patch antenna using gap-coupled method," *Progress In Electromagnetics Research*, Vol. 96, 127–139, 2009.
18. Heidari, A. A., M. Heyrani, and M. Nakhkash, "A dual-band circularly polarized stub loaded microstrip patch antenna for GPS

applications," *Progress In Electromagnetics Research*, Vol. 92, 195–208, 2009.

19. Yang, S. S., K.-F. Lee, A. A. Kishk, and K.-M. Luk, "Design and study of wideband single feed circularly polarized microstrip antennas," *Progress In Electromagnetics Research*, Vol. 80, 45–61, 2008.
20. Wu, G.-L., W. Mu, G. Zhao, and Y.-C. Jiao, "A novel design of dual circularly polarized antenna fed by L-strip," *Progress In Electromagnetics Research*, Vol. 79, 39–46, 2008.
21. Yu, A., F. Yang, and A. Z. Elsherbeni, "A dual band circularly polarized ring antenna based on composite right and left handed metamaterials," *Progress In Electromagnetics Research*, Vol. 78, 73–81, 2008.
22. Ansoft High Frequency Structure Simulation (HFSS), ver. 13, ANSYS, Inc., Canonsburg, PA, 2011.

Shorted Annular Patches as flexible antennas for space applications

Luigi Boccia, Giandomenico Amendola, Giuseppe Di Massa

Dipartimento di Elettronica, Informatica e Sistemistica
Università della Calabria
87036 Arcavacata di Rende (CS), Italy
Phone : +39-0984-494652 Fax : +39-0984-494713
E-mail: lboccia@deis.unical.it; amendola@deis.unical.it; dimassa@deis.unical.it

Abstract

This paper presents a review of the most important features of the Shorted Annular Patch antennas. These radiators have several mechanical and electrical advantages with respect to other microstrip geometries. In particular, the presence of the short in the central zone of the antenna provides increased radiation flexibility which permits to control the antenna beam aperture. In order to demonstrate the usefulness of SAP's features examples of applications in space environment are provided.

1. INTRODUCTION

In the last decades printed antennas have been largely studied due to their advantages over other radiating systems, such as light weight, reduced size, low cost, conformability and possibility of integration with active devices.

In this paper the most important features of an innovative microstrip radiator, namely the Shorted Annular Patch (SAP) antenna, will be presented and discussed.

The SAP antenna geometry is shown in Fig. 1 [1]. At variance of a conventional disk, the inner boundary of this patch is shorted to the ground plane. This antenna has several advantages with respect to the standard circular patch. In fact, a circular disk antenna has an input impedance that ranges from $0\,\Omega$ at the centre up to $200-300\,\Omega$ at the edge. To get a good match the feed should be then inserted near the centre with a small tolerance. A shorted annular patch has an input impedance of about $100\,\Omega$ at the edge, therefore the position of the feed is less critical allowing for an easier matching. Furthermore, the presence of the cylindrical conductor in the central zone of the antenna reduces the energy stored under the patch resulting in a lower antenna quality factor and in a bandwidth wider than the one of a standard circular disk.

In terms of size, weight and cost the SAP antenna has the same appealing characteristics of the standard microstrip patches.

In the following the most important SAP antenna radiation properties will be presented focusing the attention on their benefits for space applications.

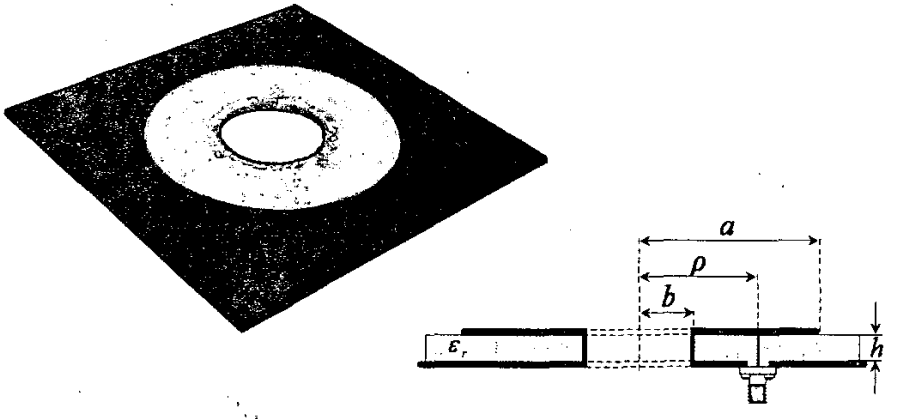

Fig. 1 – Shorted Annular Patch geometry.

2. SAP CHARACTERISTICS

SAP antennas have been extensively studied for their property to inhibit surface wave radiation. In [2] it has been demonstrated that an appropriate selection of the SAP ring external radius inhibits the excitation of the TM_0 surface wave mode avoiding the radiation pattern deterioration due to the surface waves diffraction and reducing mutual coupling in array applications [3]. The theory has been extended to elliptical SAP, for dual band or circularly polarized antennas, in [4].

Another essential feature of the antenna is that the SAP pattern can be easily controlled varying the antenna geometry without degrading the radiation characteristics. In order to clarify this aspect, let us first consider a conventional circular patch antenna resonating on its dominant mode TM_{11}. Once the resonant frequency and the dielectric characteristics are given, the external radius of the disk it is uniquely determined and the antenna radiation pattern, strictly connected to the magnetic current distribution at the external edge of the patch, can not be varied.

On the contrary, the shorted annular patch, which has the same magnetic current distribution of a conventional disk, offers much more flexibility in shaping the radiation pattern. In fact, with a proper choice of the external and internal radii, narrower beams that maintain the radiation characteristics of a circular disk can be obtained.

As example, three shorted annular patch antennas resonating at the nominal GPS L1 frequency, 1.57542GHz, with an external radius of 35, 45, and 55.7 mm, have been designed considering a substrate with dielectric constant ε_R=2.55 and thickness of 3.2 mm. The effect of a larger external radius is shown in Fig. 2 where the co-polar radiation patterns of the three SAP antennas have been compared with the one of a conventional circular patch resonating at the same frequency and designed using the same substrate. As expected, a larger outer radius of the antenna results in a narrower beam.

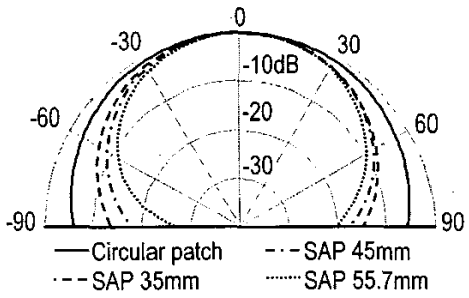

Fig. 2 – SAP radiation pattern flexibility.

Another important feature of the proposed antenna is that the gain of the shorted patch is considerably higher than other conventional microstrip antennas. For instance, the circular patch antenna taken as reference in Fig. 2 has a gain of 6.8dB while the SAP's gain varies with the outer radius of the ring following the curve reported in Fig. 3 and attaining a maximum of 10.67dB.

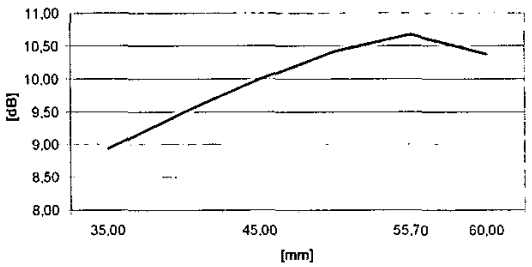

Fig. 3 – SAP gain vs. outer radius.

In addition to the radiation properties, the SAP antenna has mechanical features highly beneficial for space applications. In fact, even if the SAP designs proposed in this paper have been developed using a conventional microstrip technology, they can be easily adapted to solutions employing suspended technology and high performance materials. This opportunity eliminates the problems arising from the sensitivity of the electrical characteristics of the substrates and the distortion generated by the diffraction of surface waves seems to be advisable. This configuration is easily accomplished as the central short provides a supporting element on which single or stacked SAP's can be build.

As a further advantage of the shorted ring with respect to other microstrip geometries, it should be noticed that the central short provides a path for ESD avoiding the creation of ad-hoc circuits.

3. APPLICATIONS

So far, the SAP antenna has been successfully applied to several aerospace applications.

High Directive Antennas

The gain increase combined with the possibility to control the beam aperture can result highly beneficial in designing directive antennas of small and medium satellites. Normally for these applications where beam widths around 50degrees and a gain around 12 dB are needed, small array of printed antennas are employed. The same requirements can be easily satisfied in a more efficient way

using a single stacked SAP antenna. With this solution the beam aperture can be shaped by opportunely selecting the antenna outer radius and a parastic patch can be used to further increase the antenna gain.

High precision GPS

In the last few years the Global Positioning System (GPS) has been used in a variety of applications for which new and more restrictive requirements for the design of the receiving antenna have been introduced. In particular, for high-precision GPS applications, such as differential GPS, GPS-based spacecraft attitude determination or geodetic surveying, a receiving antenna with superior rejection to multipath signals is required.

At the radiator level, multipath can be essentially controlled in two ways. Antennas with a good rejection of LHCP signals can potentially eliminate multipath effects arising from direct reflections. Additionally, considering that reflections often impinge on the antenna at low elevations, the multipath rejection performance can be improved by shaping the antenna gain pattern to reject low-elevation signals while ensuring adequate hemispherical coverage. Furthermore, in order to satisfy the demanded precision and reliability, a high-performance GPS antenna must be capable of operation at the two GPS frequencies (L1: 1.57542GHz, L2: 1.2276GHz).

Several low multipath GPS antennas have been proposed in the past [5]. Unfortunately, most of the available solutions, including arrays or choke rings, are impractical in aerospace applications due to the operational requirements in terms of size and weight. A more effective design has been proposed in [6] where the shorted annular patch antenna, has been introduced as a possible solution for low-multipath GPS applications.

As shown in Fig. 2 the SAP radiator offers an extended radiation pattern flexibility which can be used to optimize the multipath rejection performances in consideration of the specific application constrains.

In order to demonstrate the radiation characteristics of the shorted patches, the experimental results referred to the SAP antenna having an external radius of 35mm are presented. A prototype has been fabricated using a standard milling drilling machine. An Arlon Diclad™ layer ($\varepsilon_r = 2.55$; h=3.2mm) has been used to etch the patch. The inner hole has been machined into the two dielectrics and the short circuit has been obtained using soldered copper foil. Adequate circular polarization purity is attained by feeding the antenna by means of two 50 Ω coaxial probes located 90 deg. apart and having 90 deg. of phase difference. The inner radius and the feed location are 6mm and 12mm respectively. The measured input impedance of the antenna is presented in Fig. 5, in comparison with the results of a FEM based commercial simulator [9]. As it can be seen, the predicted result is in excellent agreement with the experimental values.

Due to the precision of the simulator and the accuracy of the fabrication process, it was possible to achieve a fairly precise design that provided predictably high performance. In fact, the antenna resonates at the nominal GPS L1 frequency and is very well matched.

The multipath rejection performances of the SAP prototype have been evaluated considering both the sharpness of the antenna pattern toward the horizon and the circular polarisation purity over the whole radiation hemisphere.

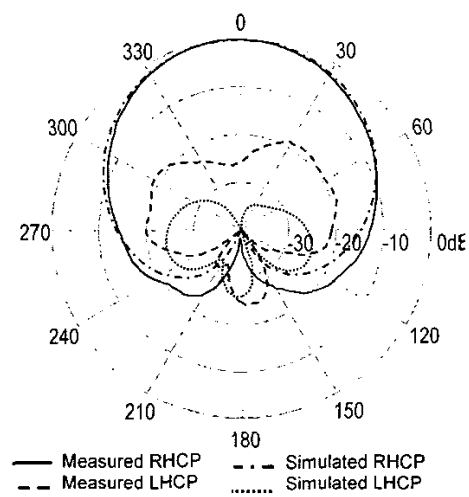

Fig. 4 - Measured and simulated radiation patterns.

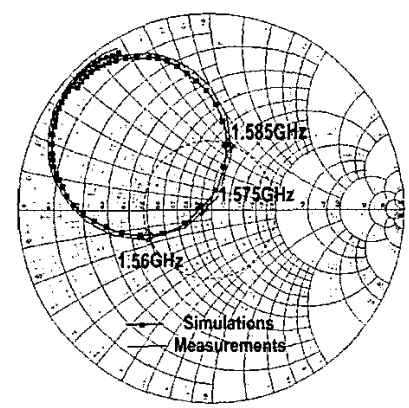

Fig. 5 - Simulated and measured input impedance.

The measured and simulated radiation patterns, reported in Fig. 4, show that the proposed SAP antenna has, as expected, an amplitude roll-off from boresight to horizon of about 15dB. It is important to note that this result, which provides a wide hemispherical coverage while sufficiently rejecting grazing signals, has been obtained using a 14 cm square ground plane so without increasing the overall dimension of the antenna. In addition to the sharpness of the radiation pattern, the SAP prototype proposed in this paper fully satisfies the polarization purity constrains required for high precision GPS applications. In fact, the axial ratio stays below 2dB within the entire coverage hemisphere.

Other geometrical configurations of SAP antennas have been proposed for high precision GPS applications. In [7] the features of the shorted annular elliptical patch antenna (SAEP) have been shown demonstrating that an effective low multipath design can be obtained using a single coaxial feed. As an extension of that design a dual band SAEP has been presented in [8]. In this latter case two shorted elliptical rings have been arranged in a stacked configuration to provide dual frequency operation.

SAP for Radio occultation applications

The implementation of the GPS network of satellites has created an opportunity for active remote sounding of the earth's atmosphere by radio occultation. In radio occultation, the ray path of a radio signal emitted by one satellite and received at another satellite in low orbit (LEO) passes through the atmosphere when the LEO satellite sets behind the Earth. The signals are delayed as they travel through the atmosphere because the refractivity varies as a function of pressure, temperature, and water vapour pressure. These delays in the GPS signals are measured in order to extract atmospheric properties through an inversion process.

Active remote sounding of the earth's atmosphere by radio occultation require high performances and different modes of operation, thus the development of suitable instruments is needed. In particular, the antennas for a radio occultation measurement require shaped beams to maximize the gain along the curved limb of the earth.

Typically, the antenna the beam in the elevation and azimuth plane must be localized between $-27.8° < \theta < -10$ and $-53° < \phi < 53°$ for both the GPS frequencies. To fulfil the radio occultation radiation requirements a number of stacked shorted annular patch antennas can be used to form a linear array. In this configuration the radiation pattern flexibility of the shorted annular patch antennas can be highly beneficial in reducing the overall dimension of the array. In fact, the azimuthal radiation pattern constraints can be enforced by opportunely selecting the outer radii of the SAP elements while the elevation shaping is controlled by the array factor. Once again, the flexible radiation properties of the SAP antenna allows for a space and complexity reduction with respect to other microstrip geometries.

4. CONCLUSIONS

The Shorted Annular Patch antenna is an innovative radiator. In addition to the features of the microstrip technology, the shorted ring has increased radiation flexibility and mechanical properties more suitable to aerospace applications.

REFERENCES

[1] G. Di Massa, G. Mazzarella, *"Shorted Annular Patch Antenna"*, MOTL, Vol.8 March 1995

[2] D. R. Jackson, J. T. Williams, Arun K. Bhattacharyya, Richard L. Smith, Stephen J. Buchheit & S. A. Long, *"Microstrip Patch Designs that do not excite Surface Waves"*, IEEE Trans. On AP, Vol. 41 No.8 Aug 1993

[3] M. Khayat, D. R. Jackson, J. T. Williams, *"Mutual Coupling Between Reduced Surface-Wave Microstrip Antennas"*, IEEE Trans. On AP, Vol. 48, No. 10, Oct 2000

[4] G. Amendola, L. Boccia, G. Di Massa, *"Surface Wave Radiation from a Shorted Elliptical Patch Antenna"* - IEEE AP-S, Volume: 2 , 2003

[5] A. M. Dinius - *"GPS antenna multipath rejection performance"*, Lincoln Laboratory Report, Aug 1995

[6] L. Boccia, G. Amendola, G. Di Massa, L. Giulicchi – *"Shorted Annular patch antennas for multipath rejection in GPS-based attitude determination"*, MOTL, January 2001.

[7] L. Boccia, G. Amendola, G. Di Massa – *"A shorted elliptical patch antenna for GPS applications"* – to be published on IEEE Antennas and Wireless Propagation Letters

[8] L. Boccia; G. Amendola; G. Di Massa – *"A high-performance dual frequency microstrip antenna for global positioning system"*- APS, 2001 IEEE International Symposium , Volume: 4 , 2001

[9] HFSS v8 – Ansoft Corporation

Performance evaluation of shorted annular patch antennas for high-precision GPS systems

L. Boccia, G. Amendola and G. Di Massa

Abstract: Even with the advances in signal processing, multipath error remains the major error source of high-precision global positioning system (GPS) applications. One of the most valid means to improve the accuracy of these systems is an appropriate design of the receiving antenna. Unfortunately, in many cases, the low-multipath-radiation requirements are very difficult to satisfy especially when physical constraints have also to be considered. As a possible solution, a study on the multipath rejection performances of shorted annular patch (SAP) antennas is presented here. In the first part, the SAP radiation characteristics will be deeply analysed by designing and testing three different antennas. Then, the results of a comparative test conducted on a GPS facility will be used to assess the on-field performances of the three prototypes. This experimental validation will show that a significant improvement of the SAP performances can be achieved when the reduced surface wave criterion, which has been widely adopted as a design rule in previous works, is relaxed and a trade-off between all the low-multipath-radiation requirements is considered. Moreover, comparison with two commercial GPS antennas will reveal that SAPs can be a very attractive and useful solution in high-precision GPS systems where severe physical constraints are imposed.

1 Introduction

High-precision measurements of the global positioning system (GPS) carrier phase have been used in a wide variety of applications ranging from differential GPS to worldwide geodetic networks and aircraft control landing. More recently, GPS-based attitude-determination techniques have been developed and demonstrated for both aircraft [1] and satellite applications [2]. The key observable quantity in each of these systems is a differential measurement across two antennas of the phase of the GPS signal transmitted by a satellite. Most of the errors in these measurements, such as atmospheric delays or orbital and clock inaccuracies, are spatially correlated and are generally cancelled through the differencing process. The major limitation that reduces the accuracy of these systems is because of the multipath reflections of the GPS signal from surfaces around the antenna. When the length of a reflection path exceeds that of the direct path by more than 10–20 m, the multipath errors can then be reduced by signal processing techniques at the receiver [3, 4]. Unfortunately, in the most common case [5], the strongest reflected signal component has an excess path length of less than 10 m which makes the receiver unable to detect and remove the multipath contamination.

More effectively, the accuracy of a high-precision GPS system can be increased using an antenna capable of rejecting multipath interferences.

At the antenna level, a first distinction between direct and reflected signals can be made through polarisation discrimination. In fact, it should be noticed that the GPS signal is transmitted as a right-hand circularly polarised (RHCP) wave whose ellipticity does not exceed 1.13 dB [6]. Hence, the left-hand circularly polarised (LHCP) components of the signal are mainly because of a polarisation reversal caused by a first-order multipath reflection and they can be rejected using a receiving antenna with high co-polar (RHCP) to cross-polar (LHCP) ratio over an extended angular range.

Although GPS system operation imposes a broad hemispherical coverage to receive signals from all visible satellites, for high-precision differential carrier phase measurements, the coverage region must be reduced to avoid severe multipath effects. In fact, signals coming from low elevation angles are more likely to be reflections and their amplitude can be mitigated shaping the radiation pattern of the receiving antenna to have low gain near the horizon. Additionally, within the coverage area the antenna should ideally provide a uniform phase response so that the carrier phase measurements can be made, as much as possible, immune to the antenna–satellite orientation.

The uniformity of the phase response and the polarisation purity of the antenna-radiated field are difficult to realise when the constraint of sharp slope near the horizon is added. Attempts to simultaneously meet these requirements have been made in several ways and various types of GPS antenna designs have been proposed. This includes spiral (or helix) antennas [7], patch elements placed on choke rings [8, 9] or stealth [10] ground planes and several array configurations [11, 12].

Even if these solutions can be designed to reduce the multipath error, they result in large and heavy structures that are not well suited for aerospace applications. An innovative class of compact high-precision GPS antennas has been introduced in [13] where a shorted annular patch (SAP) [14–16] element has been demonstrated to significantly

doi:10.1049/iet-map:20060025

Paper first received 10th February and in revised form 25th July 2006

The authors are with the Dipartimento di Elettronica, Informatica e Sistemistica, University of Calabria, Via Bucci, 42-C8, Rende 87036, Italy

E-mail: boccia@deis.unical.it

reduce the multipath interferences of GPS-based attitude-determination sensors. In general, SAP antennas satisfy the low-multipath-radiation requirements as their beam can be easily narrowed by opportunely choosing the inner and outer radii of the patch. However, in spite of this extended radiation pattern flexibility, all the low-multipath SAP designs available in literature [13, 17–20] are based on the reduced surface wave (RSW) principle introduced in [21]. Following this criterion, the surface wave emissions of an SAP antenna at a given frequency can be inhibited when the external radius of the shorted ring is fixed to a critical value. Even if this vinculum results in an optimal radiation efficiency, it does not allow any further control on the antenna beam width.

The contribution of this paper is 2-fold. In the first part of the paper, an in-depth analysis of the SAP radiation characteristics is presented. This assessment was performed by relaxing the RSW vinculum and designing three shorted rings with different external radii to obtain different radiation patterns. The performances of these three prototypes were then evaluated in terms of radiation diagrams, phase centre variations and polarisation purity over all the hemispherical coverage. This comparative analysis will reveal that the multipath rejection performance evaluation uniquely based on the radiation pattern characteristics may be ambiguous. As a solution, in the second part of the paper, this ambiguity will be resolved by providing a valid means to improve the SAP's immunity to multipath signals. From the results of a comparative test campaign conducted on an on-ground GPS test facility, it will be shown that an optimal GPS antenna design can be obtained when the reduced surface wave criterion, which has been widely adopted as a design rule for all GPS shorted patch antennas presented in the past, is relaxed and when a trade-off between the beam aperture, phase response uniformity and polarisation purity is considered. Experimental results will finally demonstrate that, under this condition, the SAP immunity to multipath signals can be significantly improved with respect to previous designs, leading to performances considerably higher than the ones obtained with conventional patches. As a consequence, SAP antennas may prove very useful in those high-precision GPS applications where restrictive physical constraints are imposed, such as in the case of aerospace systems.

2 SAP design

The SAP antenna geometry is shown in Fig. 1. An annular patch with external and internal radii a and b, respectively, is printed onto a dielectric grounded slab having relative dielectric constant ε_r and height h. Contrary to conventional annular patches, the SAP inner border is shorted to the ground plane, thus making the dominant cavity mode a TM_{11} field variation [16]. The SAP radiation pattern is therefore similar to that of the circular disk. However, once the dielectric characteristics and the operating frequency are fixed, the disk radius is uniquely determined and its radiation pattern cannot be modified. Conversely, the radiation characteristics of the shorted ring can be easily controlled varying the antenna geometry so that larger patches have higher amplitude roll-off near the horizon. Thanks to this feature, SAP antennas can be in fact optimised for high-precision GPS applications choosing the outer radius to minimise the multipath interference and adjusting the inner radius to make the patch resonate at the desired frequency.

In what follows, the design of three different SAP antennas operating in the GPS L1 band (L1: 1.57542 GHz) and

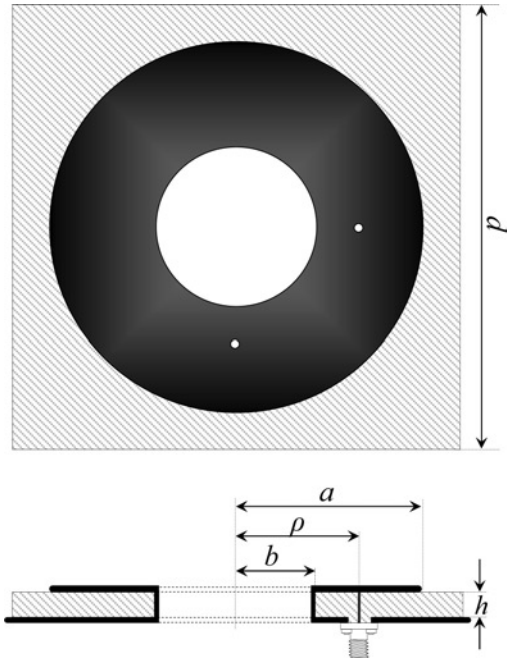

Fig. 1 *SAP geometry: top view and lateral view*

printed onto an Arlon® Diclad527 substrate having dielectric constant $\varepsilon_r = 2.55$, thickness $h = 3.2$ mm and loss tangent 0.0022 is presented. The first SAP radiator, referred to as SAP-G, was designed following the RSW criterion reported in [21]. Accordingly, the patch outer radius was selected making use of (10) in [21]

$$a = \frac{x'_{1n}}{\beta_{TM_0}} \tag{1}$$

where x'_{1n} are the zeros of the derivative of the first-order Bessel function and β_{TM_0} the propagation constant of the TM_0 surface wave mode. This equation does not depend on the dielectric permittivity, and surface wave emissions are inhibited at the nominal L1 frequency when the ring of magnetic current flowing at the external boundary of the patch has a radius of 55.78 mm. Because of the over-cutting of the machining tool, an external radius of 55.7 mm has been measured. The outer radii of the other two shorted rings, named SAP-M and SAP-P, were taken to be 45 and 35 mm, respectively. This choice was inspired by the consideration that for SAP antennas with $a > 60$ mm, side lobes will appear [19] and that causes a deterioration of the radiation pattern. In contrast, an outer radius smaller than 35 mm would lead to radiation characteristics similar to that of a conventional disk whose external radius is about 32 mm.

The circular polarisation of each antenna was obtained adopting a dual-feed arrangement realised by two 2-mm coaxial probes located 90° apart and driven with 90° of phase difference. A first crude approximation of the patch inner radii and feed locations were determined using the cavity model presented in [16] (another implementation of the cavity model for SAP antennas has also been presented in [14, 15]). The values obtained with this model for the inner radii were 29.5, 18.4 and 5.9 mm for SAP-G, SAP-M and SAP-P antennas, respectively. Similarly, the feed locations determined using the cavity model were 35.8, 24.4 and 11.8 mm, respectively. These values have been then used as a starting point for extensive full-wave finite-element method (FEM)-based simulations [22] where the accuracy was enhanced by manually refining

Table 1: Inner and outer radii, feed positions and dielectric size

Antenna	*a*, mm	*b*, mm	*d*, mm	ρ, mm
SAP-G	55.7	30.08	140	36.5
SAP-M	45.0	18.83	150	25
SAP-P	35.0	6.0	160	12

the mesh for each element of the antenna thus obtaining very reliable results as it is shown in [23]. The geometrical parameters for all the three SAP elements are shown in Table. 1.

Prototypes of the three SAP antennas were then fabricated by machining the inner hole in the dielectric substrate and shorting the internal boundary by means of a soldered copper foil. This solution has been preferred to the other equivalent techniques [17, 18] as it exactly reproduces the simulation set-up and because it has been judged the most mechanically stable. The reflection coefficient of each patch was taken, connecting the two ports to a vectorial network analyser. Results are shown in Fig. 2 and they indicate that all the three prototypes resonate around the nominal L1 frequency with reflection coefficients below 15 dB over the entire band.

In order to keep the circular polarisation characteristics of each antenna as much as possible independent from the feed network design, each prototype was driven by means of an external quadrature hybrid (Pasternack PE2051) providing $90 \pm 0.2^\circ$ of phase difference within the GPS-L1 bandwidth and having a maximum Voltage standing wave ratio (VSWR) equal to 1.07.

3 Radiation characteristics

In a first assessment, the radiation characteristics of the three shorted rings were evaluated considering different figures of merit such as the amplitude roll-off from broadside to the horizon, the polarisation purity over all the hemispherical coverage and the phase response uniformity. All the measurements presented in this section have been taken at anechoic chamber of the University of Calabria [24] using a linearly polarised probe with a co-polar to cross-polar ratio higher than 40 dB in the broadside direction. Circular polarised patterns have been then calculated by combining the linear response of each antenna under test in two orthogonal planes. The co-ordinate system has

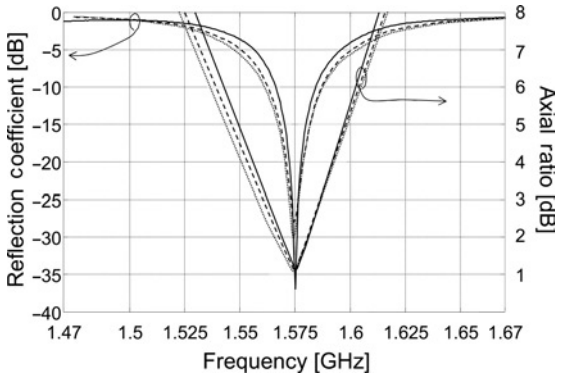

Fig. 2 *Measured reflection coefficient and axial ratio in the broadside direction for the three antenna prototypes*

Solid line: SAP-G
Dashed line: SAP-M
Dotted line: SAP-P

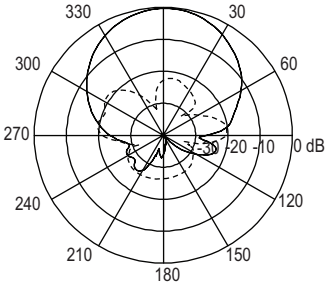

Fig. 3 *Measured radiation pattern of the SAP-G antenna in the cut plane $\Phi = 45^\circ$*

Solid line: RHCP
Dashed line: LHCP

been fixed at the centre of each antenna, at the ground plane level.

3.1 Radiation pattern

The measured co-polar (RHCP) and cross-polar (LHCP) patterns for the SAP-G antenna in the cut plane $\Phi = 45^\circ$ are shown in Fig. 3. As can be seen, for the RHCP radiation, the amplitude roll-off from broadside to horizon is around 25 dB and the antenna is circularly polarised with an on-axis RHCP to LHCP ratio around 24 dB. Both the increased directivity and the optimal radiation efficiency affect the antenna gain which is 9.85 dB on axis, a considerably higher value if compared with the one of a circular disk that is around 7 dB.

The radiation pattern of the SAP-M antenna was also measured, and the results are provided in Fig. 4. As expected, with respect to the SAP-G radiator, the SAP-M shows a reduced amplitude roll-off from broadside to the horizon that is around 20 dB. The on-axis gain is 8.97 dB, whereas the RHCP to LHCP isolation is 23 dB. Coherently, the SAP-P antenna provides a more uniform hemispherical coverage with a gain at the horizon 15 dB lower than the one on axis (Fig. 5). In the broadside direction, the gain and the RHCP to LHCP ratio are 8.06 and 26 dB, respectively.

It should be noticed that the amplitude response of the three prototypes is not uniform. However, this amplitude inhomogeneity is not so critical for a GPS system [7] as the only requirement is to have a signal level sufficient for all the coverage angles so that the receiver electronics can maintain lock with adequate signal-to-noise ratio.

The polarisation degradation against frequency has been estimated by evaluating the axial ratio (AR) bandwidth of the three prototypes. The measured results are reported in

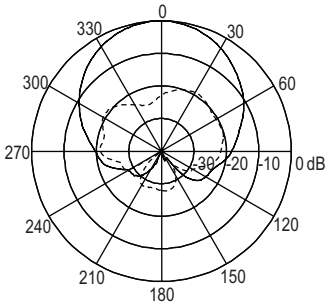

Fig. 4 *Measured radiation pattern of the SAP-M antenna in the cut plane $\Phi = 45^\circ$*

Solid line: RHCP
Dashed line: LHCP

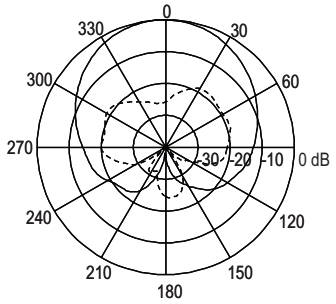

Fig. 5 *Measured radiation pattern of the SAP-P antenna in the cut plane $\Phi = 45^\circ$:*
Solid line: RHCP
Dashed line: LHCP

Fig. 2 and they show that for all the patches the polarisation purity in the broadside direction is very satisfactory for a wide range of frequencies. This is mainly because of the fact that the external hybrid which has been used to polarise each antenna provides 90° of phase difference in the range 1–2 GHz.

3.2 Phase centre

The phase response uniformity was estimated by considering the phase centre variations against the observation angle. For each prototype, the phase centre location was determined by positioning the antenna to be coaxial with the positioner axes of rotation, and the RHCP phase measurements were conducted following the procedures and algorithms proposed in [25]. The horizontal and vertical phase centre offsets with respect to the mechanical centres in the cut planes $\Phi = 0^\circ$, 45°, 90° and 135° are shown in Figs. 6–8, respectively. As can be seen, for all the antennas, both the horizontal and vertical phase centre locations diverge when the observation angle is taken near the horizon. However, a fair evaluation can be obtained taking into account only the variations achieved for observation angles comprised between $\pm 80^\circ$. Under this condition, the maxima of the horizontal and vertical phase offsets calculated for the three prototypes are reported in Table 2.

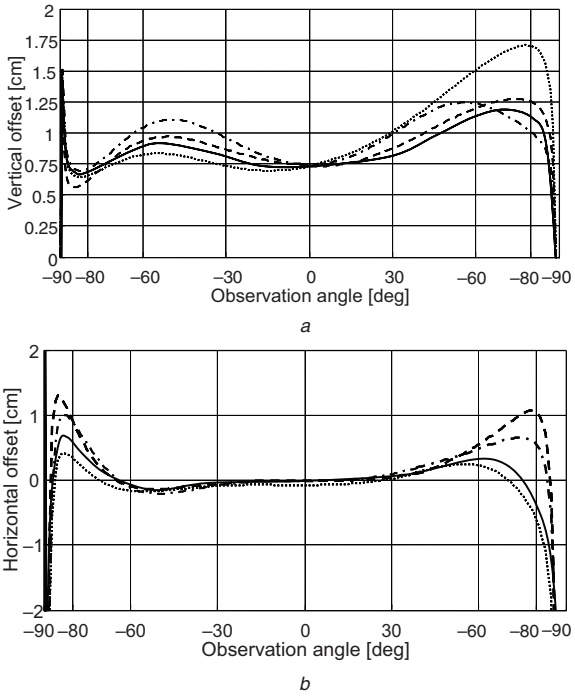

Fig. 7 *SAP-M phase centre variations against observation angle θ with respect to the mechanical centre of the antenna*
a Vertical offset
b Horizontal offset
— $\Phi = 0^\circ$; – – – $\Phi = 45^\circ$; – · – $\Phi = 90^\circ$; ··· $\Phi = 135^\circ$

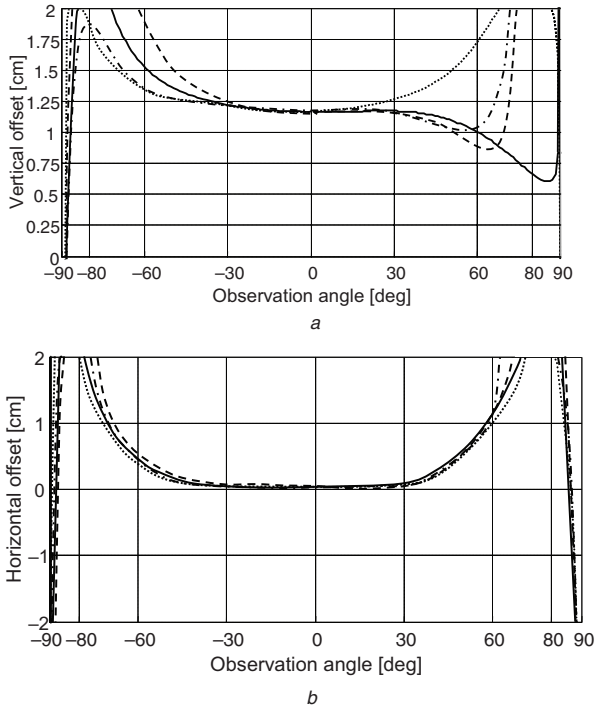

Fig. 6 *SAP-G phase centre variations against observation angle θ with respect to the mechanical centre of the antenna*
a Vertical offset
b Horizontal offset
— $\Phi = 0^\circ$; – – – $\Phi = 45^\circ$; – · – $\Phi = 90^\circ$; ··· $\Phi = 135^\circ$

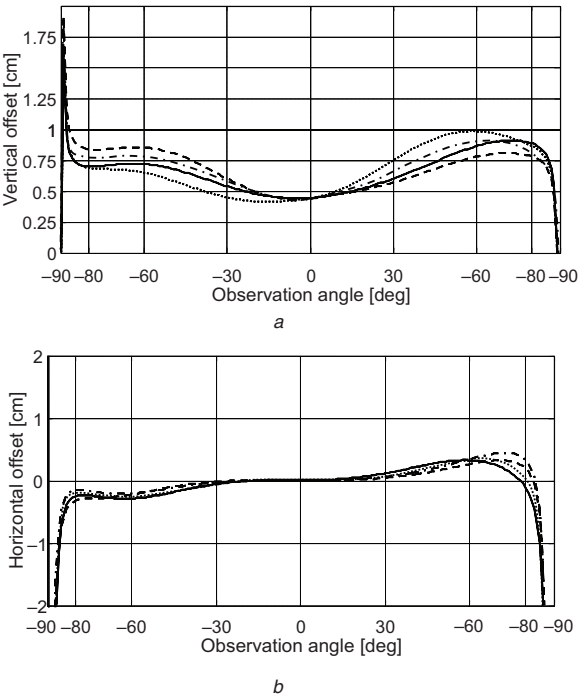

Fig. 8 *SAP-P phase centre variations against observation angle θ with respect to the mechanical centre of the antenna*
a Vertical offset
b Horizontal offset
— $\Phi = 0^\circ$; – – – $\Phi = 45^\circ$; – · – $\Phi = 90^\circ$; ··· $\Phi = 135^\circ$

Table 2: Maximum horizontal and vertical phase centre variations for the SAP-G, -M, and –P

Antenna	Vertical, cm	Horizontal, cm
SAP-G	±2.24	±2.53
SAP-M	±0.543	±0.812
SAP-P	±0.29	±0.40

These results indicate that the larger the antenna radius, the more distributed is the phase centre. However, this effect is not exclusively related to shorted rings as a similar behaviour can be observed in many other antennas such as horns [26] or helixes [7]. In fact, the pattern cut-off near the horizon in creases in antennas with a wide radiating surface. This is because of a process of phase interference which in turn deteriorates the antenna phase front and polarisation [7].

3.3 Polarisation purity

The circular polarisation purity of each antenna was assessed by evaluating also the axial ratio within all the hemispherical coverage. Sufficient discrimination between RHCP and LHCP signals for proper GPS operation is obtained when the AR stays below 3 dB for a wide angular range. Results for the three SAP prototypes are shown in Fig. 9. It can be observed that the SAP polarisation purity declines near the horizon. Furthermore, for the same rationale outlined in the previous section, this deterioration in-creases as the outer radius increases. In particular, the SAP-G radiator is well polarised only for angles comprised between -60° and 60°, whereas the AR of the SAP-P antenna stays below 2 dB within all the hemispherical coverage.

4 On-field assessment

The results presented in the previous section indicate that the axial ratio and the phase stability of SAPs deteriorate as the external radius increases. Thus, although larger SAP antennas have higher amplitude roll-off near the horizon and therefore better immunity to grazing signals, they lack in terms of phase uniformity and polarisation purity. As has been noticed before, this consideration is not limited to shorted rings, but it can be extended to many other radiators. In fact, it is very difficult to have a single GPS antenna that simultaneously satisfies all the high-precision radiation requirements, especially when physical constraints such as limited size are also considered. As a consequence, the performance evaluation uniquely based on the radiation characteristics can be ambiguous

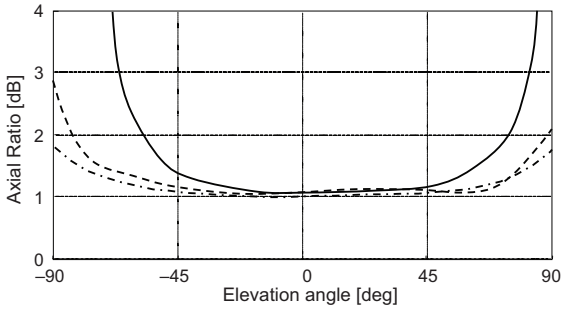

Fig. 9 *Measured axial ratio at $\Phi = 45^\circ$ of the SAP-G, M and -P antenna against elevation angles*

—: SAP-G; – – –: SAP-M; – · –: SAP-P

and an experimental on-field assessment is necessary to find the optimal design.

To clearly identify the SAP design with best immunity to the multipath error, a comparative test campaign was conducted at the GEO-GPS facility, an on-ground GPS test range of the National Research Centre (Centro Nazionale delle Ricerche, CNR) in Rende (Cs), Italy. This facility, normally used to test DGPS-based geodetic systems, consists of two identical GPS receivers with 10 Hz reporting capability connected to a workstation. Each receiver is paired with a 30 dB amplifier and with an antenna mounted atop a rigid support and aligned with True North. The system is fixed on the rooftop of a 15-m tall building located in a dense urban zone and with an unobstructed view for elevations above 7°. The basic measurable quantity of this differential GPS configuration is the baseline separation between the two antennas which essentially depends upon the differential path delay of the received GPS signal. Therefore this kind of measurement provides a valid means to assess the performances of a GPS antenna, as it is the major error source owing to multipath interferences. In fact, other inaccuracies such as differential line bias can be easily cancelled correcting the baseline reference vector through a calibration process. However, it should be noticed that the test set-up used in these experiments is not intended to be representative of the best multipath performances attainable with the antennas under test. Indeed, a precise assessment would be strongly influenced by the configuration of the environment surrounding the receiving antennas and by the baseline distance. As a consequence, a fair evaluation can be only inferred on the basis of a comparative test campaign.

The low-multipath performances of the three SAP antennas were evaluated by fabricating pairs of identical prototypes and performing 24-h tests to collect differential baseline displacements. This experiment duration is optimal because it evens out daily temperature oscillations and is equal to the repeatability period of the GPS constellation as seen from the ground. Thanks to the high gain of the SAP antennas and to the amplifier present in the receiving chain, it was possible to lock the GPS signals coming from all the satellites with elevations above 10°. Furthermore, to provide an additional reference for the evaluation of the SAP performances, two pairs of commercial GPS antennas were also tested in the same facility, namely a single feed patch (Ma-Com 1141 [27]) and a dual-band multi-feed GPS antenna (AT2775-42AW from AeroAntenna Technology, Inc. [28]). These radiators are referred to as Ref-1 and Ref-2, respectively. The Ref-2 element is a high-precision antenna [29] specifically designed for GPS-based geodetic applications and it was tested in the GEO-GPS facility with a ground plane extension having 20 cm of external radius. Both the Ref-1 and the Ref-2 antennas having an internal amplifier, it was possible to test these two radiators without any additional amplifiers.

For each antenna under test, the measured data were statistically evaluated considering the root mean square (RMS) of the differential baseline displacement, whereas the nominal baseline length was 5 m in all the experiments. For uniformity, the data collected from satellites with elevation lower than 10° were filtered out in all the test cases and the Ref-2 data for the L2 band were discarded. The experimental results are presented in Table 3, showing that the three SAP elements have very different performances. As expected, the accuracy achieved with all the shorted rings is better than the one of the Ref-1 patch. In particular, the minimum baseline displacement is

Table 3: Experimental results, RMS of the differential baseline displacement

Antenna under test	RMS calculated with a mask on satellites having elevation lower than 10° on the horizon, mm	RMS calculated with a mask on satellites having elevation lower than 30° on the horizon, mm
Ref-1	2.021	1.988
SAP-G	1.697	1.163
SAP-P	1.215	1.157
Ref-2	0.979	0.890
SAP-M	0.759	0.684

obtained with the SAP-M antenna whose RMS is 0.759 mm, whereas the SAP-G and SAP-P errors are 1.697 and 1.215 mm, respectively. Hence, the SAP-M performances are 55% better than the ones of the SAP-G antenna and this result might be even optimised designing and testing other SAP prototypes and using a multi-feed arrangement. However, this is beyond the scope of this work which shows that the SAP accuracy can be significantly improved when the RSW criterion is abandoned and a trade-off between all the antenna radiation parameters is considered. As an additional achievement, it should be noticed that under this condition, the SAP performances are competitive even when compared with other high-accuracy GPS antennas such as the Ref-2 antenna whose measured error is 0.979 mm.

As a further result, in Table 3 are also presented the differential baseline displacement obtained filtering out the data collected from satellites having elevation lower than 30°. Owing to the fact that the antenna polarisation performances degrade near the horizon and that signals impinging at the antenna from low elevation angles are significantly corrupted by multipath reflections, an improvement of the system accuracy can be observed in all the five antennas under test. Even if this result is useless for many high-precision GPS applications being the hemispherical coverage limited to only 120°, it is interesting to note that the performance improvement is not uniform for all the antennas. The most significant improvement can be, in fact, observed in the test of the SAP-G radiator which is the antenna most affected by a degradation of the axial ratio at low elevation angles (see Fig. 9).

5 Conclusions

A study on the multipath rejection capability of SAP antennas has been presented. With the intent to fully explore the SAP potential in high-precision GPS applications, three prototypes were designed to have different radiation characteristics. In a first assessment, the behaviour of these three patches was evaluated in terms of radiation pattern, phase centre variations and polarization purity over all the hemispherical coverage. Results showed that the identification of the best SAP design may be ambiguous even when such an in-depth analysis of the radiation characteristics is conducted. In fact, the amplitude roll-off near the horizon and the uniformity of the phase response and polarisation purity have been demonstrated to be mutually exclusive requirements. Hence, to solve this ambiguity, an experimental analysis was conducted by comparing the on-field performances of the three shorted rings antennas with two commercial GPS antennas. The experiments showed that the SAP accuracy can be significantly improved when a trade-off between all the low-multipath-radiation requirements is considered and the reduced surface wave criterion, which has been widely adopted in the past, is abandoned.

In conclusion, shorted rings revealed performances comparable to other high-precision GPS radiators with some additional peculiarities. First, SAPs are planar light-weight elements and they do not require any ground plane extension, thus keeping the overall antenna dimension very small. Furthermore, the fabrication costs are similar to that of conventional microstrip antennas as the inner short can be realised using a set of vias as shown in [17, 18]. Moreover, shorted patches are well suited for aerospace applications. In fact, the central short provides a natural path for electrostatic discharges and it can even be used as a supporting element to develop SAPs in suspended technology.

6 Acknowledgments

The authors thank Ing. Salvatore Gabriele and all the personnel of the GEO-GPS facility, the on-ground GPS test range of the National Research Centre (Centro Nazionale delle Ricerche, CNR) in Rende (Cs), Italy. The authors are also grateful to Steven Best for providing the program needed to calculate antennas phase centre. This work was partly supported by the European Space Agency under contract 14358/00/NL/FM.

7 References

1 Choen, C.E.: 'Attitude determination using GPS'. PhD thesis, Stanford University, 1992
2 Stein, B.A., and Sang, T.: 'Satellite attitude determination using GPS'. IEEE Position Location and Navigation Symp., 1992
3 Weill, L.R.: 'Conquering multipath: the GPS accuracy battle', *GPS World*, 1997, **8**, (4), pp. 59–66
4 Braasch, M.: 'Autocorrelation sidelobe considerations in the characterization of multipath errors', *IEEE Trans. Aerosp. Electron. Syst.*, 1997, **33**, pp. 290–295
5 Ray, J.K., and Cannon, M.E.: 'Characterization of GPS carrier phase multipath'. Proc. ION National Technical Meeting, San Diego, January 1999, pp. 243–252
6 Kaplan, E.D.: 'Understanding GPS: principles and applications' (Artech House, 1996)
7 Tranquilla, J.M., and Best, S.R.: 'A study of quadrifilar helix antenna for global positioning system applications', *IEEE Trans. Antennas Propag.*, 1990, **38**, (10), pp. 1545–1550
8 Dinius, A.M.: 'GPS antenna multipath rejection performance'. Lincoln Laboratory Technical Report, August 1995
9 Tranquilla, J.M., Cam, J.P., and Al-Rizzo, H.M.: 'Analysis of a choke ring ground plane for multipath control in global positioning system (GPS) applications', *IEEE Trans. Antennas Propag.*, 1994, **42**, (7), pp. 905–911
10 http://www.trimble.com
11 Padros, N., Ortigosa, I., Baker, J., Iskander, F., and Thornberg, B.: 'Comparative studies of high-performance GPS receiving antenna designs', *IEEE Trans. Antennas Propag.*, 1997, **45**, (4), pp. 698–706

12 Counselman, C.C., III: 'Multipath-rejecting GPS antennas', *Proc. IEEE*, 1999, **87**, (1), pp. 86–91
13 Boccia, L., Amendola, G., Di Massa, G., and Giulicchi, L.: 'Shorted annular patch antennas for multipath rejection in GPS-based attitude determination', *Microw. Opt. Technol. Lett.*, 2001, **28**
14 Lin, Y., and Shafai, L.: 'Properties of centrally shorted circular patch microstrip antennas'. IEEE AP-S, Syracuse, 1988, pp. 700–703
15 Lin, Y., and Shafai, L.: 'Characteristics of concentrically shorted circular patch microstrip antennas', *IEE Proc.*, 1990, **137**, (1), pp. 18–24
16 Di Massa, G., and Mazzarella, G.: 'Shorted annular patch antenna', *Microw. Opt. Technol. Lett.*, 1995, **8**, pp. 222–226
17 Basilio, L.I., Williams, J.T., and Jackson, D.R.: 'A reduced-surface-wave GPS antenna with low susceptibility to multipath interference'. AP Symp., 2002
18 Basilio, L.I., Williams, J.T., Jackson, D.R., and Khayat, M.A.: 'A comparative study of a new GPS reduced-surface-wave antenna', *Antennas Wireless Propag. Lett.*, 2005, **4**, pp. 233–236
19 Boccia, L., Amendola, G., and Di Massa, G.: 'A shorted elliptical patch antenna for GPS applications', *IEEE Antennas Wirel. Propag. Lett.*, 2003, **2**, pp. 6–8
20 Boccia, G., Amendola, G., and Di Massa, G.: 'A dual frequency microstrip patch antenna for high-precision GPS applications', *IEEE Antennas Wirel. Propag. Lett.*, 2004, **3**, pp. 157–160
21 Jackson, D.R., Williams, J.T., Bhattacharyya, A.K., Smith, R.L., Buchheit, S.J., and Long, S.A.: 'Microstrip patch designs that do not excite surface waves', *IEEE Trans. Antennas Propag.*, 1993, **41**, (8), pp. 1026–1037
22 Ansoft HFSS
23 Boccia, L., Amendola, G., and Di Massa, G.: 'Design a high-precision antenna for GPS', *Microw. RF*, 2003, **1**, pp. 91–93
24 Antenna Measurement Services of the Antenna Centre of Excellence (ACE), available online at: http://ace.deis.unical.it
25 Best, S., and Tranquilla, J.M.: 'A numerical technique to determine antenna phase centre location from computed or measured phase data', *ACES J.*, 1995, **10**, (2), pp. 46–62
26 Schrank, H., and Hakkak, M.: 'Antenna designer's notebook – design of pyramidal horns for fixed phase center as well as optimum gain', *IEEE Antennas Propag. Mag.*, 1991, **33**, (3), p. 53–55
27 http://www.macom.com/
28 http://www.aeroantenna.com/
29 http://www.ngs.noaa.gov/

THE SHORTED ANNULAR PATCH AS A MULTI-PATH SUPPRESSING ANTENNA

G.J.K. Moernaut*, G.A.E Vandenbosch †

*Orban Microwave Products, Belgium, Gerald.Moernaut@orbanmicrowave.com
†KULeuven, Belgium, Guy.Vandenbosch@esat.kuleuven.be

Keywords: patch antenna, reduced surface wave, multi-path suppression, GNSS

Abstract

This paper presents an overview of the multi-path phenomena and the performance of the **S**horted **A**nnular **P**atch (SAP) in suppressing unwanted multi-path signals caused by ground reflections. It is shown that the SAP's previously derived multi-path suppressing optimum is in fact sub-optimal. An improved design rule based on the **M**ulti-**P**ath **R**atio (MPR) is proposed.

1 Introduction

This paper discusses the multi-path caused by ground reflections and quantifies the antenna susceptibility to this multi-path, namely the **M**ulti-**P**ath **R**atio (MPR). The basic topology of the **S**horted **A**nnular **P**atch (SAP) is briefly outlined. The original multi-path suppression optimum is given. The performance of the SAP antenna is studied making use of the MPR definition. An improved multi-path suppression optimum is defined based on the MPR definition. A theoretical link between the old and new multi-path suppression optimum is established.

2 The multi-path problem in GNSS

Multi-path is a prime source of navigation errors in GNSS-based navigation systems. Multi-path errors arise from interference between the received direct and reflected signals in the receiver. Multi-path mitigation algorithms have been developed and are embedded within the digital part of most high-end receivers. Since it is not possible to provide any multi-path suppression in the RF part of the receiver, the antenna remains the only possibility to provide additional multi-path suppression. Multi-path signals arrive mainly at low elevations, due to vertical obstacle reflections, and from the bottom, due to ground reflections. The antenna's susceptibility to multi-path signals is mainly due to its radiation properties at low elevations. This low elevation radiation can largely be subscribed to surface wave propagation on the ground plane. These surface waves are scattered at the ground plane edge, giving rise to unwanted radiation towards the back of the antenna and at low elevations. The antenna's multi-path performance is popularly quantified with the **M**ulti-**P**ath **R**atio (MPR).

The MPR for ground reflections can be straightforwardly arrived at by inspecting figure 1 depicting the multi-path problem caused by ground reflections. The desired GNSS signals are **R**ight **H**and **C**ircularly **P**olarized while the undesired ground reflected signals might be **L**eft **H**and **C**ircular **P**olarized as well as RHCP.

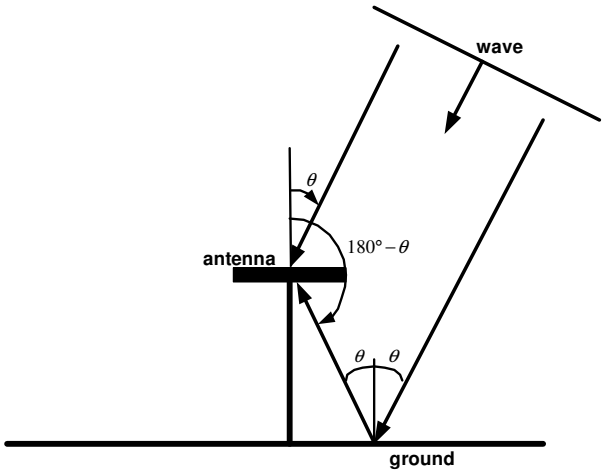

Figure 1: The multi-path problem quantified.

The multi-path susceptibility of a GNSS antenna can be quantified by the MPR defined as:

$$MPR = \frac{E_{RHCP}(\theta)}{E_{RHCP}(180° - \theta) + E_{LHCP}(180° - \theta)} \quad (1)$$

Where E_{RHCP} and E_{LHCP} are the antenna's directivity (or gain) at θ or θ's supplement angle 180°-θ.
Equation 1 clearly demonstrates the importance of two antenna characteristics, namely:

- The front-to-back ratio:
  If there is no radiation sensitivity towards the ground, the denominator becomes zero and as a result the MPR becomes infinite. Hence, the antenna has perfect multi-path performance for ground reflections.
- The axial ratio:
  The MPR formula has an RHCP to LHCP ratio embedded within, which at 0° elevation, or θ = 90° becomes an RHCP to LHCP ratio at the same 0°

elevation. This is popularly designated as the axial ratio of an antenna.

3 The shorted annular patch

The **S**horted **A**nnular **P**atch (SAP), whose topology is shown in figure 2, was originally proposed by D.R. Jackson et al. as a **R**educed **S**urface **W**ave (RSW) patch antenna [2]. This patch antenna was shown not to excite surface waves when a certain RSW condition is met. Unwanted low elevation radiation is minimized when surface wave excitation is avoided. This leads to an increased gain roll-off towards lower elevations. This increased gain roll-off is the reason the SAP was given the multi-path suppression capable status [1].

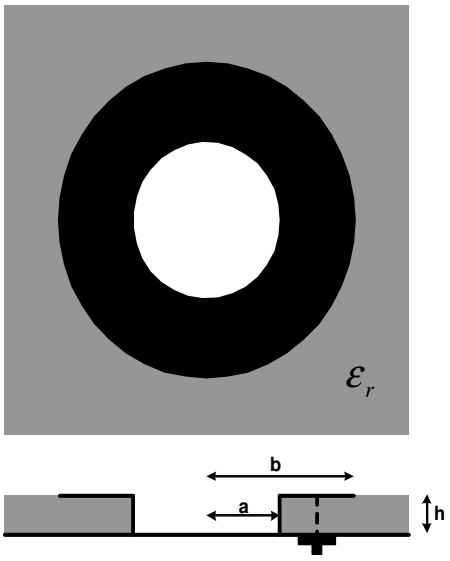

Figure 2: The SAP topology.

The resonance condition of an SAP antenna as derived using the classic cavity model and is given by [2,3]:

$$J_n'(\frac{b}{a}\mathrm{X}_{nm})Y_n(\mathrm{X}_{nm}) - J_n(\mathrm{X}_{nm})Y_n'(\frac{b}{a}\mathrm{X}_{nm}) = 0 \quad (2)$$

With,

$$f_{nm} = \frac{\mathrm{X}_{nm}c}{2\pi a\sqrt{\varepsilon_r}} \quad (3)$$

The variables in equation 2 and 3 are:

- b and a are the outer and inner radius of the SAP.
- X_{nm} is a root of equation 2 corresponding with mode n (radial) - m (axial).
- $J_n(.)$ and $Y_n(.)$ are the Bessel functions of the first and second kind of order n.
- $J'_n(.)$ and $Y'_n(.)$ are the derivates of the Bessel functions of the first and second kind of order n with respect to their argument.
- f_{nm} is the resonance frequency of the nm-mode.
- c is the velocity of light in free space.
- ε_r is the dielectric constant of the SAP's substrate.

Calculating the resonance frequency of the SAP involves solving the transcendental equation 2 for which an iterative procedure is required. Another simplified way for calculating the SAP's resonance frequency avoiding an iterative procedure has been published in [3].

The original multi-path suppression condition, which is in fact the RSW condition, is [2]:

$$J_1'(\beta_{TM_0}b) = 0 \quad (4)$$

or

$$\beta_{TM_0}b = x_{1m} = 1.8412 \quad (5)$$

The variables in equation 4 and 5 are:

- $J'_1(.)$ is the derivate of the Bessel functions of the first kind of order 1 with respect to its argument.
- β_{TM_0} is the TM_0 surface wave wave number. The TM_0 surface wave is the only surface wave present in a thin low permittivity dielectric slab [4].
- χ_{nm} is a root of equation 4 and is referred to as the RSW figure. The MPR condition remains described as in terms of RSW in order to keep the relation to its original conception.

Note that only the first solution of equation 4 is considered because this results in the smallest SAP outer radius and excites the SAP in its fundamental TM_{11} mode.
The surface wave root can be found using the procedure outlined in [4]. β_{TM_0} can be approximated by k_0, the free space wave number, for thin low permittivity dielectric slabs.

4 Shortcomings of the original multi-path suppression condition

This multi-path suppression condition is in fact a reduced surface wave condition. If the condition is met, the antenna does not excite surface waves. These surface waves give rise to radiation at low elevations and scattering at the substrate-ground plane truncation. This scattering results in backward radiation worsening the front-to-back ratio of the antenna. However, the front-to-back ratio is not the only important parameter. The axial ratio is very important as well; especially a good axial ratio at low elevations is desired. Unfortunately, blocking radiation at low elevation leads to degraded axial ratio performance since a minimum radiation is needed in order to ensure good circular polarization radiation.
In order to demonstrate the axial ratio degradation when the SAP's outer radius meets the original RSW optimum, an SAP on a RO4003 substrate from Rogers Corporation™ of 1.524 mm thickness was simulated with CST Microwave Studio™. Fringing field compensation has been applied according to the procedure in [3]. The substrate and ground plane radii were

taken 20 mm larger than the SAP's outer radius. This topology is referred to as TOPA. Figure 3 and 4 show a 2-dimenional cross section of the RHCP and LHCP radiation pattern for three RSW figures, namely 1.75 (-), 1.85 (x), which is close to 1.8412 being the original RSW optimum, and 1.95 (o).

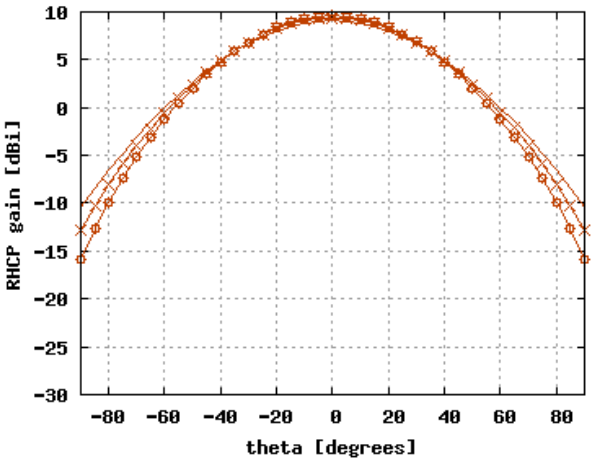

Figure 3: RHCP gain vs. theta.

The RHCP gain roll-off increases with increasing RSW figure as expected, while the LHCP gain is higher as well for increased RSW figures.

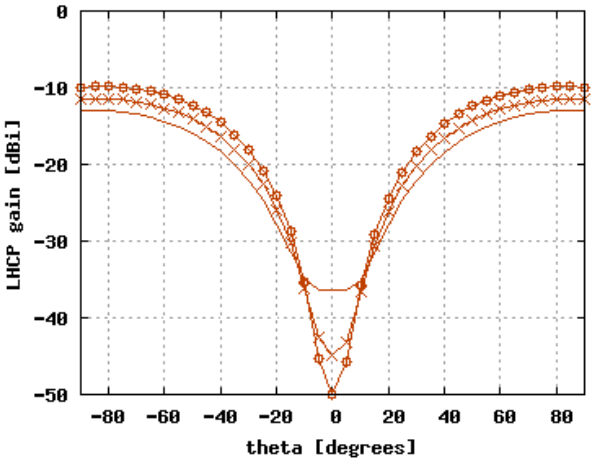

Figure 4: RHCP gain vs. theta.

Figure 5 displays the axial ratio for the same SAP implementations.

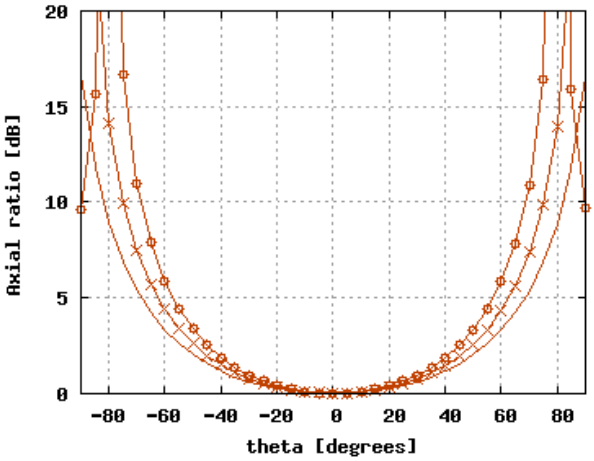

Figure 5: Axial ratio vs. theta.

Axial ratio degradation with increasing RSW figure is readily observed. Since the axial ratio has a profound influence on the multi-path performance, the MPR of the same SAP implementations is plotted in figure 6.

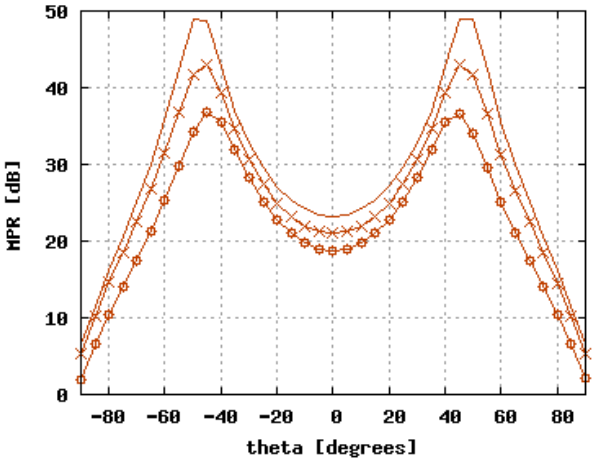

Figure 6: Multi-path ratio vs. theta.

Figure 6 clearly demonstrates the multi-path performance degradation with increasing RSW figure including the original RSW optimum. The MPR and axial ratio are seen to improve for decreasing RSW figure. However, since the radiation at low elevation increases with decreasing RSW figure. This leads to a lower gain roll-off implying a degraded front-to-back ratio, which is vital for proper multi-path performance as well. An MPR optimum RSW figure is expected from this observation.

5 Improved multi-path suppression condition

In order to find a multi-path optimum RSW figure the SAP was simulated over a wider range of RSW figures. The MPR was plotted as a function of the RSW figure for three elevations, namely 5°(-), 10°(x) and 15°(o) in figure 7. An MPR optimum around an RSW figure of 1.73 is observed.

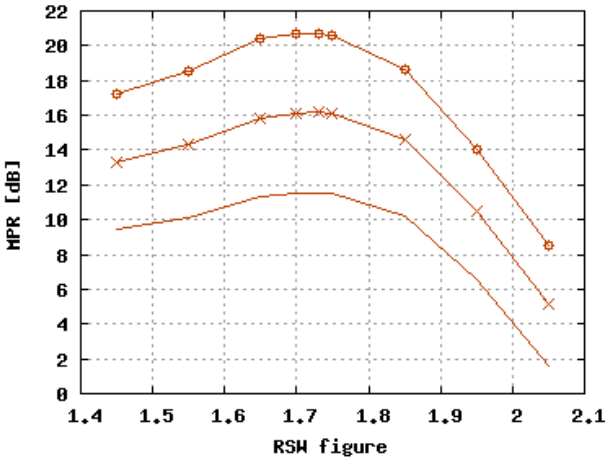

Figure 7: MPR vs. RSW figure at three elevations.

The RHCP gain and axial ratio for the same elevations are plotted as a function of the RSW figure in plots 8 and 9. These figures clearly demonstrate the common misunderstanding that a higher gain roll-off automatically yields a higher multi-path suppression, which is definitely not the case. The discussion clearly shows the axial ratio has an underestimated role in multi-path suppression.

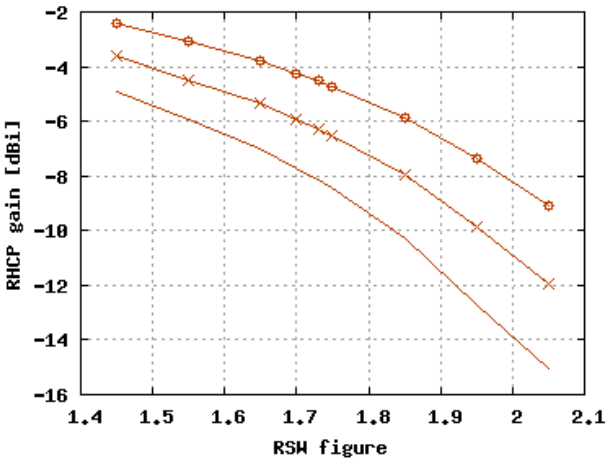

Figure 8: RHCP gain vs. RSW figure at three elevations.

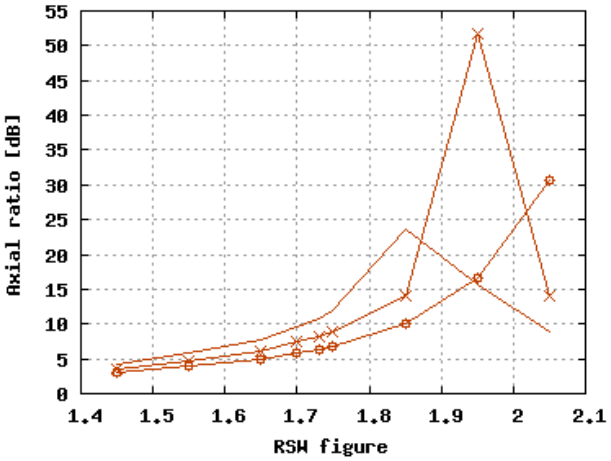

Figure 9: Axial ratio vs. RSW figure at three elevations.

A serious axial ratio degradation for larger RSW figures is observed in figure 9 accompanied with an increasing RHCP gain roll-off as seen in figure 8.

In order to verify the generality of the new MPR optimum RSW figure, the SAP was simulated on a 3.25 mm thick RO4003 substrate with 20 mm ground plane extension (TOPB), a 1.524 mm thick RO4003 substrate with 40 mm ground plane extension (TOPC) and a 1.28 mm RO3006 substrate with 20 mm ground plane extension (TOPD). The discussion is limited to the SAP's first mode only. This limits the dielectric constant to 8.4, the critical dielectric constant [2]. The MPR as a function of the RSW figure for 5°(-), 10°(x) and 15°(o) elevations is shown in figures 10 to 12.

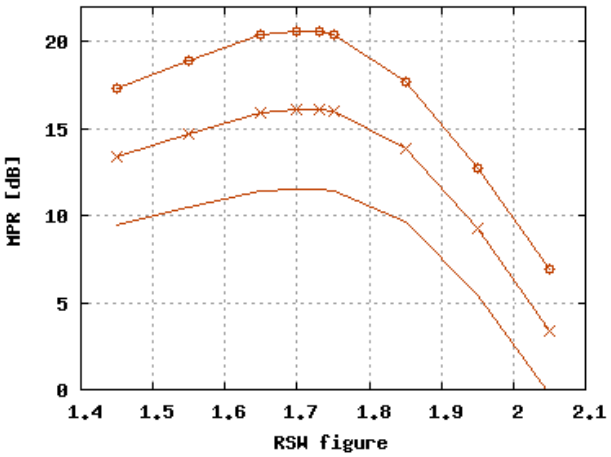

Figure 10: MPR vs. RSW figure at three elevations of TOPB.

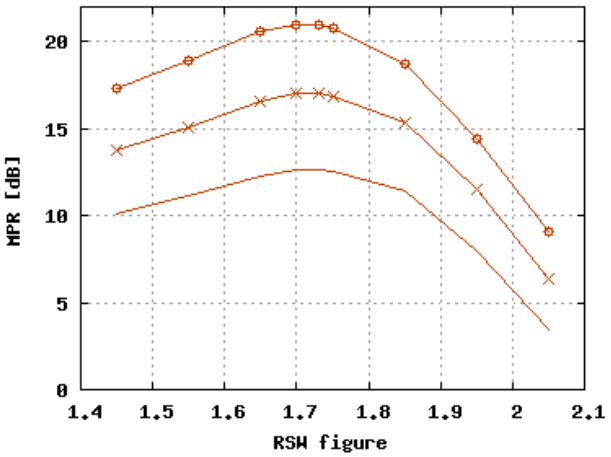

Figure 11: MPR vs. RSW figure at three elevations of TOPC.

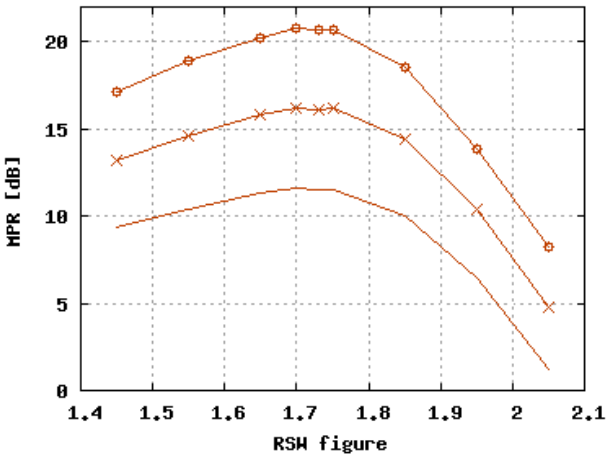

Figure 12: MPR vs. RSW figure at three elevations of TOPD.

Figure 10 to 12 clearly demonstrate the generality of the new optimum RSW figure equal to 1.73. This new optimum agrees well with the intuitively expected, namely:

- The new MPR optimum value is lower than the original one. This results in increased radiation at lower elevations needed for good circular polarization radiation.
- The new MPR optimum remains close to the original value, which minimizes gain roll-off degradation. Hence, the front-to-back ratio of the new multi-path optimum remains within the vicinity of the old multi-path optimum.

6 Link with the original RSW condition equation

The original RSW definition as given in equation 4 (-) is plotted as a function of the RSW in figure 13 and 14.

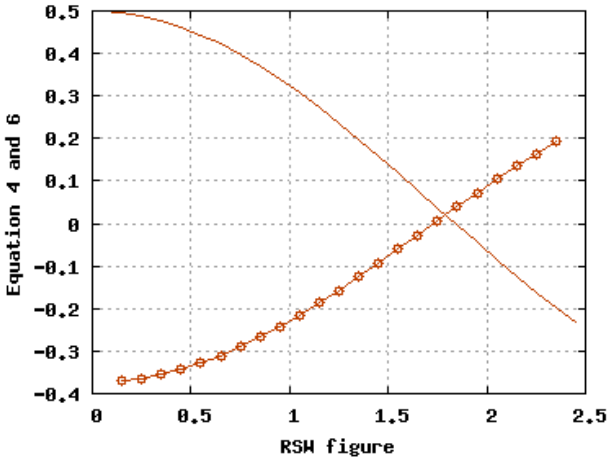

Figure 13: Equation 4 and 6 vs. RSW figure coarse.

Figure 13 is enlarged in the vicinity of both the old and the new optimum for clarity.

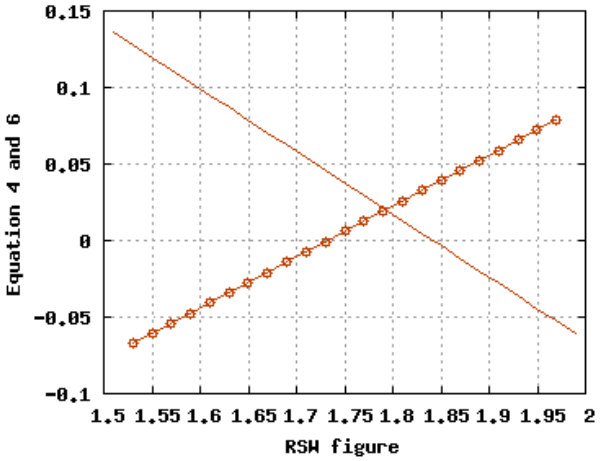

Figure 14: Equation 4 and 6 vs. RSW figure in the vicinity of both the old and the new MPR optimum.

Closely inspecting the curvature in figure 13 just below the original MPR optimum reveals that the new optimum appears to be the point where the curve has its steepest decent towards the original RSW condition. This point can be calculated by determining the second derivative of the original RSW function (equation 4), which is the same as the third derivative of the Bessel function of the first kind and order 1 with respect to its argument. The result is:

$$J_1^{(3)}(\beta_{TM_0} b) = 0 \qquad (6)$$

or

$$\beta_{TM_0} b = x_{1m}^{(3)} = 1.732 \qquad (7)$$

The original RSW definition as given in equation 6 (o) is plotted as a function of the RSW figure 13 and 14 as well. The theoretical MPR optimum RSW figure corresponds very well with the experimentally found value.

7 Conclusion

This paper showed that the original reduced surface wave based multi-path suppression optimum is sub-optimal when it comes to multi-path signals caused by ground reflections.
An improved multi-path suppression optimum was defined based on the MPR definition. A theoretical link between the old and new multi-path suppression optimum is established.

Acknowledgements

The first author would like to thank Daniël Orban, CEO and founder of **O**rban **M**icrowave **P**roducts, for the ability to pursue the PhD degree while working at OMP.

References

[1] L. Boccia, et al., "A dual frequency microstrip patch antenna for high-precision GPS applications", IEEE Antennas and Wireless Propagation Letters, Vol. 3 Is. 1, pp. 157-160, 2004
[2] D.R. Jackson, et al., "Microstrip patch designs that do not excite surface waves", IEEE Trans. Ant. & Prop., Vol. 41 Is. 8, pp. 1026-1037, 1993
[3] G.J.K. Moernaut & G.A.E. Vandenbosch, "Simple pen and paper design of shorted annular ring antenna", IEE Electronics Letters, Vol. 39 Is. 25, pp. 1784-1785, 2003
[4] D.M. Pozar, "Microwave engineering (2^{nd} edition)", Wiley

Concept Study of a Shorted Annular Patch Antenna: Design and Fabrication on a Conducting Cylinder

Gerald J. K. Moernaut, *Member, IEEE*, and Guy A. E. Vandenbosch, *Member, IEEE*

***Abstract*—This paper presents the shorted annular patch (SAP) antenna on an electrically conducting cylinder. The SAP antenna has been credited with superior multipath suppressing properties which makes it interesting for global navigation satellite system (GNSS) applications. GNSS applications demand integration of filters and low noise amplifiers as close to the radiating structure as possible. To this goal, the SAP is mounted on an electrically conducting cylinder which serves as a quality shielded housing for accompanying electronics.**

***Index Terms*—Global navigation satellite system (GNSS), Shorted annular patch (SAP) antenna.**

I. Introduction

THIS paper outlines the design of a shorted annular patch (SAP) antenna located on an electrically conducting (aluminum) cylinder. The SAP antenna has been considered very useful for global navigation satellite system (GNSS) applications [2], [3] because of its good multipath suppressing properties, excellent radiation pattern symmetry and low cost because it is a single substrate patch antenna. The SAP remains the topic of many research papers, e.g., [1], [4]–[7]. Commercial GNSS antennas always contain additional circuitry such as power dividers, low noise amplifiers and filters. It is vital that at least part of the RF circuitry is as close to the antenna radiating element as possible from a noise figure point of view. It is also desired that this electronics is electromagnetically shielded from the radiating structure. Amplification of the GNSS signals combined with parasitic radiation by the circuitry results in a feedback loop to the radiating structure. This likely results in low noise amplifier oscillations. Until now, in literature the SAP has always been described without the presence of such an electronics housing. In this paper, the aluminum cylinder is included to emulate a real life GNSS antenna as closely as possible. The SAP is being designed with maximum azimuthal symmetry in order to minimize phase center and axial ratio variation in azimuth. An important issue for GNSS antennas is the phase center (PC). It is the electrical center of the antenna. The position of the receiver is actually the position of the receiver antenna with respect to its PC and not the physical center of the antenna. The physical center of the antenna is often referred to as the antenna reference point (ARP). A stable and calibrated phase center is a must when a high degree of accuracy is required. GNSS receivers for high-end applications such as geodesy usually have azimuthally symmetric radiation patterns minimizing phase center deviation in azimuth from the geometrical center. Therefore, the SAP is mounted on an aluminum cylinder rather than, e.g., a cube. Some degree of azimuthal phase center asymmetry is always present as a result of manufacturing tolerances, feed network inaccuracies and component spreading. There still is a phase center variation with respect to elevation.

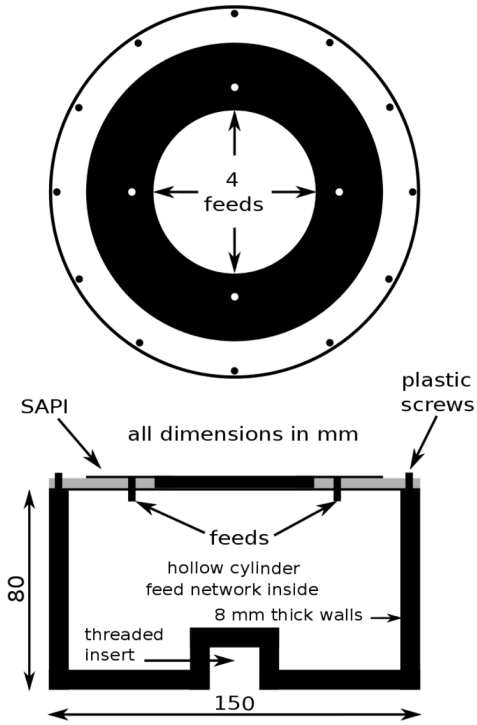

Fig. 1. The SAP on cylinder topology.

II. Topology Outline

The SAP on cylinder topology is depicted in Fig. 1. The structure consists of a SAP etched on a 3.25 mm FR4 substrate ($\varepsilon_r = 4.5$ and $\tan\delta = 0.01$). The SAP was designed according to the procedure described in [5]. The SAP's inner radius was fixed on the calculated value while the SAP's outer radius was optimized for correct resonance frequency using CST Microwave Studio [9]. This is required to compensate for fringing field edge extension. The final SAP's inner and outer radii are 34.53 and 53.8 mm, respectively. The shorting wall is made as a plated through via hole. The four 1.5 mm diameter feed probes are

Manuscript received May 24, 2010; revised October 07, 2010; accepted November 25, 2010. Date of publication April 19, 2011; date of current version June 02, 2011.

G. J. K. Moernaut is with Orban Microwave Products, Remylaan 4C, 3018 Wijgmaal, Belgium (e-mail: Gerald.Moernaut@orbanmicrowave.com).

G. A. E. Vandenbosch is with the Department of Electrical Engineering (ESAT), Division TELEMIC, KULeuven, 3001 Heverlee, Belgium (e-mail: Guy.Vandenbosch@esat.kuleuven.be).

Digital Object Identifier 10.1109/TAP.2011.2143685

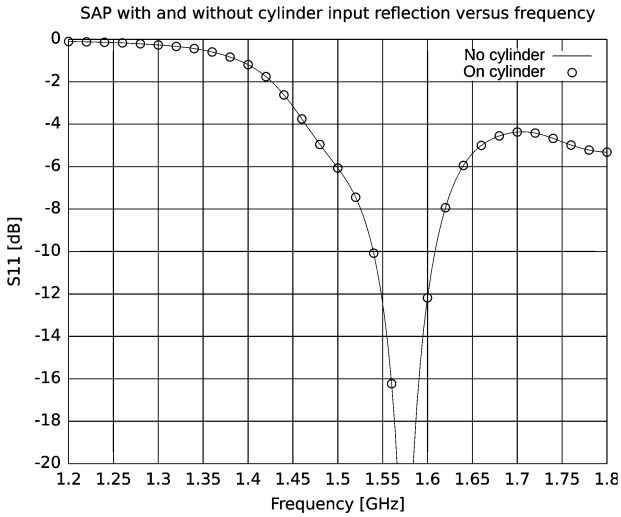

Fig. 2. SAP with and without cylinder input reflection versus frequency.

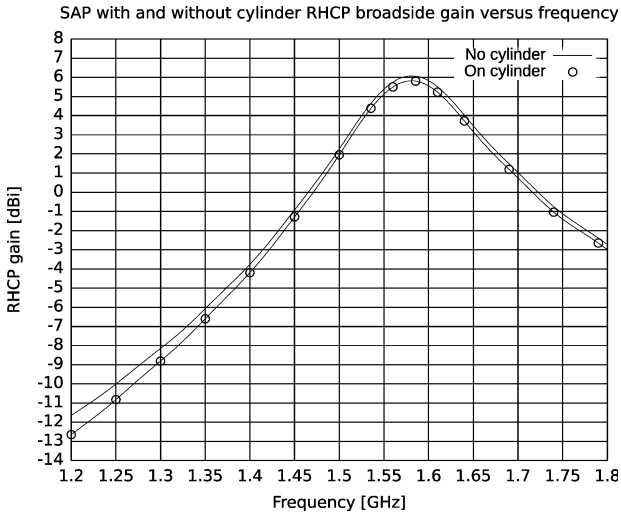

Fig. 3. SAP broadside RHCP gain versus frequency.

located at 14 mm from the shorting wall of the SAP and are 90 degree sequentially rotated. The four feed points are connected to a power divider. This power divider splits the power into 4 equal parts with a 90 degree sequential phase shift. This technique is a well-known circular polarization creation technique [8]. Although the technique works with 2 feed points, 4 symmetric feed points offer the advantage of a higher degree of azimuthal symmetry in the radiation patterns. This feature is desired since the goal is to achieve geodetic optimal performance with respect to radiation pattern symmetry. The ground plane and printed circuit board are 150 mm in diameter. The SAP is placed upon a hollow aluminum cylinder and fixed with 12 plastic (nylon) screws. Note that the nylon screws have little or no effect on the antenna behavior and therefore have been excluded from the simulation model. The hollow cylinder contains the RF circuitry; in this concept study only a feed network is present. It should be stressed that previous studies of the SAP exclude the presence of an RF housing. The cylinder is 150 mm in diameter and 80 mm high. Note that the cylinder diameter is

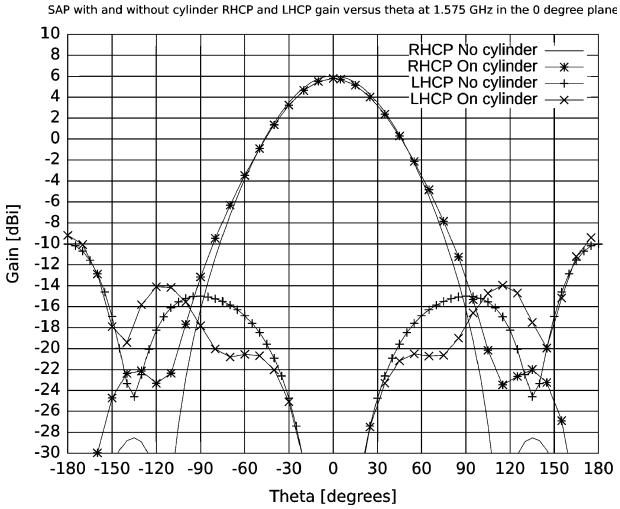

Fig. 4. SAP gain versus theta in the azimuth 0 degree plane.

the same as the substrate diameter. In real life the antenna has a radome. Radomes can be designed to have minimum impact on the radiation characteristics. Therefore, no radome has been included in this concept study.

III. Comparison of a SAP With and Without Cylinder

This comparison is being done with simulations only because it is impractical to measure an SAP with feeding hardware behind it without proper shielding and mounting hardware in an anechoic chamber. At this point, the SAP has been simulated under a perfect feed network assumption, i.e., perfect amplitude and phase balance, and no losses.

Special attention has been paid to the meshing of the SAP. Three mesh cells were forced along the SAP's substrate thickness. This denser mesh was extended one substrate thickness below and above the SAP. A mesh density of 20 cells per wavelength was taken within the SAP plane. The bounding box surrounds the simulation model 1/8 wavelength at the design frequency. Figs. 2 and 3 show the input reflection and RHCP gain versus frequency, respectively.

Figs. 4–6 depict the RHCP and LHCP gain versus theta at the center frequency for several cross sections. Figs. 7 to 9 depict the axial ratio versus theta at the center frequency for several cross sections.

The following can be concluded from the simulations of an SAP with and without a cylinder:

- The cylinder has no influence on the SAP's resonance frequency.
- The gain versus frequency in broadside is slightly (about 0.3 dB) lower for the SAP on cylinder.
- The front-to-back ratio is lightly lower (about 0.4 dB) for the SAP on cylinder.
- The SAP on cylinder has increased co-polar (RHCP) back lobes at around theta 135 degrees.
- The cross-polar (LHCP) side lobes shift to lower elevations for the SAP on cylinder. Thus, the axial ratio is considerably better (several dB's) at lower elevations.
- The SAP's radiation patterns exhibit a high degree of symmetry in azimuth.

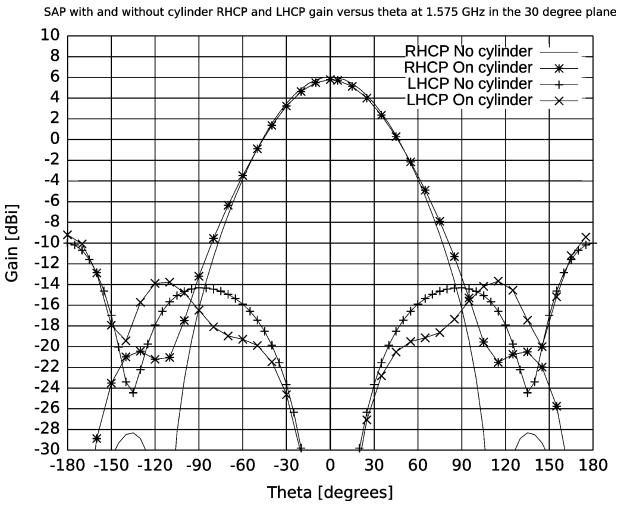

Fig. 5. SAP gain versus theta in the azimuth 30 degree plane.

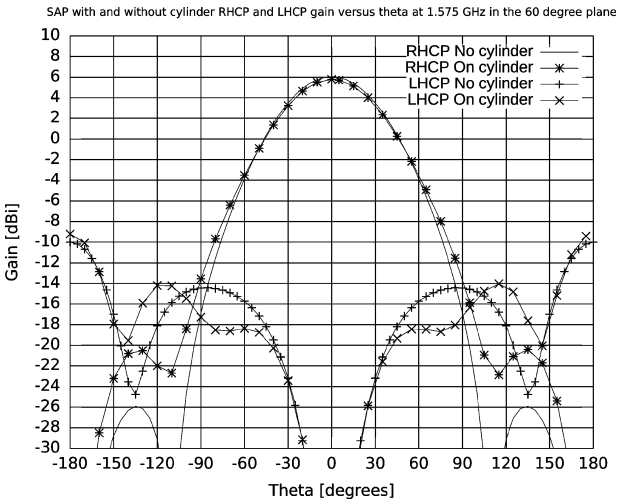

Fig. 6. SAP gain versus theta in the azimuth 60 degree plane.

The overall conclusion is that the cylinder has a positive influence on most radiation characteristics with only a small (negligible) penalty on the front-to-back ratio and broadside gain. Good axial ratio is more vital for GNSS applications.

The contribution of the conducting cylinder on the overall radiation pattern can be understood as an alteration in the scattering of the fields at the substrate truncation. Without the cylinder, the fields are partially scattered towards the back of the PCB. Simulations indicate that these backwards scattered fields are more LHCP than RHCP. When mounted on the cylinder, the fields are partially scattered towards the cylinder. Since the cylinder is electrically conductive (PEC) the tangential electric field component vanishes at the cylinder surface, while the normal electric field component does not. This means that at least part of the LHCP back scattered fields become RHCP. The net effect is an RHCP field increase and an LHCP field decrease due to the cylinder at low elevations.

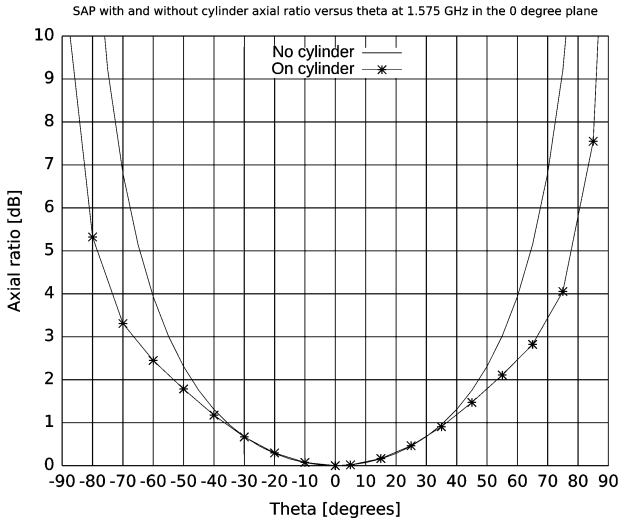

Fig. 7. SAP axial ratio versus theta in the azimuth 0 degree plane.

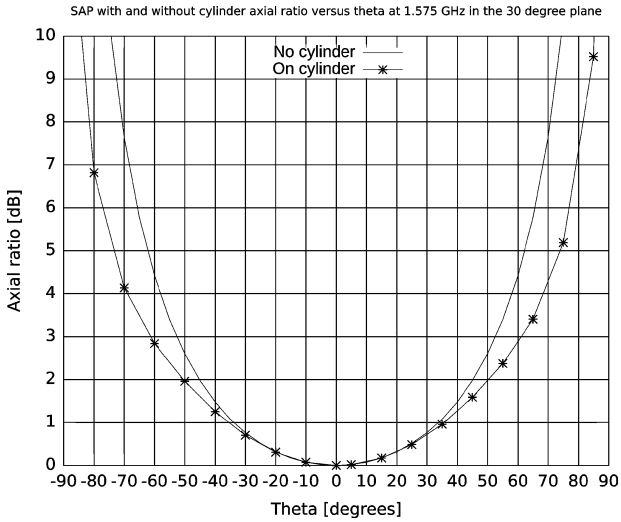

Fig. 8. SAP axial ratio versus theta in the azimuth 30 degree plane.

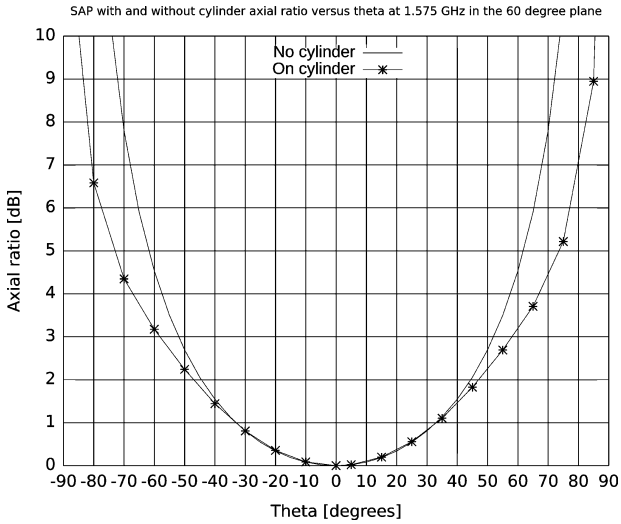

Fig. 9. SAP axial ratio versus theta in the azimuth 60 degree plane.

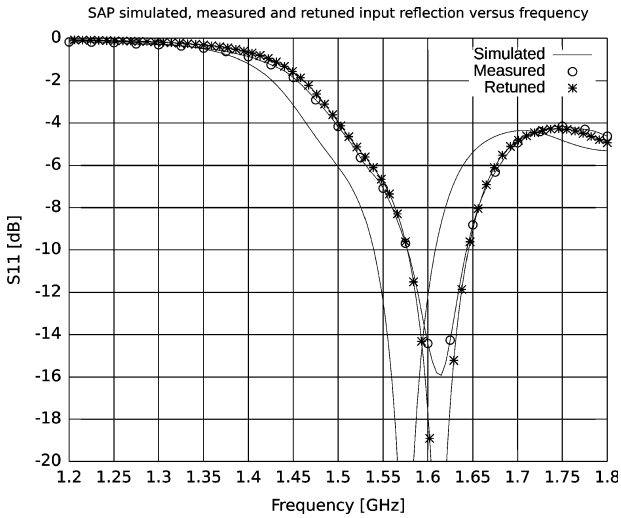

Fig. 10. SAP on cylinder simulated, measured and retuned input reflection versus frequency.

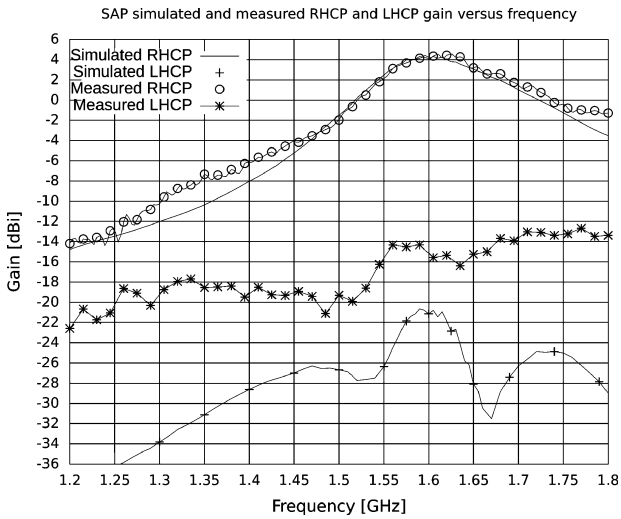

Fig. 11. SAP on cylinder simulated and measured RHCP and LHCP gain versus frequency.

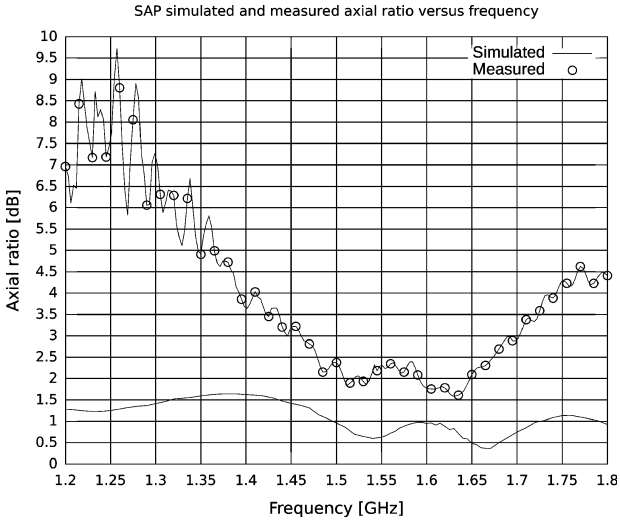

Fig. 12. SAP on cylinder measured broadside axial ratio versus frequency.

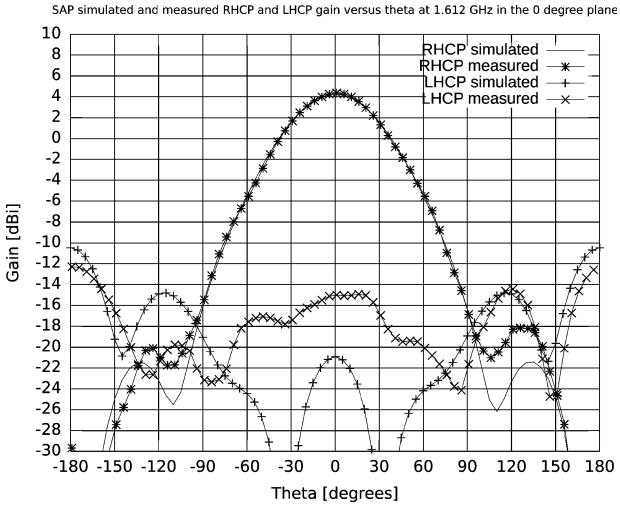

Fig. 13. SAP on cylinder simulated and measured RHCP and LHCP gain versus theta in the azimuth 0 degree plane.

IV. Simulation and Measurements of a SAP on Cylinder

Fig. 10 shows the simulated and measured input reflection of a SAP feed point versus frequency. SAP radiation pattern measurements require the use of a four phase feed network. The SCQ-4-1650+ of MiniCircuits with its evaluation board has been used here [10]. Four equally long RG-316 cables connect the four outputs of the splitter to the four SAP inputs. Simulation results in this section were done with measured splitter S-parameters.

A frequency shift can be observed for the measured input reflection. This is due to material and manufacturing tolerances. The substrate thickness was 3.25 mm in simulations while the measured substrate thickness is 3.10 mm. This deviation is normal as the required 3.25 mm is not a standard available thickness. The relative permittivity in simulations is 4.5. Resimulating with the measured substrate thickness and a different relative permittivity reveals that the latter is 4.35 instead of 4.5. This 4.35 is a normal deviation of the low cost FR4 substrate material. These two discrepancies explain the frequency shift entirely. For correct comparison between simulations and measurements, the retuned simulation results are used here.

Fig. 11 depicts the simulated and measured RHCP and LHCP gain in broadside versus frequency.

Fig. 12 depicts the simulated and measured broadside axial ratio versus frequency.

Figs. 13–15 show the simulated and measured RHCP and LHCP gain versus theta at 1.612 GHz in different cross sections at azimuth 0, 30, and 60 degrees.

Figs. 16 and 18 show the simulated and measured axial ratio versus theta at 1.612 GHz in different cross sections 0, 30, and 60 degrees. Other cross sections results are similar because of the SAP's symmetry.

The following can be concluded from the measurements of a SAP on a cylinder:

- The measured front-to-back ratio is about 3 dB better compared to the simulations.

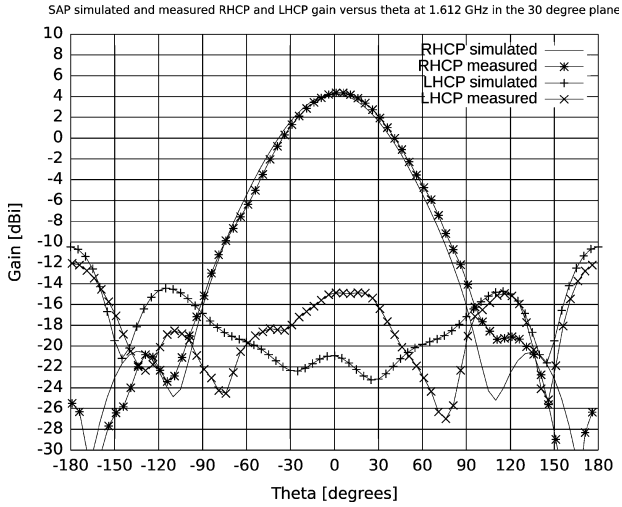

Fig. 14. SAP on cylinder simulated and measured RHCP and LHCP gain versus theta in the azimuth 30 degree plane.

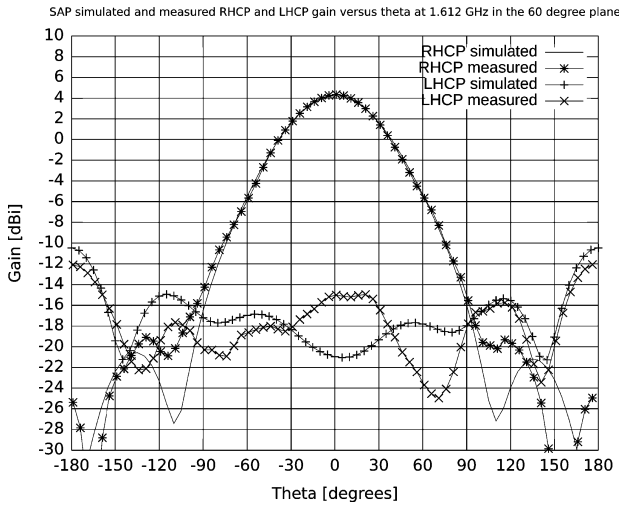

Fig. 15. SAP on cylinder simulated and measured RHCP and LHCP gain versus theta in the azimuth 60 degree plane.

- The broadside cross-polar (LHCP) component is higher in the measurements. This leads to an increased axial ratio at elevations around broadside. This can be blamed on feed network inaccuracies.
- The measured axial ratio at low elevations is better than the simulations.
- The co-polar (RHCP) component is quite similar for simulations and measurements.
- The SAP's radiation patterns exhibit a high degree of symmetry in azimuth.

V. Conclusion

Commercial GNSS antennas always contain additional RF circuitry such as power dividers, low noise amplifiers and filters which should be as close to the antenna radiating element as possible from a noise figure point of view. It is desired that this electronics is electromagnetically shielded from the radiating structure in order to avoid low noise amplifier oscillations.

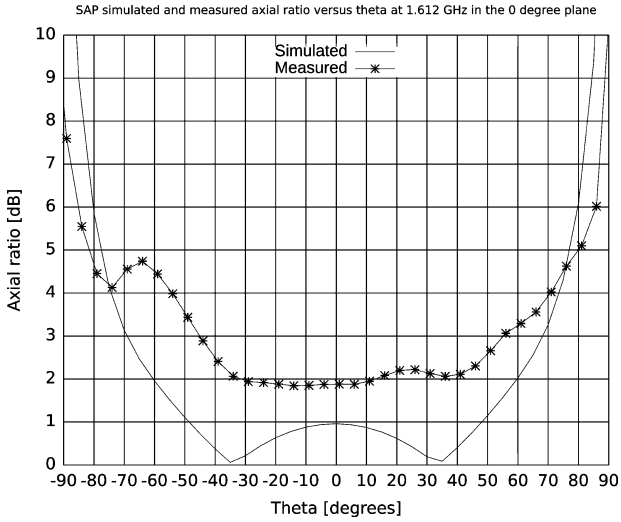

Fig. 16. SAP on cylinder simulated and measured axial ratio versus theta in the azimuth 0 degree plane.

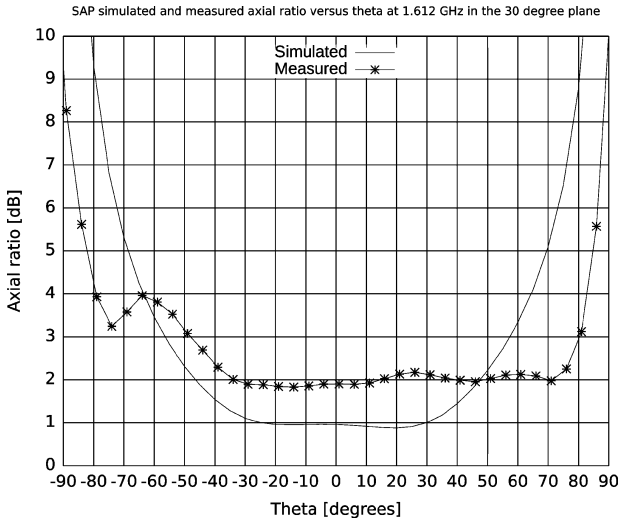

Fig. 17. SAP on cylinder simulated and measured axial ratio versus theta in the azimuth 30 degree plane.

On top of that a proper antenna mounting is required for GNSS antennas. A cylinder shaped housing is the most logical candidate because it is expected to maintain the SAP's inherent radiation pattern symmetry in azimuth.

The overall conclusion of our work is that the cylinder has a positive influence on most radiation characteristics with only a small (negligible) penalty on the front-to-back ratio and broadside RHCP gain. The axial ratio at lower elevations is improved considerably even with increased cross-polar (LHCP) radiation in broadside due to feed network imperfections. A good axial ratio at low elevations is vital for GNSS applications. The SAP's radiation patterns exhibit a high degree of symmetry in azimuth for both co- and cross-polar radiation. This is important for GNSS applications and proofs the SAP's particular suitability as a cheap alternative to expensive geodetic type GNSS antennas when mounted on a cylindrical housing.

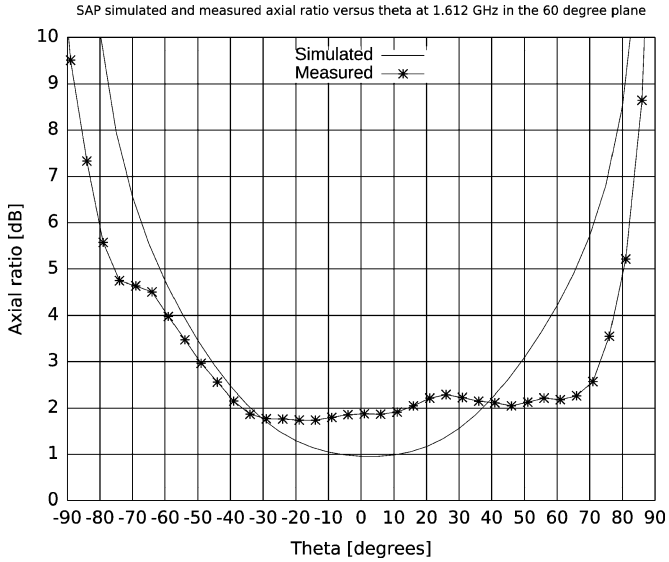

Fig. 18. SAP on cylinder simulated and measured axial ratio versus theta in the azimuth 60 degree plane.

ACKNOWLEDGMENT

G. J. K. Moernaut would like to thank D. Orban, CEO and founder of Orban Microwave Products, for his support.

REFERENCES

[1] D. R. Jackson *et al.*, "Microstrip patch designs that do not excite surface waves," *IEEE Trans. Antennas Propag.*, vol. 41, no. 8, pp. 1026–1037, Aug. 1993.

[2] L. Boccia, G. Amendola, and G. D. Massa, "Performance evaluation of shorted annular patch antennas for high-precision GPS systems," *IET Microw. Antennas Propag.*, vol. 1, pp. 465–471, Apr. 2007.

[3] G. J. K. Moernaut and G. A. E. Vandenbosch, "The shorted annular patch as a multi-path suppressing antenna," in *Proc. 2nd Eur. Conf. Antennas Propag. (EuCAP 2007)*, Nov. 11–16, 2007, pp. 1–6.

[4] L. Boccia, G. Amendola, and G. Di Massa, "Shorted annular patches as flexible antennas for space applications," in *Proc. 17th Int. Conf. Appl. Electromagn. Commun. (ICECom 2003)*, Oct. 1–3, 2003, pp. 189–192.

[5] G. J. K. Moernaut and G. A. E. Vandenbosch, "Simple pen and paper design of shorted annular ring antenna," *Electron. Lett.*, vol. 39, no. 25, pp. 1784–1785, Dec. 11, 2003.

[6] G. J. K. Moernaut and G. A. E. Vandenbosch, "Shorted annular patch with coplanar 90-degree hybrid feed for circular polarization," in *Proc. INICA 2003*, Berlin, Germany, Sep. 17–19, 2003, pp. 29–31.

[7] W. M. Dorsey and A. I. Zaghloul, "Dual-substrate capacitive loading for size reduction in shorted annular ring antennas," *IEEE Trans. Antennas Propag.*, vol. 57, no. 10, pp. 3339–3342, Oct. 2009.

[8] R. Garg *et al., Microstrip Antenna Design Handbook*. Dedham, MA: Artech House, 2001.

[9] [Online]. Available: http://www.cst.com

[10] [Online]. Available: http://www.minicircuits.com/

Gerald J. K. Moernaut (M'10) was born in Dendermonde, Belgium, on January 10, 1978. He received the M.Sc. (Industrieel Ingenieur, Ing. M.Sc.) degree in electrical engineering (electronic design) from the Hogeschool voor Wetenschap en Kunst, De Nayer Instituut, Belgium, in 2000, and the M.Sc. (Burgerlijk Ingenieur, ir. M.Sc.) degree in electrical engineering (telecommunications) in 2002, and the Ph.D. degree in October 2010, both from the Katholieke Universiteit Leuven (K. U. Leuven), Belgium.

From September 2002 until December 2004, he was a Research Assistant with the Department of Electrical Engineering (ESAT), Division of Telecommunications and Microwaves (TELEMIC), the Katholieke Universiteit Leuven. Since January 2005, he has been working as an antenna engineer with Orban Microwave Products.

Guy A. E. Vandenbosch (M'91) was born in Sint-Niklaas, Belgium, on May 4, 1962. He received the M.S. and Ph.D. degrees in electrical engineering from the Katholieke Universiteit Leuven (K. U. Leuven), Belgium, in 1985 and 1991, respectively.

He was a Research and Teaching Assistant from 1985 to 1991 with the Telecommunications and Microwaves section, K. U. Leuven, where he worked on the modeling of microstrip antennas with the integral equation technique. From 1991 to 1993, he held a Postdoctoral Research Position with the K. U. Leuven. Since 1993, he has been a Lecturer, and since 2005, a Full Professor with the same university. He has taught courses on Electrical Engineering, Electronics, and Electrical Energy, Wireless and Mobile Communications, part Antennas, Digital Steer- and Measuring Techniques in Physics, and Electromagnetic Compatibility. His research interests are in the area of electromagnetic theory, computational electromagnetics, planar antennas and circuits, electromagnetic radiation, electromagnetic compatibility, and bioelectromagnetics. His work has been published in approximately 100 papers in international journals and has been presented at about 160 international conferences.

Dr. Vandenbosch has convened and chaired numerous sessions at many conferences. He was Co-Chairman of the European Microwave Week 2004 in Amsterdam, and chaired the TPC of the European Microwave Conference within this week. He was a member of the TPC of the European Microwave Conference in 2005, 2006, 2007, and 2008. He has been a member of the Management Committees of the consecutive European COST actions on antennas since 1993, where he is leading the working group on modeling and software for antennas. Within the ACE Network of Excellence of the EU (2004–2007), he was a member of the Executive Board and coordinated the activity on the creation of a European antenna software platform. He holds a certificate of the postacademic course in Electro-Magnetic Compatibility at the Technical University Eindhoven, The Netherlands. Since 2001, he has been President of SITEL, the Belgian Society of Engineers in Telecommunication and Electronics. Since 2008, he has been a member of the Board of FITCE Belgium, the Belgian branch of the Federation of Telecommunications Engineers of the European Union. During 1999–2004, he was Vice-Chairman, and during 2005–2009, he was Secretary of the IEEE Benelux Chapter on Antennas en Propagation. Currently, he holds the position of Chairman of this Chapter. From 2002 to 2004, he was Secretary of the IEEE Benelux Chapter on EMC.

ANALYSIS OF SHORT CIRCUITED RING PATCH OPERATED AT TM_{01} MODE

Vicente González P.[1] Daniel Segovia V.[2] Eva Rajo I.[2] José Luis Vázquez R.[2] Carlos Martín P.[2]

Recibido el 5 de noviembre de 2004, aceptado el 21 de junio de 2005

ABSTRACT

This paper presents a comprehensive study of the theory of the short circuited annular-ring patch based on the cavity model. An analytical expression for frequency, fields, radiation pattern, efficiency and input impedance based on this model is shown. Simulations and experimental results are given to show the resonant frequencies, illumination fields, radiation patterns and input impedances for the 0 and 1 modes. Furthermore, it provides a simple formulation to design this type of antennas.

Keywords: Patch antenna, cavity model, short circuited annular ring patch, input impedance.

RESUMEN

Este artículo muestra un estudio sencillo de la antena en anillo cortocircuitado en base al modelo de cavidad. Se han extraído y mostrado en base al modelo de cavidad expresiones sencillas para la frecuencia de trabajo, campos en el interior de la antena, diagramas de radiación, eficiencia e impedancia de entrada. Resultados experimentales y simulaciones de las frecuencias de resonancia, de los campos de iluminación, de los diagramas de radiación y de las impedancias son mostradas para el anillo en cortocircuito trabando en modo 0 y 1.

Palabras clave: Antena impresa, parche, modelo de cavidad, anillo cortocircuitado, impedancia de entrada.

INTRODUCTION

Among the various shapes of microstrip antennas, the rectangular and circular patches are the ones that have been more extensively studied [1], [4]. These patch antennas have a ring version that has been chosen as an alternative to the standard shape. These annular antennas are geometrically and electrically an intermediate step between printed loops and patches. Several interesting properties are associated with annular ring antennas. First of all, the size of the resonant ring is substantially smaller than that of the corresponding patch. Secondly, using annular topologies allows increasing the gain margin of the patch antenna in comparison with compact (circular or rectangular) ones.

A second alternative is the short circuited ring patch done by incorporating a shorting rod at the center of a circular patch; for this geometry, the resonant ring (TM_{11} mode) becomes greater than the original patch and, then, exhibits greater gain values. This makes margin of gain extend even more than the achievable with patches. The main drawback that this type of patch presents is that side lobes can be important when the size of the short circuited patch is big. Figure 1 shows a comparison between the different circular geometries and the margin of gains that can be obtained with each of them. This last property makes annular topologies particularly suitable for their integration in array antennas, allowing the optimum the optimum combined choice of the elementary radiator and the inter element spacing. From the theoretical point of view, ring patch antennas differ from traditional patch antennas by having an additional contour condition in the inner side of patch. This inner contour may be an open circuit or a short circuit. The open circuited annular patch antenna has been totally studied, so attention will be paid to the short circuited one. Figure 2 shows the geometry of a circular short circuited ring patch. The fundamental radiation mode in the open circuited patch antenna is the TM_{11} as in the corresponding circular patch. However there is an important difference when working with short circuited ring patches: the TM_{01} mode (the first index corresponds

[1] Instituto Tecnológico de Zacatecas México, aspirante al grado de doctor, depto. de Ingeniería Audiovisual y Comunicaciones, E.U.I.T. de Telecomunicación, Universidad Politécnica de Madrid - Campus Sur, Ctra. Valencia Km 7, E-28031, Madrid, España. vgonzalz@diac.upm.es.

[2] Depto. de Teoría de la Señal y Comunicaciones, Escuela Politécnica Superior, Universidad Carlos III de Madrid, Avda. Universidad 30, 28911 Leganés. Madrid, España.

to the azimuth variation) presents its resonance at much lower frequencies (depending on both radiuses) than in the circular and open ring patches, becoming the "fundamental" mode (lowest resonant frequency). This mode is often called Mode 0 and behaves slightly different from traditional circular patches since there is no cutoff frequency. It is evident that high order indexes in the radial variation have no sense from the practical point of view since they lead to bigger surfaces causing a strongly decreased efficiency. On the other hand, higher order modes in azimuth have been used, in practice, only for mobile applications. This means that almost all the practical patches work in the "dipolar" mode (TM_{01} for rectangular geometries and TM_{11} for circular ones). However, according to the above statements concerning the short circuited ring patch, two modes must be considered: Mode 0 (TM_{01}) that provides the lowest resonance frequency and mode 1 (TM_{11}) that behaves in a similar way to the corresponding mode in traditional circular patches.

Although the cavity model has been applied to study the short circuited annular-ring patch [5], [6], there are important omissions such as the field distribution is not analyzed and the 0 mode impedance is not considered at all (besides, values of directivity up to 12-14 dB are proposed which are impossible to reach in real patch antennas). A comprehensive study of the theory and the characteristics of the short circuited annular patch is given.

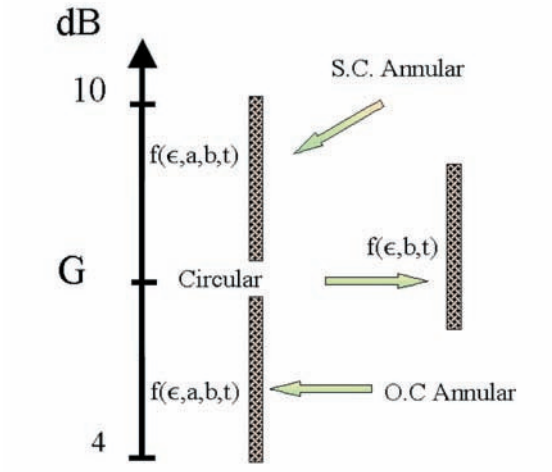

Fig. 1 Comparison between the different circular geometries.

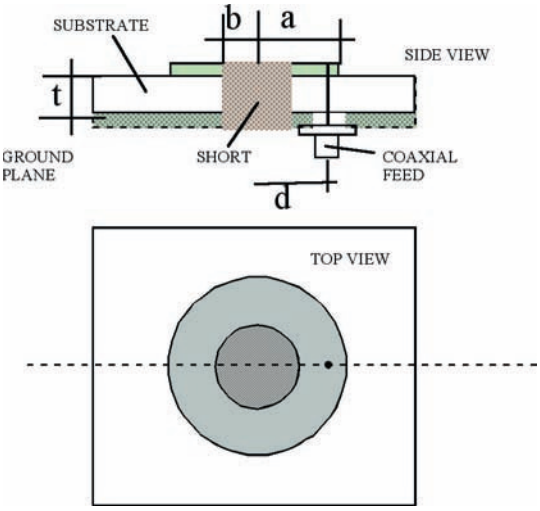

Fig. 2 Short Circuited Annular Ring Patch Antenna.

ANALYSIS OF THE SHORT CIRCUITED RING PATCH

A. Resonant frequencies

The geometry of the short circuited annular ring patch is shown in Figure 2. It has an outer radius *a*, an inner radius *b*, and is printed on the top of a substrate of thickness *t*. The model in the figure is fed through a coaxial probe located at a distance *d* from the center of the patch.

In the simple cavity model, the region between the patch and the ground plane is considered as a cavity bounded by electric walls on the top, bottom and inner edge, and a magnetic wall along the outer edge. If it is assumed that there is only TM modes propagating in the cavity, the resonant frequencies are determined by equation 1. It has also been assumed that the field distribution under the patch does not vary with the thickness of the patch (*t*) since $t<<\lambda$.

$$f_{mn} = \frac{k_{mn}}{2\pi a \cdot \sqrt{\mu_o \cdot \varepsilon}} = \frac{k_{mn} \cdot c}{2\pi a \cdot \sqrt{\varepsilon_r}} \qquad (1)$$

where the sub indexes mn represent the corresponding TM mode, *e* is the permittivity of the substrate, μ_0 is the vacuum permeability, *c* is the light velocity, ε_r is the substrate relative permittivity and $k_{mn,}$ are the roots of the following characteristic equation (2).

$$J'_m(k_{mn})N_m(k_{mn}c) - J_m(k_{mn})N'_m(k_{mn}c) = 0 \qquad (2)$$

Equation 2 comes from the boundary conditions in a ring cavity (electric wall for the inner edge and magnetic wall for the outer one); c is the ratio b/a, $J_m(x)$ and $N_m(x)$ are the first and second kind m^{th} order Bessel functions and the prime denotes the first derivative. Figure 3 shows the roots of equation 2 for different ratios b/a; it can be seen that the n^{th} subindex of the corresponding TM_{mn} mode has been fixed to 1 while the m^{th} one is varied from 0 to 4 (modes will be generally denoted according to the m^{th} subindex). It must be emphasized that the lowest resonance frequency is the corresponding to the 0 mode.

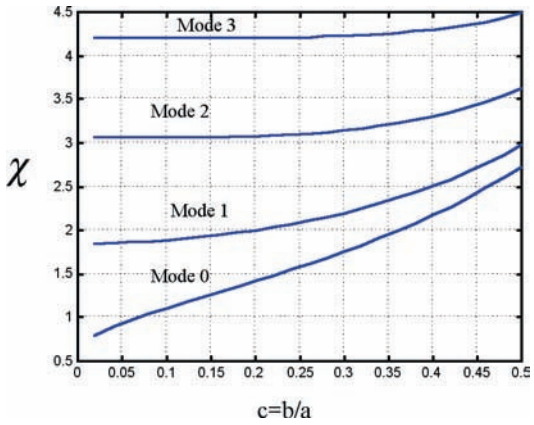

Fig. 3 Values of Roots of equation 2 for the short circuited Ring Patch.

A correction on the value of the outer radius, *a,* has been proposed as a technique to find out the value of the resonance frequency. Some authors [7] consider a suitable approach to model the antenna as a circular microstrip patch with radius *r=a-b*. This approach behaves well for higher modes but, only in a small variation margin of c, for lower ones. Schneider [8] has proposed to use an effective permittivity to take into account the effects of the fringing fields. Moreover a modification in the outer radius has also been suggested in [2], [8] resulting in the following empirical formula (3).

$$a' = a + (3/4)\cdot t \qquad (3)$$

This expression can be considered as correct in most cases.

B. Cavity fields

For the coaxial feeding case, the electromagnetic field excitation is due to a density current defined as

$$\vec{J} = I(\phi - \phi_o)\frac{\cdot\delta(r-d)}{d}\hat{z} \qquad (4)$$

Where *d* and Φ_0 denote the position of the feeding coaxial probe.

The fields within the cavity corresponding to the TM_{mn} mode are given by:

$$E_z^{mn} = A_{mn}\Big[J_m(k_0\sqrt{\varepsilon_r}r)N_m(k_0\sqrt{\varepsilon_r}b) + \\ -J_m(k_0\sqrt{\varepsilon_r}b)N_m\ \Big]\cdot\cos m\phi$$

$$H_\Phi^{mn} = -\frac{j}{\omega\mu}A_{mn}\Big[J'_m(k_0\sqrt{\varepsilon_r}r)N_m(k_0\sqrt{\varepsilon_r}b) + \\ -J_m(k_0\sqrt{\varepsilon_r}b)N'_m(k_0\sqrt{\varepsilon_r}r\Big]\cdot\cos m\phi$$

$$H_r^{mn} = -\frac{j}{\omega\mu}\frac{m}{r}A_{mn}\Big[J_m(k_0\sqrt{\varepsilon_r}r)N_m(k_0\sqrt{\varepsilon_r}b) + \\ -J_m(k_0\sqrt{\varepsilon_r}b)N_m(k_0\sqrt{\varepsilon_r}r)\Big]\cdot\sin m\phi \qquad (5)$$

where A_{mn} is a constant depending on the corresponding *mn* mode and ϕ, *r* and *z* are the coordinates in a cylindrical system. When the patch is excited, for a general situation, several modes can appear. Then, the fields can be expressed as:

$$E_z^{mn} = j\omega\mu I\sum_{n=1}^{\infty}\sum_{m=0}^{\infty}\Big[R_{mn}\Big[J_m(k_0\sqrt{\varepsilon_r}r)N_m(k_0\sqrt{\varepsilon_r}b) - J_m(k_0\sqrt{\varepsilon_r}b)N_m(k_0\sqrt{\varepsilon_r}r)\Big]\cdot\cos m\phi\Big]$$

$$H_\Phi^{mn} = I\sum_{n=1}^{\infty}\sum_{m=0}^{\infty}\Big[R_{mn}\Big[J'_m(k_0\sqrt{\varepsilon_r}r)N_m(k_0\sqrt{\varepsilon_r}b) - J_m(k_0\sqrt{\varepsilon_r}b)N'_m(k_0\sqrt{\varepsilon_r}r)\Big]\cdot\cos m\phi\Big]$$

$$H_r^{mn} = \frac{I}{r}\sum_{n=1}^{\infty}\sum_{m=0}^{\infty}m\cdot\Big[R_{mn}\Big[J_m(k_0\sqrt{\varepsilon_r}r)N_m(k_0\sqrt{\varepsilon_r}b) - J_m(k_0\sqrt{\varepsilon_r}b)N_m(k_0\sqrt{\varepsilon_r}r)\Big]\cdot\sin m\phi\Big] \qquad (6)$$

Where R_{mn} is the amplitude of each mode present in the patch and is related to the corresponding A_{mn} and to the amount of energy associated to each propagating mode. Where w is the diameter of the probe that provides a uniform current [8]. Although equation 6 relates to a double infinite series, in most practical cases it converges very fast for m,n values lower than 5. Figures 4 and 5 represent the electrical fields inside the cavity as a function of the radius and the azimuthal angle. Figure 6 represents the current line distribution and 3D Ez field in the short circuited ring patch for the modes 0 and 1.

$$R_{mn} = \begin{cases} \dfrac{\pi w k_0^{\,2} \varepsilon_r \left[J_0(k_{0n}d)N_0(k_{0n}b) - J_0(k_{0n}b)N_0(k_{0n}d) \right]}{\left[\left(k_0\sqrt{\varepsilon_r} \right)^2 - k_{0n}^{\,2} \right] \cdot \left[\dfrac{J_0(k_{0n}b)}{J_0(k_{0n}a)} - 1 \right]}; m = 0 \\ \dfrac{\pi k_0^{\,2} \varepsilon_r \sin mw \cos m\pi \left[J_m(k_{mn}d)N_0(k_{mn}b) - J_m(k_{mn}b)N_m(k_{mn}d) \right]}{m \cdot \left[\left(k_0\sqrt{\varepsilon_r} \right)^2 - k_{0n}^{\,2} \right] \cdot \left[\dfrac{J_m(k_{mn}b)}{J_m(k_{mn}a)} \cdot \left(1 - \dfrac{m^2}{\pi k_0^{\,2} \varepsilon_r a^2} \right) - \left(1 - \dfrac{m^2}{\pi k_0^{\,2} \varepsilon_r b^2} \right) \right]}; \forall m \neq 0 \end{cases} \tag{7}$$

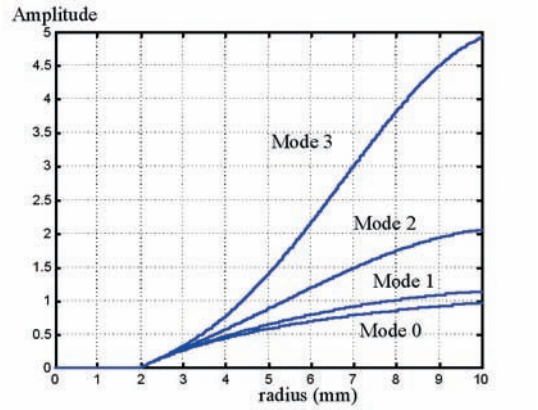

Fig. 4 Ez field versus radius of the patch.

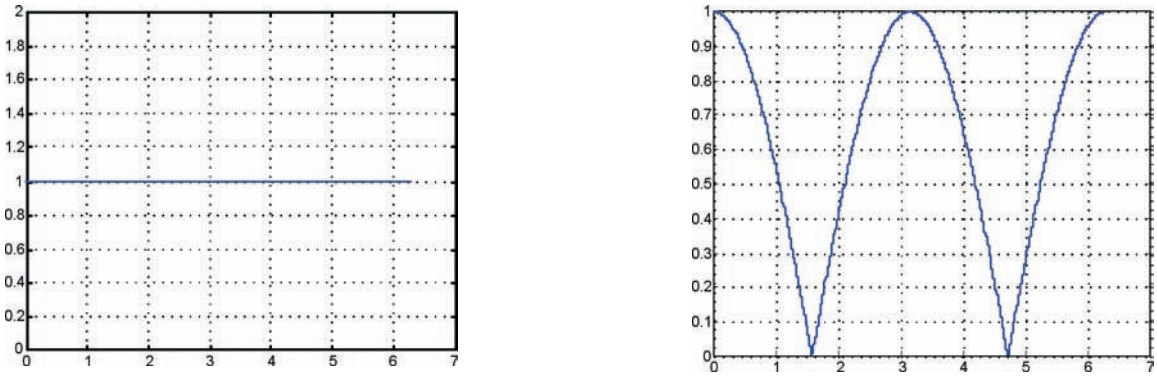

Mode 1 Mode 2

Fig. 5.1 Ez versus azimuthal angle in radians.

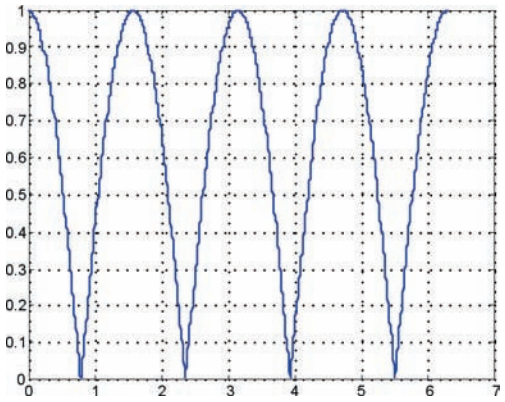

Mode 2

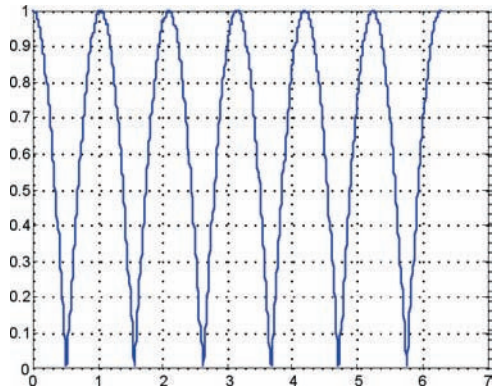

Mode 3

Fig. 5.2 Ez versus azimuthal angle in radians.

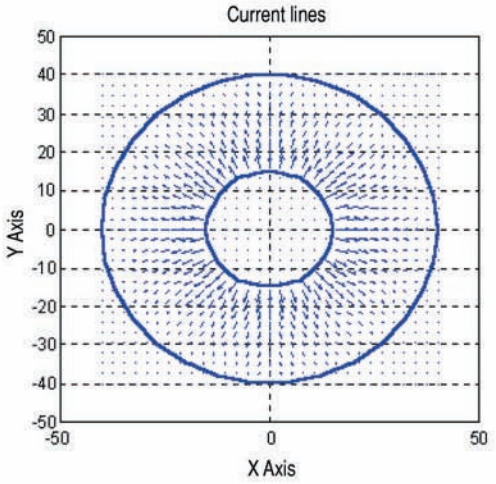

Mode 0

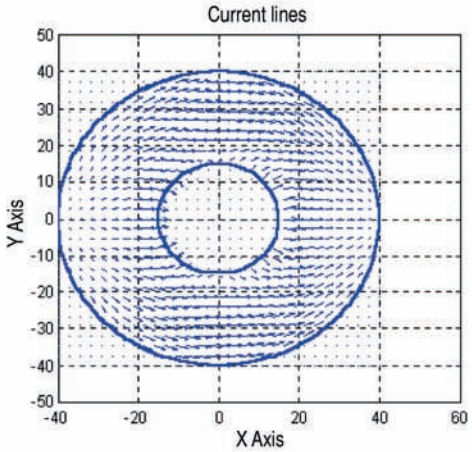

Mode 1

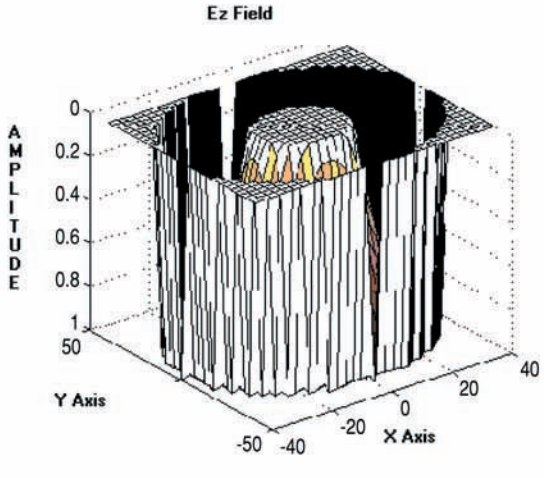

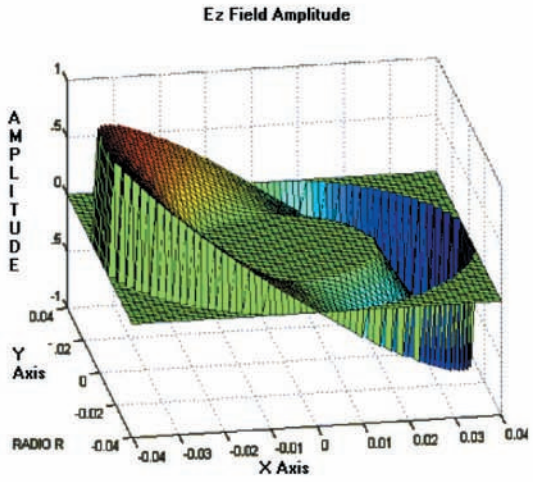

Fig. 6 Current line distribution in the patch (upper side) and 3D Ez Field for modes 0 and 1 side.

C. Input Impedance

The input impedance allows the definition of the antenna operation bandwidth and the analysis of the possibility of adding resonance to increase its bandwidth.

Although the input impedance of the shorted annular ring patch has not been calculated yet by using the cavity model, the method of calculation is well established [1], [2]. It involves the introduction of an effective loss tangent to take into account for the various losses in the cavity, namely the radiation, the dielectric, the conductor and the surface wave losses. The last quantity is quite small and can usually be neglected, for the case where the ratio between the substrate thickness and the wavelength (h/λ) be lower than 0.05 (e.g.). However, real patches have limited substrate and ground plane; then, when the surface wave reaches these edges, it transforms into a volume wave without decreasing the antenna efficiency although distorting (even strongly) the radiation pattern.

Then, the input impedance can be formulated as [1], [9] and [10], see (8).

The first term in brackets represents the contribution from the 0 mode while the double sum represents the contribution from all other modes, k_{eff} is the effective wave number which is given as:

$$k_{eff} = k_0\sqrt{\varepsilon_e(1 - j\delta_{eff})} \tag{9}$$

where δ_{eff} is the effective loss tangent given by [10]:

$$\delta_{eff} = \tan\delta + \frac{1}{t\sqrt{\sigma\mu\pi f}} + \frac{2\omega\cdot\mu\cdot t\cdot M}{\eta_0\cdot\varepsilon_r\cdot\left[\frac{J_m\left(k_{mn}\cdot a\right)}{J_m\left(k_{mn}\cdot b\right)}\cdot\left(1-\frac{m^2}{k_{mn}^2\cdot b^2}\right)-\left(1-\frac{m^2}{k_{mn}^2\cdot a^2}\right)\right]} \tag{10}$$

The quantity M is the following integral: see (11).

Note that the first term in the previous integral is zero for the 0 mode. Besides the double sum in (8) mainly affects to the upper modes so for the analysis of the TM_{01} or TM_{11} modes they must be discarded. It must also be noted that the mode 0 presents, in the same way as any other mode, an equivalent resonant RLC circuit. However, for low frequencies this mode behaves as a short circuit; for that reason it can be thought that at these frequencies another RC circuit looms. This RC circuit is composed of a resistor (with a very low value depending on the frequency) paralleled with a capacitor whose effect is negligible at the corresponding resonant frequency of the TM_{01}. This last effect at very low frequencies (quasi static) can be included in the overall equivalent circuit of the TM_{01} mode what would result in a double series resonant circuit (an RC circuit for low frequencies and the traditional RLC circuit for the corresponding resonant frequency of the TM_{01} mode). Although it could be thought of having a dual resonant antenna for the TM_{01} mode by tuning the RC circuit with an appropriate inductive coaxial probe, this is not so since the radiation properties of the lower frequencies are very poor.

$$Z_{IN} = R + jX = j\omega\mu\left\{\sum_{n=1}^{\infty}\frac{(J_0(k_{0n}t)N_0(k_{0n}b)-J_0(k_{0n}b)N_0(k_{0n}t))^2}{4(k_{eff}^2-k_{0n}^2)\left[\frac{J_0^2(k_{0n}b)}{J_0^2(k_{0n}a)}-1\right]}\pi k_{0n}^2+\sum_{m=1}^{\infty}\sum_{n=1}^{\infty}\frac{\left(\frac{\sin(mw)}{mw}\right)^2\left[N_m(k_{mn}a)J_m(k_{mn}t)-J_m(k_{mn}a)N_m(k_{mn}d)\right]^2}{\frac{2(k_{eff}^2-k_{mn}^2)}{\pi k_{mn}^2}\left[\frac{J_m(k_{mn}a)}{J_m(k_{mn}b)}\left(1-\frac{m^2}{k_{mn}^2b^2}\right)-\left(1-\frac{m^2}{k_{mn}^2a^2}\right)\right]}\right\} \tag{8}$$

$$M = \int_0^{\pi}\frac{m^2\cdot\cos^2\theta}{k_0^2\cdot\sin\theta}\cdot\left\{\frac{J_m\left(k_o\cdot b\cdot\sin\theta\right)}{b}-\frac{J_m\left(k_o\cdot a\cdot\sin\theta\right)}{a}\cdot\frac{J_m\left(k_{mn}\cdot b\right)^2}{J_m\left(k_{mn}\cdot a\right)^2}\right\}^2 d\theta +$$
$$+\int_0^{\pi}\sin\theta\cdot\left\{J_m\left(k_o\cdot b\cdot\sin\theta\right)-J_m\left(k_o\cdot a\cdot\sin\theta\right)\cdot\frac{J_m\left(k_{mn}\cdot b\right)}{J_m\left(k_{mn}\cdot a\right)}\right\}^2 d\theta \tag{11}$$

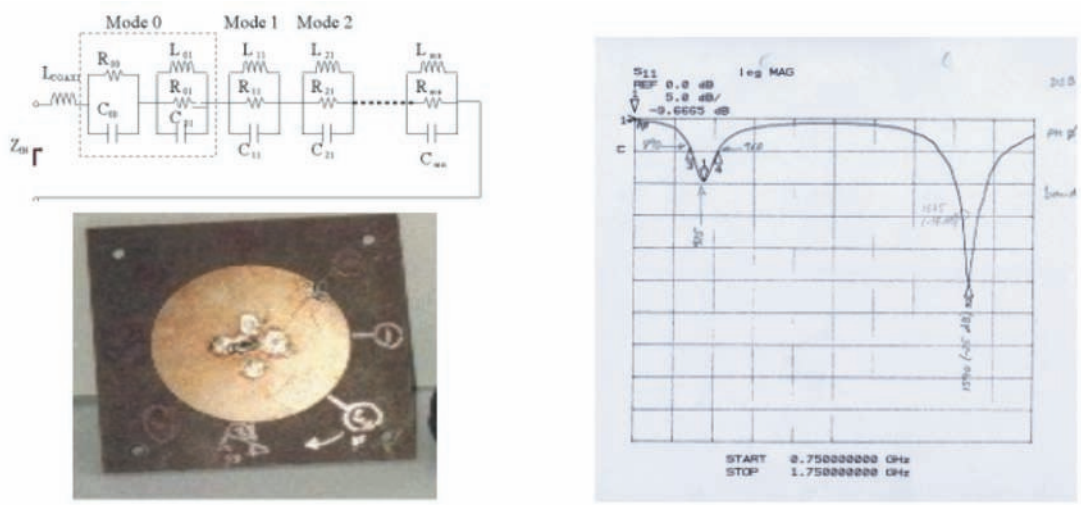

Fig. 7 Impedance model and prototype measured (left) with two resonances (right).

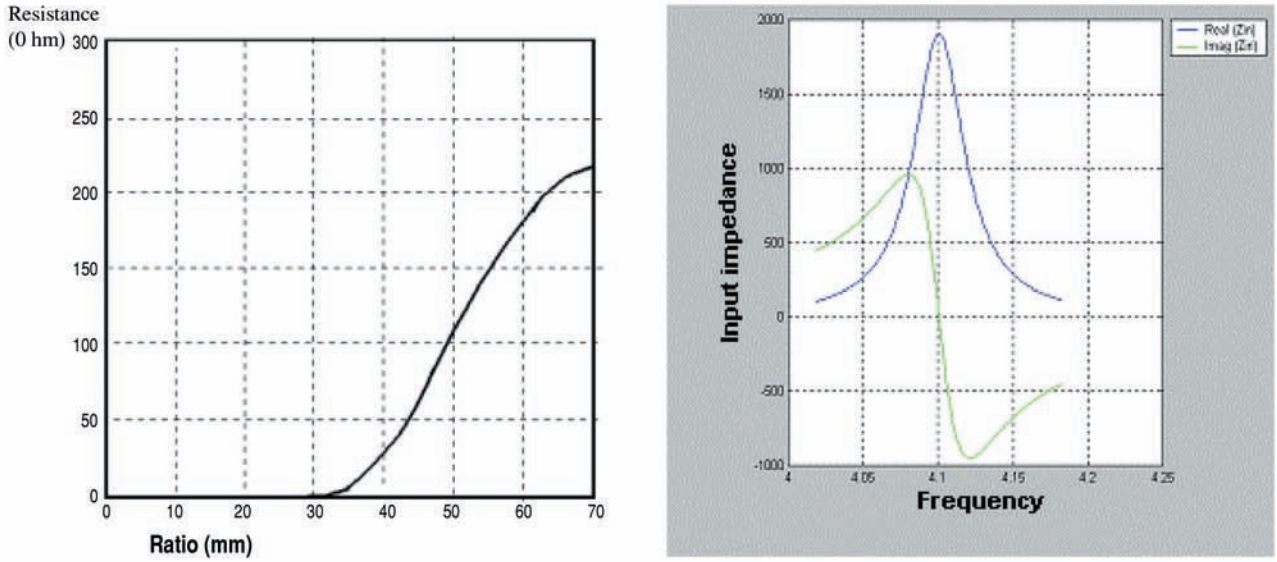

Fig. 8 Impedance vs radii (left) and Impedance vs frequency (right) in the mode 0.

According to the previous comments the complete equivalent circuit for the short circuited patch antenna is shown in figure 7. Figure 7 shows the two frequencies resonance and sc ring measured. The values for any element in the equivalent circuit are given as a function of the corresponding modes. By using previous equations, the input impedances for different modes can be easily plotted. Then figure 8 shows the input impedance for mode 0 as a function of the outer radius or frequency.

D. Radiated Fields

Once the internal fields and input impedance in the cavity have been determined, the radiated fields of a short circuited ring patch can be obtained either from the magnetic current approach on the fictitious magnetic wall in the outer region or the electric current distribution on the surface of the ring.

$$E_\theta = j^{m+1} A \frac{e^{-jk_0 r}}{r}\left[(J_m(k_{mn}a)N_m(k_{mn}b) - J_m(k_{mn}b)N_m(k_{mn}a)\right]J_m'(k_0 b sen\theta)\cos m\phi$$

$$E_\phi = -j^{m+1} mA \frac{e^{-jk_0 r}}{r}\left[J_m(k_{mn}a)N_m(k_{mn}b) - J_m(k_{mn}b)N_{\boldsymbol{m}}(k_{mn}a)\right]\frac{J_m(k_0 a sen\theta)}{k_0 a sen\theta}\frac{\cos\theta}{sen\theta}senm\phi \quad (12)$$

where:

$$A = \frac{2tk_0 E_{mn}}{\pi k_{mn}}$$

The previous expressions represent the radiated field by only one mode without considering the effect of the probe. Mode 0 or 1 will be chosen according to the application required. The other modes are less interesting because of their smaller bandwidths and polylobed radiation patterns. Figures 9 and 10 show the radiation patterns simulated and measured for 0 and 1 modes.

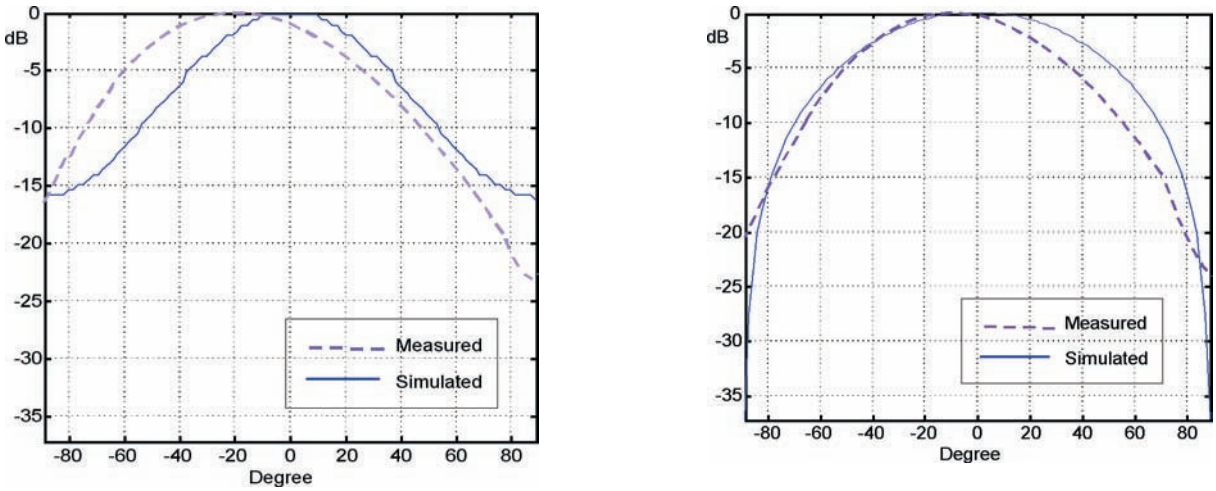

Fig. 9 Simulated and Measured radiation pattern in E (left) and H (right) plane (Mode 1).

The fundamental mode in the short circuited ring antenna is the mode 0 that has the characteristic of having a null in the zenith and a maximum in the azimuthal direction. For the same radiation mode, the radiation pattern is similar to that of a circular patch, although this antenna presents a better performance than the one using a circular geometry. It can be emphasized that this structure has a bigger gain. The directivity and gain can be given [1], [9] as: see (13).

$$D = \frac{4\pi}{\Omega_A} = \frac{4}{M\varepsilon_m} \quad (13)$$

M is the integral shown in 11. The gain is

$$G = \eta \cdot D \quad (14)$$

where the efficiency is given approximately [10]: see (15).

$$\eta = \frac{\dfrac{k_0^2 t}{\eta_0 k_{mn}^2 I}}{\dfrac{k_0^2 t}{\eta_0 k_{mn}^2 I_2} + \left[\dfrac{J_m^2(k_{mn}a)}{J_m^2(k_{mn}b)}\left(1 - \dfrac{m^2}{k_{mn}^2 b^2}\right) - \left(1 - \dfrac{m^2}{k_{mn}^2 a^2}\right)\right]\left[\dfrac{R_s}{\pi\omega^3\mu_0^2} + \dfrac{\varepsilon t\delta}{2\pi k_{mn}^2}\right]} \quad (15)$$

Where R_S is the surface resistance.

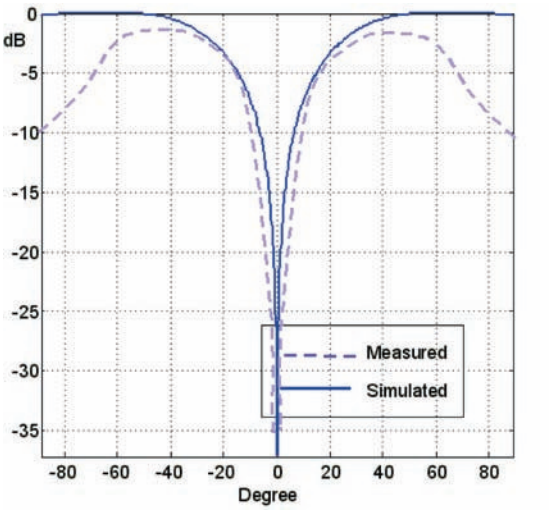

Fig. 10 Simulated and measured Radiation pattern in E and H plane (Mode 0).

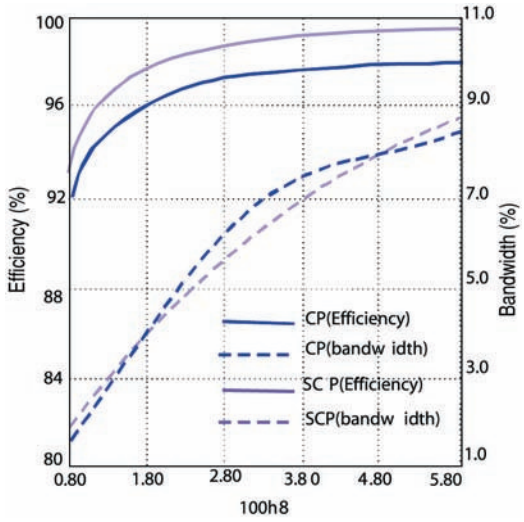

Fig. 11 Efficiency and Bandwidth versus thickness. CP(circular patch with b=28mm ε_r=2.5) and SCP(short circular patch with b=28mm a=19.3mm ε_r=2.5).

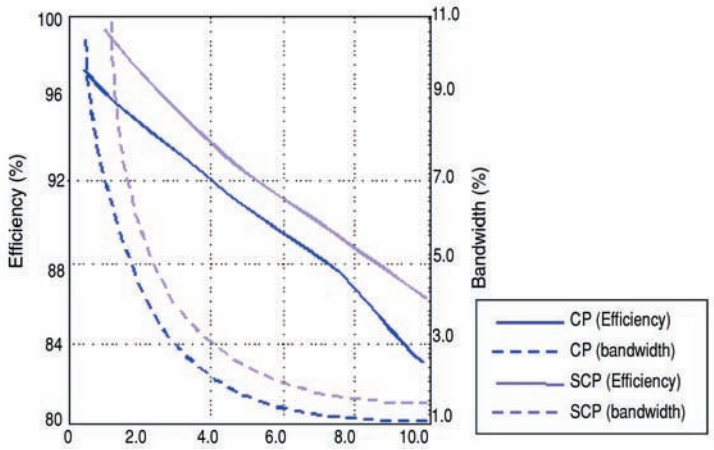

Fig. 12 Efficiency and Bandwidth versus permittivity. CP (circular patch with b=28mm h=1.58) and SCP (short circular patch with b=28mm a=19.3mm h=1.58).

Figures 11 and 12 represent the efficiency and bandwidth as a function of the thickness and the permittivity of substrate by circular patch (CP) and short circular patch (SCP).

As the radiating edge in this kind of patches is the outer bound, its radiation pattern is very similar to the corresponding one for the circular patch, but with a bigger efficiency. Besides, according to figure 1, note that the size of the short circuited patch can be modified in such a way that can be bigger than the corresponding circular patch. For that reason the radiating edge is bigger and its radiating performance is better than the conventional circular patch. It would also be possible to reduce the size of the short circuited patch by tuning externally the mode 0. This would yield a reduction in the size of the resonant patch what would reduce the antenna efficiency and gain getting a resonant structure that would hardly radiate.

Shorted annular patch with coplanar 90-degree hybrid feed for circular polarization

G. J. K. Moernaut; G.A. E. Vandenbosch, Katholieke Universiteit Leuven, ESAT-Telemic, Kasteelpark Arenberg 10, B-3001 Leuven, Belgium

Abstract

This paper presents the design of a circular polarized shorted annular patch (SAP). Circular polarization is realized using 2 feed points fed by a coplanar 90-degree hybrid coupler. The inner space of the ring is large enough to permit placement of a feeding network, eliminating the need for an extra feeding layer and thus reducing cost. Simulations and measurements show a good matching and a well-behaved circular polarization radiation pattern can be achieved.

1 Introduction

This paper outlines the design procedure of a circular polarized SAP and the feeding network accompanied with simulation and measurement results. The design procedure for the SAP is based on cavity model analysis while the hybrid is a widely known microwave component.

2 Design procedure

The proposed configuration is displayed in figure 1 and consists of an SAP with a 90-degree hybrid placed in the center (short circuited zone) of the antenna. By exciting either port 1 or port 2, left hand respectively right hand circular polarization is achieved.

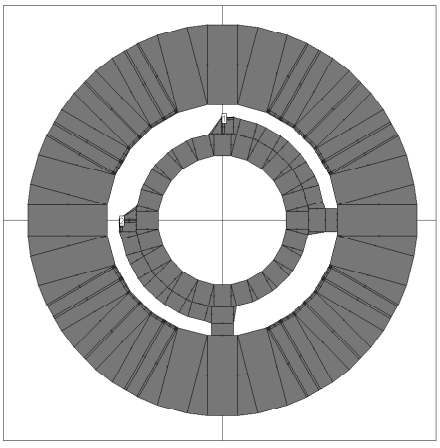

Figure 1: SAP-hybrid configuration.

The resonance frequencies of a shorted annular patch (SAP) are determined by the following formula,

$$J_n'(kb)Y_n(ka) - J_n(ka)Y_n'(kb) = 0 \qquad (1)$$

derived using cavity model analysis [1], where a and b are the SAP's inner and outer radius respectively and $J_n(.)$ and $Y_n(.)$ are the Bessel functions of the first and second kind of order n respectively. Since the average circumference of a 90-degree hybrid coupler is about 1 wavelength at the operating frequency, the inner radius of the SAP must be large enough to allow placement of the coupler in the short-circuited area of the SAP. This results in the obligation to use a relatively thin ring as radiating element since the same substrate material is used for both hybrid and SAP. For convenience some roots X_{nm} (= $k_{nm}a$) of equation 1 for different ratios of the ring outer-to-inner radius b/a are presented in table 1.

Table 1: Roots of equation 1 for different ratios b/a.

b/a	1.5	1.6	1.7	1.8	1.9	2
X_{nm}	2.61	2.15	1.83	1.59	1.4	1.25

Using formula

$$f_{nm} = \frac{X_{nm}c}{2\pi a\sqrt{\varepsilon_r}} \qquad (2)$$

the inner radius of the ring can be determined. In this formula f_{nm} denotes the resonance frequency of the desired mode, c is the speed of light and ε_r is the relative permittivity of the substrate material used.

The development of the 90-degree hybrid coupler is straightforward. A good design reference is [2]. Simulations have shown that placing the hybrid in the short-circuited zone has little effect on its performance and that the shorting wall should be as symmetrical as possible for polarization purity.

3 Simulations & measurements

Simulations where done with IE3D of Zeland™ using an infinite ground plane and measurements where done on an antenna with a ground plane of 78mm x 78mm. The RO4003 substrate of Rogers Corporation™ with ε_r of 3.38, tg δ 0.0027 and thickness 1.524 mm was used. A ratio b/a of about 1.7, an operating frequency of 2.45 GHz and left hand circular polarization where chosen. Shorting pins approximate the shorting wall. The 2 90-degree hybrid ports not connected to the SAP are probe fed. By choosing one of the 2 probe fed ports switching between right hand and left hand circular polarization is possible.

Figure 2 shows good matching of port 1 (port 2 is equivalent). The 2 possible feed points are well isolated around 2.45 GHz according to simulations. However, the measurement results show a frequency shift and a degrading in isolation. This means that the isolation is critical and further tuning is necessary.
Despite the problem with the isolation, rather good circular polarization behavior can be seen in figure 3 presenting the axial ratio versus frequency. The axial ratio is expected to further improve when the isolation problem is solved.

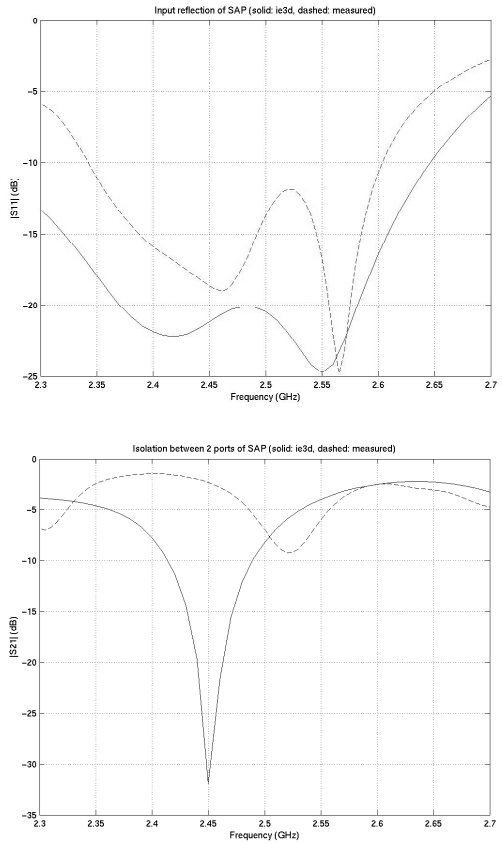

Figure 2: Input reflection (left) of port 1 and isolation (right) between port 1 and 2.

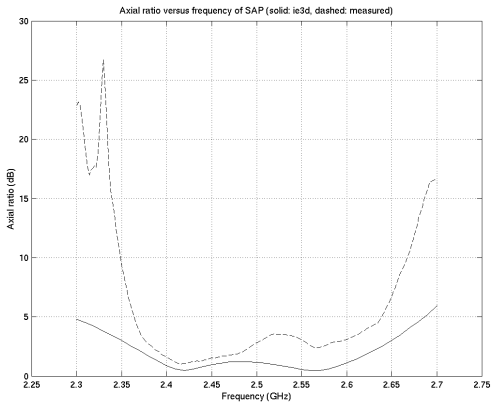

Figure 3: Axial ratio versus frequency.

Figure 4 displays the radiation pattern at 2.55 GHz (in the vicinity of best measured matching and isolation) in 2 orthogonal planes. There is good agreement between simulations and measurements.

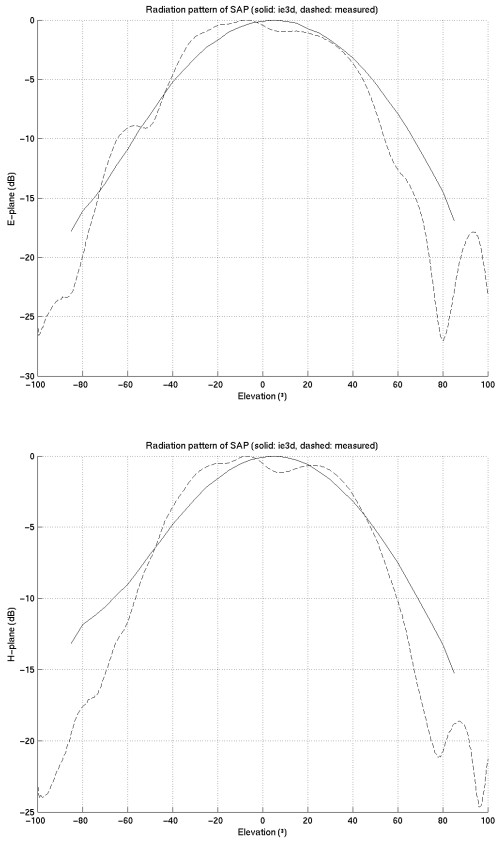

Figure 4: Radiation patterns in E-plane (left) and H-plane (right).

4 Conclusions

Simulation and measurement results show that a circular polarized SAP can be build with the proposed topology. However, measurement results also show a problem with isolation between the 2 feed ports. This deficiency can be solved with further tuning.

5 Literature

[1] Microstrip Patch Designs That Do Not Excite Surface Waves, D.R. Jackson, J.T. Williams, Arun K. Bhattacharyya, Richard L. Smith, Stephen J. Buchheit, and S.A. Long, IEEE trans. on Antennas and propagation, vol. 41, No. 8, august 1993

[2] Microwave Engineering (second edition), David M. Pozar, John Wiley & Sons Inc., 1998

A last comment can be made concerning the mode 0 for the conventional circular patch where this mode is a higher order one. In this case, the mode 0 does not present the quasi-static and tuning performance of the corresponding one in the short circuited patch. For that reason, the radiation pattern of the short circuited patch is less directive than the one for the circular patch. Besides, the lower the resonant frequency (for instance, by external tuning) the lower the directivity is.

CONCLUSIONS

The cavity model has been applied to analyze the short circuited ring antenna. This model has been applied to show the performance of the short circuited patch in front of the dielectric constant and its physical radius. Formulas for the resonant frequency, radiated field have been provided; an explicit expression for the input impedance has also been obtained and experimental results have been obtained. The accurate expressions for the radiation fields and an explicit formula for the input impedance constitute, from our point of view, new contributions to the study of short circuited patches.

One the major advantages of short circuited patch antenna is the possibility of constructing bigger resonant radiators than the conventional ones. For that reason, bigger efficiency and antenna gains can be achieved by properly choosing the resonant patch size. Other important characteristic is the fact that the fundamental mode is no longer TM_{11} (mode 1) but the TM_{01} which is the one that presents the lower cut-off frequency. This mode can be found in all the circular geometries but in the short circuited patch presents a quasi-static behavior that allows its tuning at a lower frequency than its natural resonant frequency.

REFERENCES

[1] R. Garg, P. Bhartia, I. Bahl, A. Ittipiboon. "Microstrip Antenna Design Handbook". Artech House, 2001.

[2] I.J. Bahl and P. Bhartia. "Microstrip Antennas", Artech House, Mass. 1980.

[3] M.D. Deshpande and M.C. Bailey. "Input Impedance of Microstrip Antenas", IEEE Trans. on Antennas and Prop, Vol. AP-30, no. 4, July 1982: 645-650.

[4] W.F. Richards, Y.T. Lo and D.D. Harrison. "An Improved Theory for Microstrip Antennas". IEEE Trans. MTT, 29 , no. 1, USA 1981: 38-46.

[5] Y. Lin and L. Shafai. "Properties of Centrally Shorted Circular Patch Microstrip Antennas", IEEE AP-S, Syracuse 1988: 700-703.

[6] Y. Lin and L. Shafai. "Characteristics of Concentrically Shorted Circular Patch Microstrip Antennas", IEE Proceedings, Vol. 137, no. 1, 1990: 18-24.

[7] Q. García. "Contribución al Estudio de las Antenas Autodiplexadas", Ph. Thesis, Chapter 3, Sevilla, May 1996.

[8] M.V. Schneider. "Microstrip Lines for Microwave Integrated Circuits", Bell Sist. Tech. Journal, USA 1969: 1421-1444.

[9] Y. S. Wu and F. J. Rosenbaum. "Mode Chart for Microstrip Ring Resonators". IEEE Trans. MTT, 21, USA 1973: 487-489.

[10] K.F. Lee and J.S. Dahele. "Characteristics of Annular Ring Microstrip Antenna", Electronic Letters, 1982, 28, no. 24-10: 1051-1052.

[11] Ch. Delaveaud, Ph. Leveque, B. Jecko. "New Kind of Microstrip Antenna: the Monopolar Wire-Patch Antenna", Electronic Letters, January 94: 1-2.

VOL. 4, NO. 8, OCTOBER 2009 ISSN 1819-6608
ARPN Journal of Engineering and Applied Sciences

www.arpnjournals.com

BANDWIDTH ENHANCEMENT OF INNER SHORTED ANNULAR MICROSTRIP ANTENNAS

Abdulkareem Abd Ali Mohammed[1] and Ali Hussain Ali Yawer[2]
[1]Space Observatory and Simulation Research Center, Aeronautics and Space Directorate, Baghdad, Iraq
[2]Electronic and Communications Department, College of Engineering, Al-Nahrain University, Baghdad, Iraq
E-Mail: eng.ali_hussain@Yahoo.com

ABSTRACT

An inner shorted annular micro-strip antenna was designed using Bessel function relations and then two techniques of bandwidth enhancement has been suggested and designed and the current distribution and the radiation field with the frequency and the feed point location has been studied.

Keywords: inner shorted annular microstrip antennas, bandwidth, stacked patches, Bessel function.

INTRODUCTION

Among the various shapes of microstrip antennas, the rectangular and circular patches are the ones that have been more extensively studied. The annular patch antennas have been chosen as an alternative to the standard shape. These anular antennas are geometrically and electrically an intermediate step between printed loops and patches [1].

Annular antennas have many interesting features, first, for a given frequency, the size of annular antennas is substantially smaller than that of the circular patch when both operated in the lowest mode. Second, it can be easily designed for dual band operation by using a concentric ring structure, or by employing another circular patch [2].

One of the many types of annular antennas is the inner shorted annular microstrip antennas (ISAMA), the inner boundary of this patch is shorted to the ground plane, the presence of the cylindrical conductor in the central zone of the antenna reduces the energy stored under the patch resulting in a lower antenna quality factor and in a bandwidth wider than circular disk. This will lead to a greater gain [3].

The inner shorted annular is shown in Figure-1 it has an inner shorted (a) and an outer radius (b) and printed on a substrate matreial of thickness (t) with a dielectric constant (ε_r) , The lower order modes in circular patch antenna is TM_{11} while in inner shorted patch it is TM_{01} which is the fundamental mode and it is sometimes called mode 0 ,the patch has been modeled as a cavity where the bounded by an electric wall from top and bottom and a magnetic wall from the outer periphery so the frequency can be calculated by,

$$f = \frac{x_a \, c}{2\pi\sqrt{\varepsilon_r}} \quad (1)$$

Where c is the velocity of light and (x_a) is the root of the characteristic equation

$$J_n(x_a).Y_n'(x_b) - J_n'(x_b).Y_n(x_a) = 0 \quad (2)$$

and ε_r is the dielectric constant

The input impedance of inner shorted is calculated from transmitted power and energy stored and the losses in the patch as [4]:

$$Z_{in} = \frac{\frac{1}{2} V V^*}{P_t + 2j\omega(W_e - W_m)} \quad (3)$$

Where V is the voltage in the patch, P_t is the transmitted power where:

$$P_t = P_r + P_d + P_c \quad (4)$$

And W_e is the electric energy stored and W_m is the magnetic energy stored and the bandwidth is dependent on the Q-factor and the VSWR of the patch and it is:

$$\text{B.W} = (VSWR - 1)/Q\sqrt{VSWR} \quad (5)$$

And the Quality factor is computed as follows:

$$Q = 2\omega W_e / P_t \quad (6)$$

The far field radiation with the two components of φ and θ components are shown below:

$$E_\varphi = +(j)^n \left(\frac{e^{-jk_0 r}}{r}\right)\left[\frac{k_o V_o}{2} F_{nm}(f)\right] \cos\theta \sin n\varphi * [b * F_{nm}(a)\{J_{n-1}(k_o\, b\, \sin\theta) - J_{n+1}(k_o\, b\, \sin\theta)\}] \quad (7)$$

$$E_\varphi = +(j)^n \left(\frac{e^{-jk_0 r}}{r}\right)\left[\frac{k_o V_o}{2} F_{nm}(f)\right] \cos\theta \sin n\varphi * [b * F_{nm}(a)\{J_{n-1}(k_o\, b\, \sin\theta) - J_{n+1}(k_o\, b\, \sin\theta)\}] \quad (8)$$

Where $V_o = h E_z(a)$

ANTENNA DESIGN

An inner shorted annular microstrip antennas has been designed according to the characteristic equation:

$$J_n(x_a).Y_n'(cx_a) - J_n'(cx_a).Y_n(x_a) = 0 \quad (9)$$

Where $cx_a = x_b$

So the characteristic equation can be written as

$$J_n(x_a) \cdot Y'_n(x_b) - J'_n(x_b) \cdot Y_n(x_a) = 0$$

The antenna was designed to work at mode TM_{01} which is the lower mode in the inner shorted annular microstrip antennas, it is designed at a resonance frequency of 800 MHz with an inner radius of 0.73 cm and outer radius of 6.68 cm printed on a substrate of a thickness of 0.159 cm and a dielectric constant of 2.62 ,the top layer was set to have the properties of air with dielectric constant of 1 and thickness of 1 cm in order to increase the bandwidth of the patch ,a capacitor has been added ,this is done by printing the patch on a capacitor strip printed on the ground plane, the thickness between the patch and the capacitor strip and between the capacitor strip and the ground plane was 0.02 cm and 0.96cm respectively. The third technique used to improve bandwidth combines the two techniques of stacked configuration and adding a capacitive element to the patch forming a structure shown in Figure-1 this technique will provide bandwidth by removing the reactance effect of the long probe. it consists of two inner shorted patches the printed one on the other ,the lower one is the radiating patch which has an inner radius a = 0.73 cm and an outer radius b = 6.68 cm is printed on a capacitor –strip on the top of a ground plane, the dielectric constant of the capacitor–strip (ε_{rcap}) = 2.62 have the same dielectric constant of the radiating patch (ε_{rrad}) = 2.62 and thickness of 1 cm, the other one is the parasitic patch has the dimensions of a = 1.47 cm, b = 7.15 cm printed on a substrate of dielectric constant of (ε_{rrad}) = 2.62 and thickness of 1 cm, the thickness of the layers between of the capacitor strip and the ground plane and the radiating patch and the capacitor-strip are 0.02 cm and 1 cm, respectively.

RESULTS

An inner shorted annular antenna designed according to equation (1) , Figure-2 shows the return loss of the single inner shorted patch, Figure-3 represent the real and imaginary parts of the input impedance and Figure-4 a and b represents the E-plane and the H-plane respectively, the return loss shows that the bandwidth is 12 MHz and resonance frequency of 790 MHz

The technique of capacitive-fed patch is shown in Figures (5, 6, and 7), this technique improves the bandwidth to 75 MHz (about 10.08 % of the resonance frequency) with shifting of the resonance frequency to 744 MHz

The second technique is shown in Figures (8, 9, and 10); this configuration gives a bandwidth of 174 MHz (about 22.715 % of the resonance frequency which is 766 MHz).

The above results show that the radiation field has not been affected by the different methods of enhancement and the matching between the probe feed and the antenna is about 50 ohm which is a good matching with the effect of shifting the resonance frequency from its original location.

The effect of feed location was studied for the three designs in which for every case the feed point was taken at the resonance point and the edge and the center of the patch , the radiation field for each design with three cases is shown in Figures (11,12,13), as it is seen from the figures that the radiation field is not affected too much when changing the feed point from resonance point to the edge of the patch ,on the other hand the radiation field is affected when the feed is putted at the center of the circle ,this implies for the three designs.

Figures (14, 15, and 16) represent the current distribution on the patch of the three designs for three frequencies, the resonance frequency, a frequency less than the resonance, a frequency greater than the resonance, the figures indicates the current at the resonance frequency has a maximum current indicated as the red distribution of the color, for the capacitively-fed ISAMA and capacitively-fed stacked ISAMA the current distribution is not affected by the frequency change. Figure-17 represents the radiation field at the resonance for the three designs.

REFRENCES

[1] Vicente Gonzalez P., Daniel Segovia V., Eva Rajo I., José Luis Vazquez R., Carlos Martin P. 2005. Analysis of Short Circuited Ring Patch operated at TM_{01} Mode. Rev. Fac. Ing. - Univ. Tarapaca. 13(2): 21-30.

[2] H. Liu and X.-F. Hu. Input Impedance Analysis of a Microstrip Annular-Ring Antenna with a Thick Substrate.

[3] L. Boccia, G. Amendola, G. Di Massa, L. Giulicchi- Shorted Annular Patches as Flexible Antennas for Space Applications Dipartimento di Elettronica, Informatica e Sistemistica Università Della Calabria, 87036 Arcavacata di Rende (CS), Italy.

[4] Y. LIN, L. Shafai. 1990. Characteristics of concentrically shorted circular patch microstrip antennas. IEE Proc. Vol. 137, Pt. H, No.1. February.

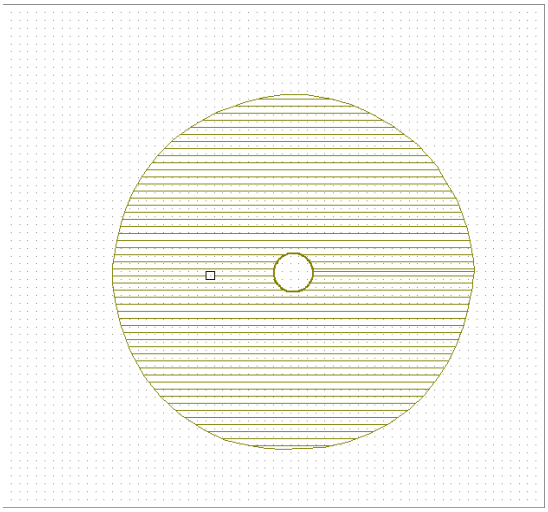

Figure-1. The structure of inner shorted annular microstrip antennas.

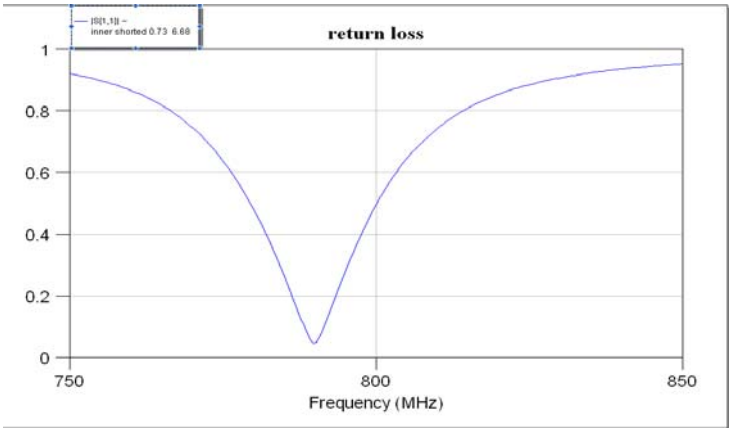

Figure-2. The return loss of an inner shorted annular patch.

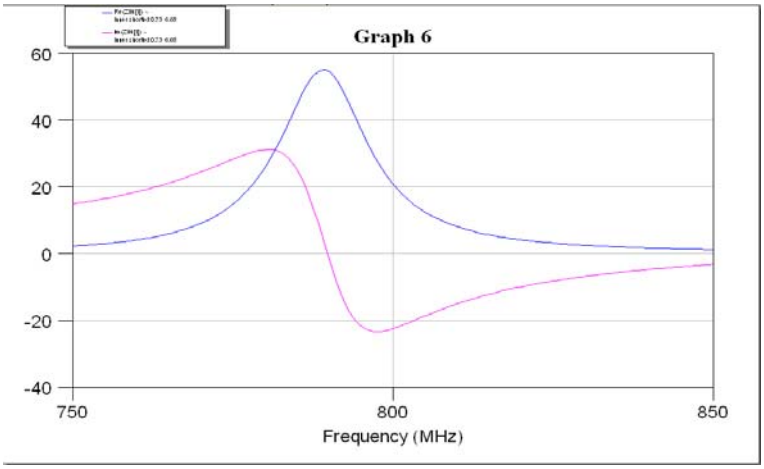

Figure-3. The input impedance of the inner shorted annular patch.

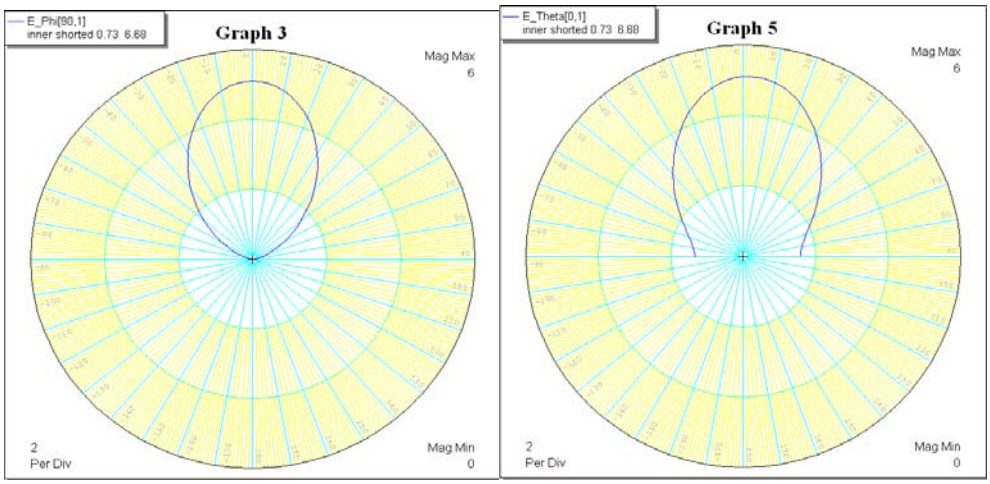

(a) (b)

Figure-4. Radiation field of inner shorted patch (a) E-plane (b) H-plane.

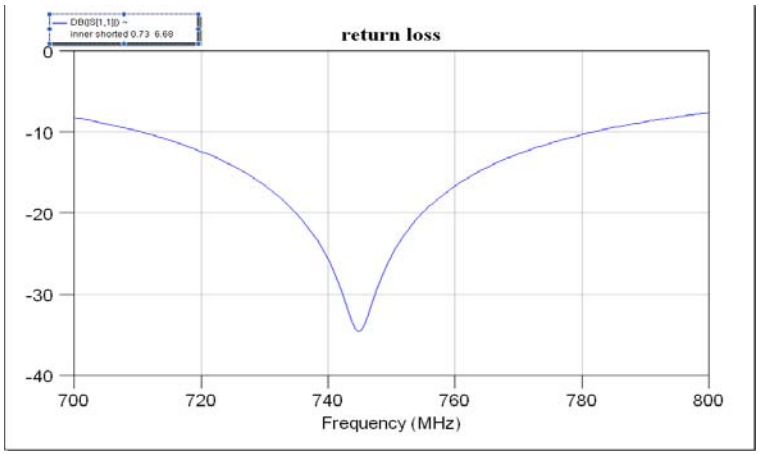

Figure-5. The return loss of a capacitively-fed ISAMA.

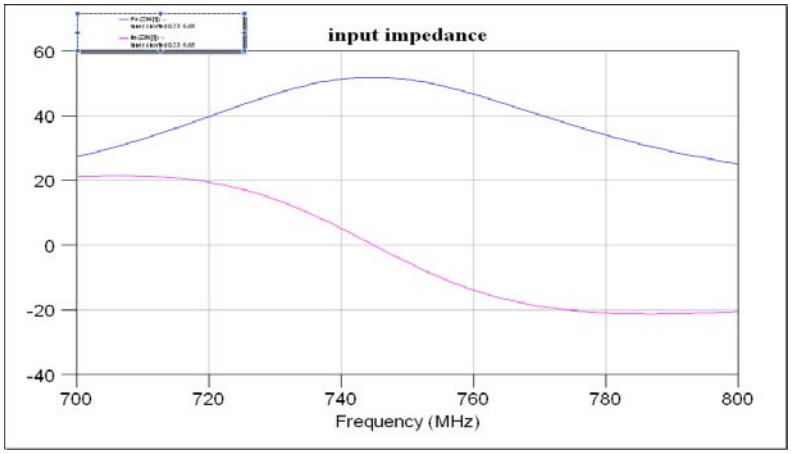

Figure-6. Real and imaginary parts of the impedance of capacitively-fed ISAMA.

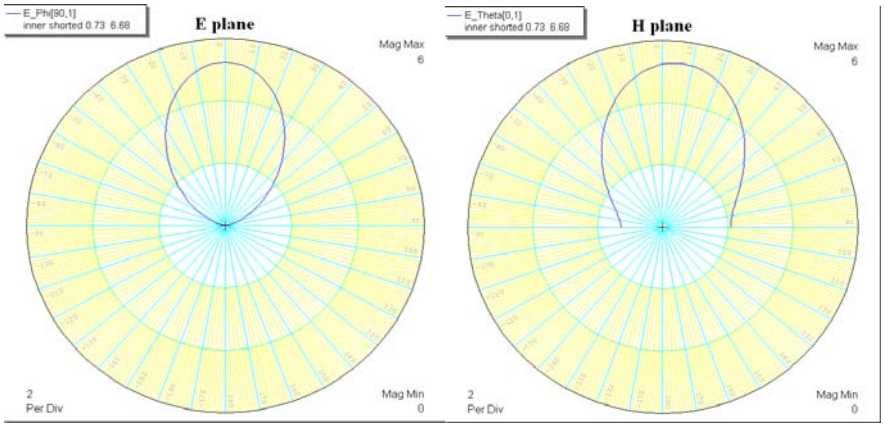

(a) (b)

Figure-7. Radiation field of capacitive-fed ISAMA (a) E-plane (b) H-plane.

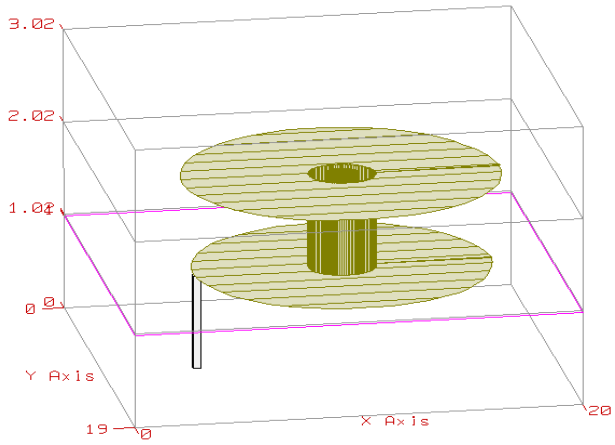

Figure-8. The configuration of capacitevely fed stacked ISAMA.

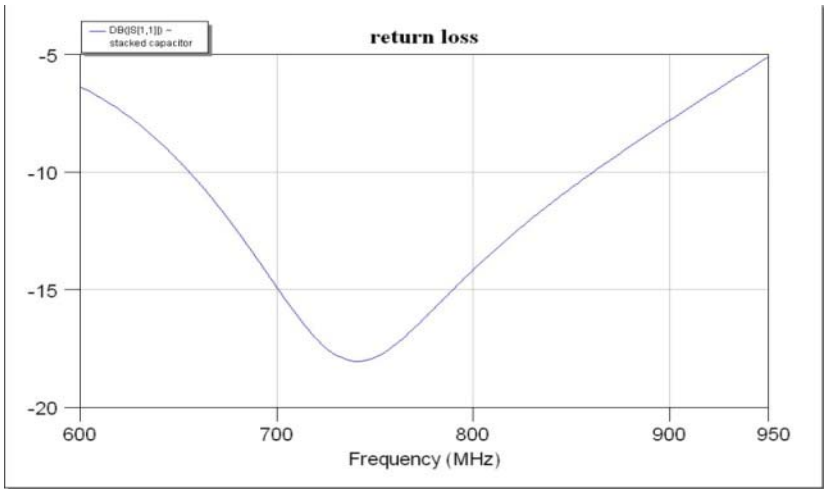

Figure-9. Return loss of the capacitevely-fed ISAMA.

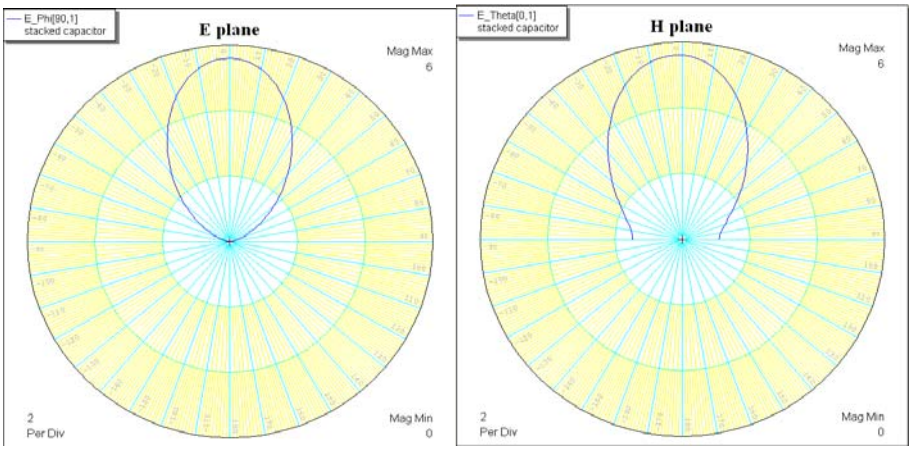

(a) (b)

Figure-10. The Radiation pattern of capacitively-fed stacked ISMA (a) E-plane (b) H-plane.

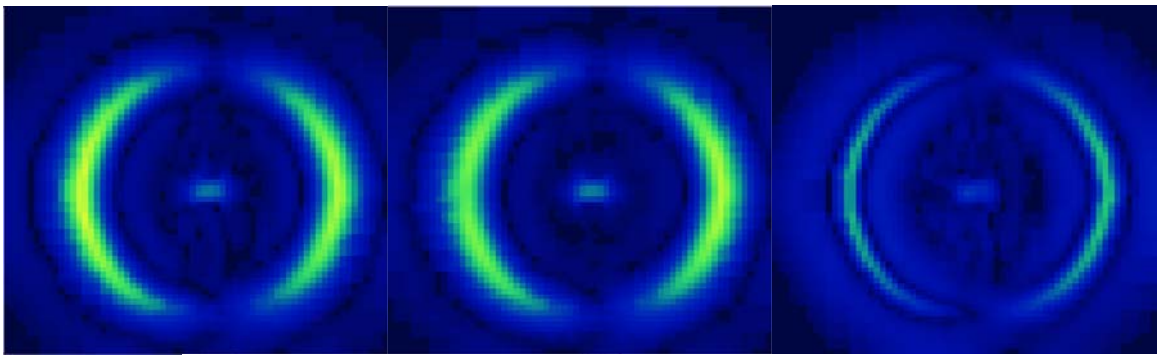

(a) (b) (c)

Figure-11. The far field of a single ISAMA when the feed is at resonance point (b) the edge (c) the center.

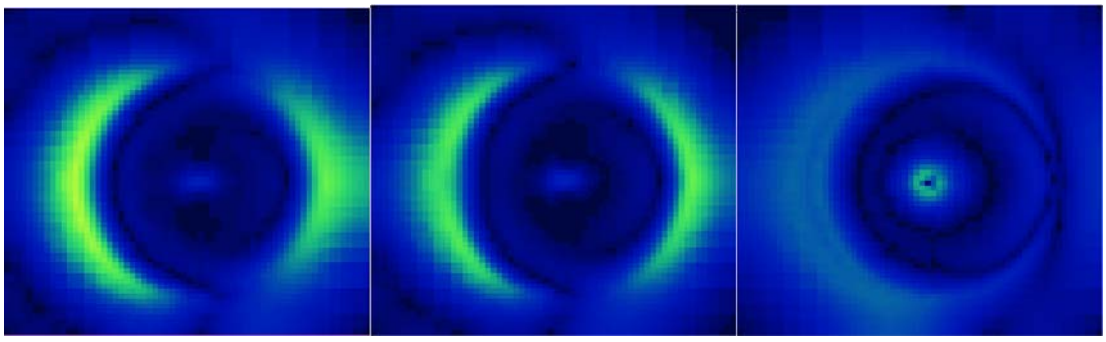

(a) (b) (c)

Figure-12. The far field of capacitively-fed Inner shorted annular patch (ISAMA) when the feed is at (a) resonance point (b) the edge (c) the center.

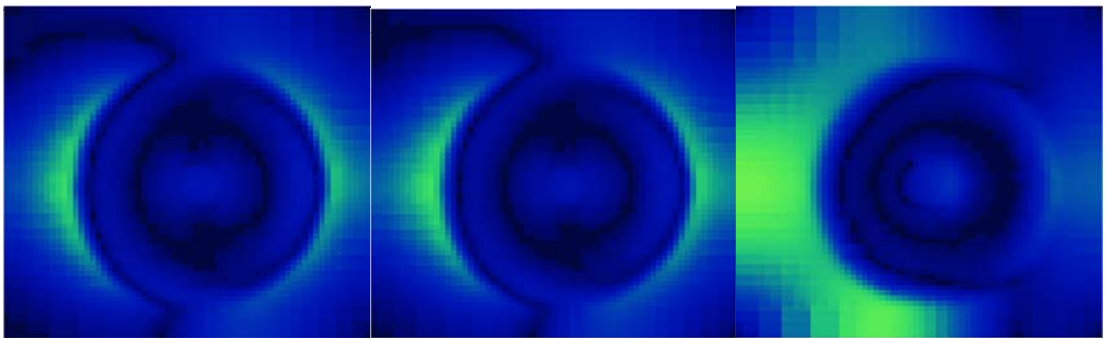

(a) (b) (c)

Figure-13. The far field of a capacitively-fed stacked Inner shorted annular patch (ISAMA) when the feed is at (a) resonance point (b) the edge (c) the center.

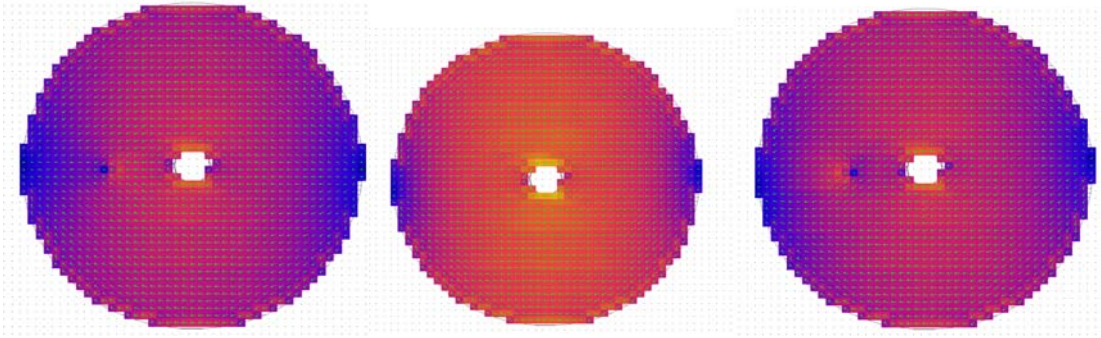

(a) (b) (c)

Figure-14. The current distribution for single ISAMA at frequency (a) 770 MHz (b) 790 MHz (resonance frequency) (c) 810 MHz.

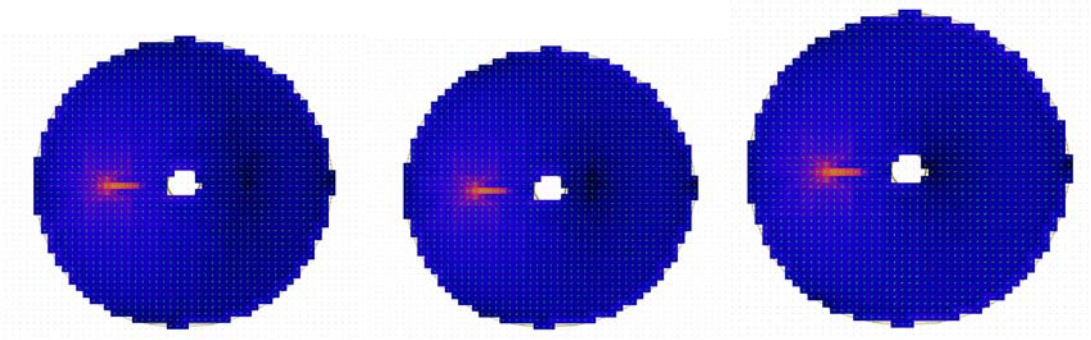

(a) (b) (c)

Figure-15. The current distribution of capacitively-fed ISAMA at frequency (a) 725 MHz (b) 745 MHz (resonance frequency) (c) 765 MHz.

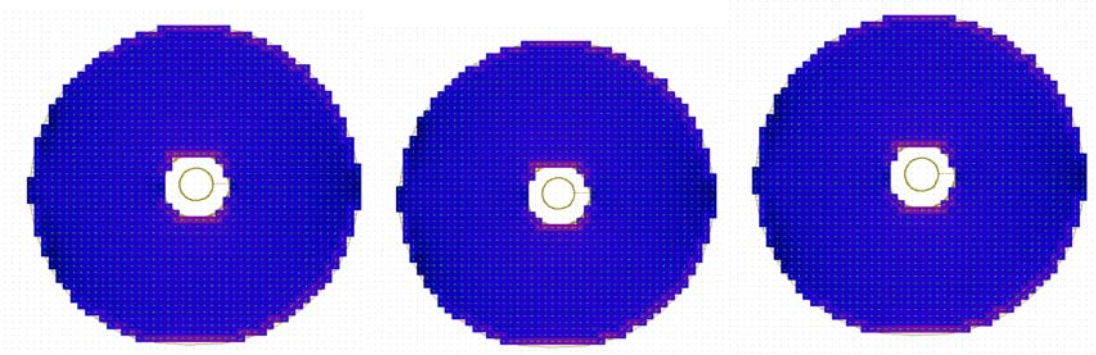

(a) (b) (c)

Figure-16. The current distribution of capacitively-fed stacked ISAMA at frequency (a) 773 MHz (b) at 793 MHz (resonance frequency) (c) 810 MHz.

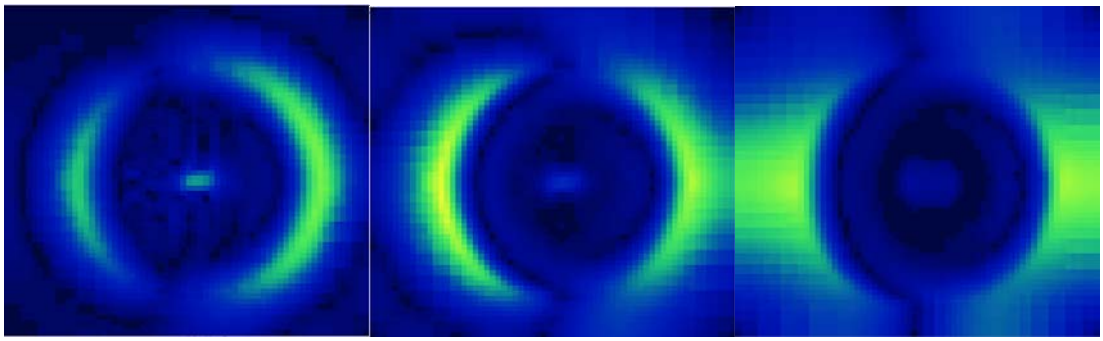

(a) (b) (c)

Figure-17. The far field of the (a) Inner Shorted Microstrip antenna (b) capacitively-fed ISAMA (c) capacitively-fed stacked ISMA.

Design A High-Precision Antenna For GPS

Proper modeling using an FEM electromagnetic simulator leads to the design of a low-cost, lightweight GPS patch antenna capable of excellent multipath rejection.

LUIGI BOCCIA
Ph.D. Student
University of Calabria, Dipartimento di Elettronica, Informatica e Sistemistica, 87036 Arcavacata di Rende (CS), Italy; (39) 0984-494743, FAX: (39) 0984-484713, e-mail: lboccia@deis.unical.it.

GIANDOMENICO AMENDOLA
Associate Professor
University of Calabria, Dipartimento di Elettronica, Informatica e Sistemistica, 87036 Arcavacata di Rende (CS), Italy; (39) 0984-494611, FAX: (39) 0984-484713, e-mail: amendola@deis.unical.it.

GIUSEPPE DI MASSA
Full Professor
University of Calabria, Dipartimento di Elettronica, Informatica e Sistemistica, 87036 Arcavacata di Rende (CS), Italy; (39) 0984-494700, FAX: (39) 0984-484713, e-mail: dimassa@deis.unical.it.

Global Positioning System (GPS) receivers (Rxs) are becoming ubiquitous, as part of the electronics packages of new automobiles, in cellular telephones, and in compact electronic devices. Unfortunately, multipath errors continue to plaque the performance of discrete and embedded GPS Rxs, even with advances in signal processing. However, an innovative low-profile, lightweight antenna may offer a possible solution for reducing the multipath error in GPS systems. As will be shown, it may be possible to achieve high-performance GPS requirements with the aid of a shorted annular patch antenna.

In recent years, the number of GPS applications requiring an augmented accuracy is considerably increased spanning from geodetic surveying to aircraft landing control and satellite attitude determination. The major limitation affecting the precision of the system is the multipath error. Multipath interference is generated by the reflections and diffractions of the GPS transmitted signal from surfaces around the antenna. Since multipath effects are dependent upon the surrounding environment, they are difficult to quantify, and available signal-processing techniques do not help in solving the problem completely under all conditions. A more effective way to limit the deleterious effects of spurious reflections is by means of an antenna with superior multipath rejection capability.

At the radiator level, multipath can be essentially controlled in two ways. Since GPS signals are right-hand circularly polarized (RHCP), odd reflections are left-hand circularly polarized (LHCP). Hence, the use of antennas with a good rejection of LHCP signals can potentially eliminate multipath effects arising from direct reflections. Effects due to double reflections will remain, but these are normally much

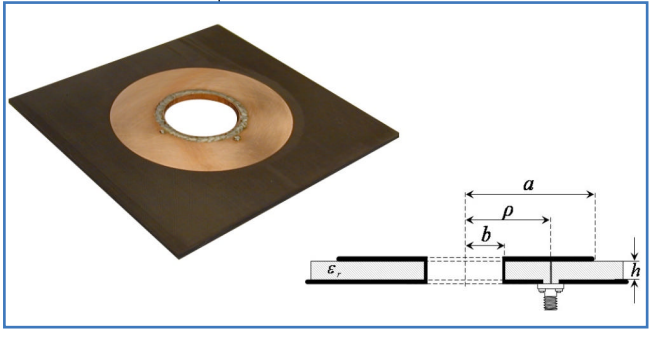

1. This cross-sectional view shows the inner radius and feed locations (a, b, and ρ) of a shorted-annular-patch (SAP) antenna.

weaker than the direct reflections. Additionally, considering that reflections often impinge on the antenna at low elevations, multipath rejection performance can be improved by shaping the antenna gain pattern to reject low-elevation signals while ensuring adequate hemispherical coverage.

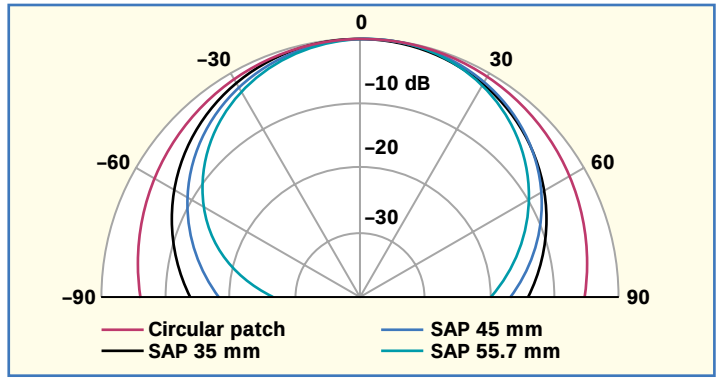

2. The SAP antenna offers a great deal of radiation pattern flexibility.

Several low multipath GPS antennas have been proposed in the past. Unfortunately, most of the available solutions, including arrays[1] or choke rings,[2] are impractical in aerospace applications due to the operational requirements in terms of size and weight. A more effective design has been proposed in ref. 3 where a novel compact radiator, namely the shorted-annular-patch (SAP) antenna, has been introduced as a possible solution for low-multipath GPS applications. In what follows, the main characteristics of SAP antennas will be discussed and a detailed review of a SAP design procedure will be presented.

The SAP antenna geometry is presented in **Figure 1**. At variance of a conventional disk the inner boundary of this patch is shorted to the ground plane. The presence of the conductor in the central zone of the antenna makes this geometry much more flexible with respect to other microstrip geometries allowing for a larger bandwidth and easier matching.[4]

The essential feature of the antenna is that the low-multipath radiation pattern requirements can be fulfilled using a single radiator, as the pattern of the shorted annular patch can be easily controlled varying the antenna geometry without degrading the radiation characteristics. In fact, it is easy to show that,[5] when working on the TM_{11} mode, the shorted ring has the same magnetic current distribution of a conventional disk and therefore a similar radiation pattern. As a consequence, with a proper choice of the external and internal radii, narrower radiation patterns that maintain the radiation characteristics of a circular disk can be obtained.

To design an SAP antenna, the first step is the selection of the patch outer radius. As it will be shown, this parameter essentially controls the antenna amplitude pattern toward the horizon and, in case of high-precision GPS applications, its choice must be the optimal compromise between the specific coverage requirements and the low multipath constrains. Once the external boundary of the shorted ring has been fixed, the inner radius has to be adjusted to make the patch resonating at the desired frequency.

Inner radius and feed locations of the three antenna patches

a	b	ρ
35.0 mm	6.0 mm	12.0 mm
45.0 mm	18.83 mm	25.0 mm
55.7 mm	30.08 mm	36.5 mm

As a proof of the SAP peculiarity, three shorted annular patch antennas resonating at the nominal GPS L1 frequency, 1.57542 GHz, with an external radius of 35, 45, and 55.7 mm, have been designed considering a substrate with dielectric constant, ϵ_R, of 2.55 and thickness of 3.2 mm. Adequate circular polarization purity is attained by feeding the antenna by means of two 50-Ω coaxial probes located 90 deg. apart and having 90 deg. of phase difference.

To simplify the design process, a simple analytical model[4] was used as a starting point to roughly estimate the antenna resonant frequency and feed location. The design was then optimized through extensive finite-element-model (FEM) based simulations using commercial High-Frequency Structure Simulator (HFSS) software from Ansoft Corp. (Pittsburgh, PA).[6] Accurate simulations were obtained by manually refining the mesh for each geometrical element of the antenna. The inner radius and the feed location for each of the three patches are shown in the **table**.

The effect of a larger external radius is shown in **Fig. 2** where the copolar radiation patterns of the three SAP antennas have been compared with the one of a conventional circular patch resonating at the same frequency and designed using the same substrate. As expected, a larger outer radius of the antenna results in a narrower beam.

It should be noticed that the shorted annular patch antenna having external radius of 55.7 mm was designed by considering the surface's wave reduction principle described in ref. 5. According to this criterion, the outer radius of the ring must be selected in such a way that the TM_0 surface-wave emission is inhibited avoiding the radiation pattern deterioration due to the diffraction of the waves on the dielectric truncation. However, the choice of the external radius is also influenced by

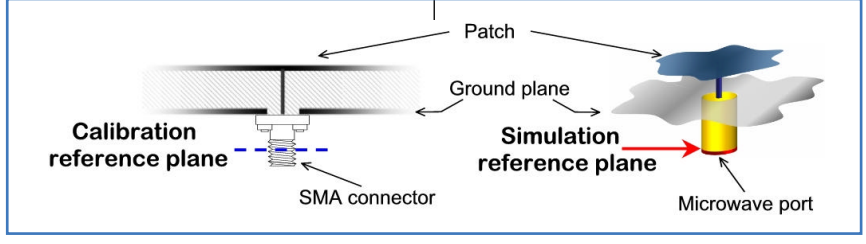

3. This diagram shows the simulation and measurement reference planes used for comparing results.

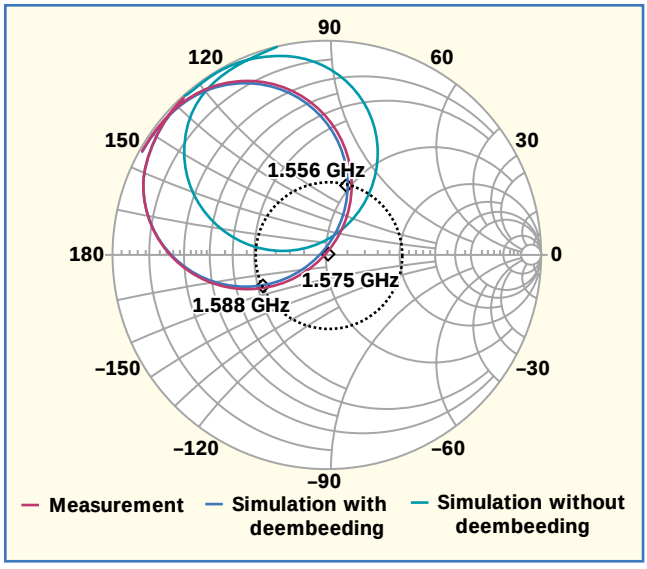

4. This comparison shows the modeled and measured input impedances of the SAP antenna.

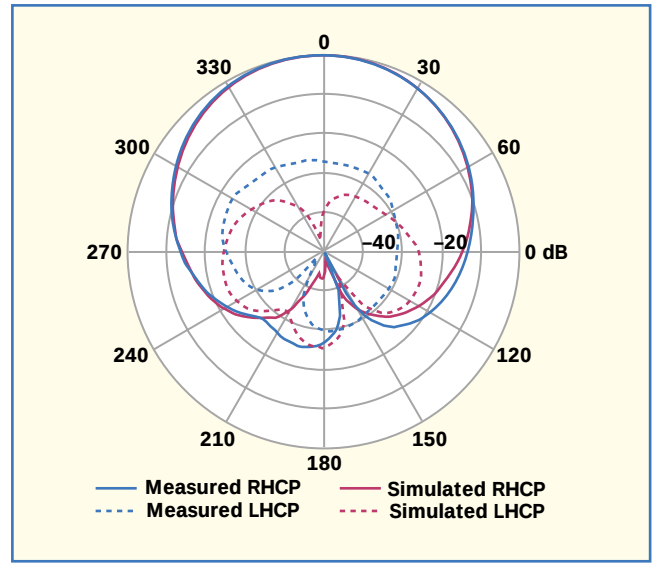

5. This is a comparison of the measured and modeled radiation patterns for the SAP antenna.

other requirements such as the extension of the radiation pattern coverage and the acceptable level of crosspolar interference.

The characteristics of the antenna and the reliability of the simulations were experimentally verified fabricating a prototype of the SAP antenna having an external radius of 35 mm.

The simulated and measured input impedances of the antenna were first compared. A comparison between numerical and experimental data often serves as a source of errors, however, due to false assumptions or poor estimations. In this case, in particular, it should be noticed that the measured input impedance is generally taken at a reference plane arbitrarily set during the calibration while the computer-generated data are calculated at the microwave port defined within the simulation environment **(Fig. 3)**.

To avoid this phase uncertainty, the two results presented here have been compared choosing the antenna ground plane as the common reference. The calibration reference plane was set by measuring and analyzing in the time domain the reflections arising from a short-ended SMA connector of the same type of the one used to feed the antenna. The calculated input impedance was coherently evaluated at the antenna ground plane by employing the de-embedding procedure included within the simulation tool environment.

In **Fig. 4**, the measured antenna input impedance is compared with the simulated data before and after the deembedding procedure was applied. As it can be seen, the predicted result is in excellent agreement with the experimental values but this outcome can be appreciated only if a coherent de-embedding method is used.

Due to the precision of the simulator and the accuracy of the fabrication process, it was possible to achieve a fairly precise design that provided predictably high performance. In fact, the antenna resonates at the nominal GPS L1 frequency and is very well matched. The multipath rejection performances of the SAP prototype have been evaluated considering both the sharpness of the antenna pattern toward the horizon and the circular polarization purity over the whole radiation hemisphere.

The measured and simulated radiation patterns **(Fig. 5)** show that the proposed SAP antenna has, as expected, an amplitude roll-off from boresight to horizon of about 15 dB. It is important to note that this result, which provides a wide hemispherical coverage while sufficiently rejecting grazing signals, has been obtained using a 14-cm-square ground plane so without increasing the overall dimension of the antenna. In addition to the sharpness of the radiation pattern, the SAP prototype proposed in this paper fully satisfies the polarization purity constrains required for high-precision GPS applications. In fact, the axial ratio stays below 2 dB within the entire coverage hemisphere.

The final antenna design, based on an SAP geometry, is inexpensive and light in weight, but offers an extended radiation pattern flexibility which can be used to optimize the multipath rejection performances in consideration of the specific application constrains. The characteristics of the antenna have been verified performing both numerical and experimental tests. Where properly considered, the simulated results are in excellent agreement with the experiments. MRF

REFERENCES

1. N. Padros, I. Ortigosa, J. Baker, F. Iskander, B. Thornberg, "Comparative studies of high-performance GPS receiving antenna designs," *IEEE Transactions on Antennas and Propagation*, Vol. 45, No. 4, April 1997.

2. A.M. Dinius, "GPS antenna multipath rejection performance," *Lincoln Laboratory Technical Report*, August 1995.

3. L. Boccia, G. Amendola, G. Di Massa, and L. Giulicchi, "Shorted Annular patch antennas for multipath rejection in GPS-based attitude determination," *Microwave and Optical Technology Letters*, January 2001.

4. G. Di Massa and G. Mazzarella, "Shorted Annular Patch Antenna," *Microwave and Optical Technology Letters*, Vol. 8, March 1995.

5. D.R. Jackson, J.T. Williams, Arun K. Bhattacharyya, Richard L. Smith, Stephen J. Buchheit, and S.A. Long, "Microstrip Patch Designs That Do Not Excite Surface Waves," *IEEE Transactions on Antennas and Propagation*, Vol. 41, No. 8, August 1993.

6. HFSS Version 8, Ansoft Corp., Pittsburgh, PA.